

**A Thermochemical Kinetic-Based Study of Ignition Delays
for 2-Azidoethanamine-Red Fuming Nitric Acid Systems:
2-Azido-N-Methylethanamine (MMAZ) Vs.
2-Azido-N,N-Dimethylethanamine (DMAZ)**

by Chiung-Chu Chen and Michael McQuaid

ARL-TR-6787

January 2014

NOTICES

Disclaimers

The findings in this report are not to be construed as an official Department of the Army position unless so designated by other authorized documents.

Citation of manufacturer's or trade names does not constitute an official endorsement or approval of the use thereof.

Destroy this report when it is no longer needed. Do not return it to the originator.

Army Research Laboratory

Aberdeen Proving Ground, MD 21005-5066

ARL-TR-6787**January 2014**

A Thermochemical Kinetic-Based Study of Ignition Delays for 2-Azidoethanamine-Red Fuming Nitric Acid Systems: 2-Azido-N-Methylethanamine (MMAZ) Vs. 2-Azido-N,N-Dimethylethanamine (DMAZ)

**Chiung-Chu Chen and Michael McQuaid
Weapons and Materials Research Directorate, ARL**

REPORT DOCUMENTATION PAGE				Form Approved OMB No. 0704-0188	
Public reporting burden for this collection of information is estimated to average 1 hour per response, including the time for reviewing instructions, searching existing data sources, gathering and maintaining the data needed, and completing and reviewing the collection information. Send comments regarding this burden estimate or any other aspect of this collection of information, including suggestions for reducing the burden, to Department of Defense, Washington Headquarters Services, Directorate for Information Operations and Reports (0704-0188), 1215 Jefferson Davis Highway, Suite 1204, Arlington, VA 22202-4302. Respondents should be aware that notwithstanding any other provision of law, no person shall be subject to any penalty for failing to comply with a collection of information if it does not display a currently valid OMB control number. PLEASE DO NOT RETURN YOUR FORM TO THE ABOVE ADDRESS.					
1. REPORT DATE (DD-MM-YYYY) January 2014		2. REPORT TYPE Final		3. DATES COVERED (From - To) November 2012–August 2013	
4. TITLE AND SUBTITLE A Thermochemical Kinetic-Based Study of Ignition Delays for 2-Azidoethanamine-Red Fuming Nitric Acid Systems: 2-Azido-N-Methylethanamine (MMAZ) Vs. 2-Azido-N,N-Dimethylethanamine (DMAZ)				5a. CONTRACT NUMBER	
				5b. GRANT NUMBER	
				5c. PROGRAM ELEMENT NUMBER	
6. AUTHOR(S) Chiung-Chu Chen and Michael J. McQuaid				5d. PROJECT NUMBER	
				5e. TASK NUMBER	
				5f. WORK UNIT NUMBER	
7. PERFORMING ORGANIZATION NAME(S) AND ADDRESS(ES) U.S. Army Research Laboratory ATTN: RDRL-WML-D Aberdeen Proving Ground, MD 21005-5066				8. PERFORMING ORGANIZATION REPORT NUMBER ARL-TR-6787	
9. SPONSORING/MONITORING AGENCY NAME(S) AND ADDRESS(ES)				10. SPONSOR/MONITOR'S ACRONYM(S)	
				11. SPONSOR/MONITOR'S REPORT NUMBER(S)	
12. DISTRIBUTION/AVAILABILITY STATEMENT Approved for public release; distribution is unlimited.					
13. SUPPLEMENTARY NOTES					
14. ABSTRACT Reaction rate expressions for paths with the potential to be rate-determining steps in the ignition of MMAZ-RFNA systems were estimated on the basis of results obtained from quantum chemistry models and transition state theory. The expressions were added to an existing finite-rate, chemical kinetics mechanism for TMEDA-DMAZ-RFNA systems to produce a TMEDA-DMAZ-MMAZ-RFNA mechanism. Homogeneous reactor simulations produced with the new mechanism predict time-to-ignition values for MMAZ-RFNA systems that are significantly longer than those for comparable DMAZ-RFNA systems. This result is consistent with experimentally measured ignition delays that have been reported for the two systems. An analysis of the computationally based results indicates that the difference in the ignition delays is attributable to differences in the rates of NO ₂ -mediated abstraction of H-atoms from the parent fuels.					
15. SUBJECT TERMS computational modeling, thermochemical kinetics, hypergolic propulsion, reaction rate, ignition delay					
16. SECURITY CLASSIFICATION OF:			17. LIMITATION OF ABSTRACT UU	18. NUMBER OF PAGES 68	19a. NAME OF RESPONSIBLE PERSON Chiung-Chu Chen
a. REPORT Unclassified	b. ABSTRACT Unclassified	c. THIS PAGE Unclassified			19b. TELEPHONE NUMBER (Include area code) 410-278-6828

Contents

List of Figures	iv
List of Tables	v
Acknowledgments	vii
1. Introduction	1
2. Methods	2
2.1 Reaction Path Characterizations.....	2
2.2 Thermodynamic Properties: $\Delta H_f^\circ(298)$, $S^\circ(298)$, and $C_p(T)$	3
2.3 Reaction Rate Expressions	3
2.4 Homogenous Reactor Simulations	4
3. Results and Discussion	4
3.1 Unimolecular Decomposition of MMAZ.....	4
3.2 Complexation of MMAZ With HNO_3	6
3.3 Abstraction of H-Atoms From MMAZ by NO_2	7
3.4 Radical + NO_2 Reactions.....	13
3.5 Comparison of Time-to-Ignition Values	19
4. Summary	21
5. References	23
Appendix A. Thermodynamic Property Estimates for Molecular Structures Involved in 2-azido-N-methylethanamine (MMAZ) Decomposition Paths	29
Appendix B. Geometric Representations, Normal Mode Frequencies, and Moments of Inertia for Molecular Structures Involved in H-Atom Abstraction Reactions	33
Appendix C. Geometric Representations, Normal Mode Frequencies, and Moments of Inertia for Molecular Structures Involved in Radical + NO_2 Addition Reaction Paths	45
Distribution List	57

List of Figures

Figure 1. Transition states for N-N ₂ bond scission with a 1,2 H-atom shift: MMAZ vs. DMAZ.	4
Figure 2. The lowest energy structures of DMAZ and MMAZ.	5
Figure 3. Equilibrium structures for MMAZ-(HNO ₃) _x complexes. (Bond distances in Å.)	6
Figure 4. Potential energy diagram for MMAZ + NO ₂ H-atom abstraction paths.	8
Figure 5. Comparison of the overall rates for R1–R4 as a function of temperature. Overall rates for H-atom abstraction from MMAZ and DMAZ by NO ₂ are also shown.	13
Figure 6. Potential energy diagram for the C•H ₂ NHCH ₂ CH ₂ N ₃ + NO ₂ system: G4-based results.	15
Figure 7. Potential energy diagram for the CH ₃ NHC•HCH ₂ N ₃ + NO ₂ system: G4-based results.	16
Figure 8. Potential energy diagram for the CH ₃ N•CH ₂ CH ₂ N ₃ + NO ₂ system: G4-based results.	17
Figure 9. QRRK-derived reaction rates (at 1 atm) as a function of temperature: (a) C•H ₂ NHCH ₂ CH ₂ N ₃ + NO ₂ , (b) CH ₃ NHC•HCH ₂ N ₃ + NO ₂ , and (c) CH ₃ N•CH ₂ CH ₂ N ₃ + NO ₂ . Note that the scale of the y-axis of (c) differs from that of (a) and (b).	18
Figure 10. QRRK rate constants at 800 K as a function of pressure: (a) C•H ₂ NHCH ₂ CH ₂ N ₃ + NO ₂ , (b) CH ₃ NHC•HCH ₂ N ₃ + NO ₂ , and (c) CH ₃ N•CH ₂ CH ₂ N ₃ + NO ₂ . Note that the scale of the y-axis of (c) differs from that of (a) and (b).	19
Figure 11. Time-to-ignition values determined in homogenous reactor simulation: MMAZ-RFNA vs. DMAZ-RFNA. Solid line: 75 atm. Dotted line: 136 atm.	20
Figure 12. Time-to-ignition values for MMAZ-DMAZ and MMAZ-TMEDA blends. Solid line: 75 atm. Dotted line: 136 atm.	21

List of Tables

Table 1. MMAZ BDE estimates. ^a	5
Table 2. Complexation exothermicities (in kcal/mol): MMAZ-(HNO ₃) _x vs. DMAZ-(HNO ₃) _x . ^a	6
Table 3. Relative energies (in kcal/mol) of stationary points for R1–R4 reaction paths.....	8
Table 4. Reaction rates (in cm ³ -mol ⁻¹ -s ⁻¹) for the abstraction of H-atoms from MMAZ by NO ₂	11
Table 5. Kinetic parameters. ^a	12
Table A-1. G4-based $\Delta H_f^\circ(298)$ estimates for equilibrium structures involved in paths for the decomposition of MMAZ.	31
Table A-2. $S^\circ(298)$ and $C_p(T)$ estimates for molecular structures involved in MMAZ decomposition paths. ^a	32
Table B-1. The Cartesian coordinates of MMAZ and MMAZ radical (MMAZ-H•) equilibrium geometries: B3LYP/6-31+G(d,p) results.	35
Table B-2. The Cartesian coordinates of (TS-E) transition states leading to <i>trans</i> -HONO formation (R1–R4): B3LYP/6-31+G(d,p) results.....	36
Table B-3. The Cartesian coordinates of (TS-H) transition states leading to HNO ₂ formation (R1–R4): B3LYP/6-31+G(d,p) results.	37
Table B-4. The Cartesian coordinates of (TS-Z) transition states leading to <i>cis</i> -HONO formation (R1–R4): B3LYP/6-31+G(d,p) results.....	38
Table B-5. The Cartesian coordinates of (COMP-E) complexes leading to <i>trans</i> -HONO formation (R1–R4): B3LYP/6-31+G(d,p) results.....	39
Table B-6. The Cartesian coordinates of (COMP-H) complexes leading to HNO ₂ formation (R1–R4): B3LYP/6-31+G(d,p) results.	40
Table B-7. The Cartesian coordinates of (COMP-Z) complexes leading to <i>cis</i> -HONO formation (R1–R4): B3LYP/6-31 +G(d,p) results.....	41
Table B-8. Normal mode frequencies and moments of inertia for MMAZ and MMAZ radicals (MMAZ-H•): B3LYP/6-31+G(d,p) results.	42
Table B-9. Normal mode frequencies and moments of inertia (MoI) for H-bonded complexes involved in reactions R1–R4: B3LYP/6-31+G(d,p) results.....	43
Table B-10. Normal mode frequencies and moments of inertia (MoI) for transition states involved in reactions R1–R4: B3LYP/6-31+G(d,p) results.....	44

Table C-1. G4-model total energies ^a and moments of inertia for molecular structures involved in MMAZ-H• + NO ₂ reactions.....	47
Table C-2. The Cartesian coordinates and normal mode frequencies of molecular structures involved in the C•H ₂ NHCH ₂ CH ₂ N ₃ +NO ₂ system. (See figure 6 in report.)	48
Table C-3. The Cartesian coordinates and normal mode frequencies of molecular structures involved in the CH ₃ NHC•HCH ₂ N ₃ +NO ₂ system. (See figure 7 in report.).....	51
Table C-4. The Cartesian coordinates and normal mode frequencies of molecular structures involved in the CH ₃ N•CH ₂ CH ₂ N ₃ +NO ₂ system. (See figure 8 in report.)	54

Acknowledgments

We are grateful to Mr. Darren Thompson (U.S. Army Aviation and Missile Research Development and Engineering Center [AMRDEC]) and Dr. William Stevenson (ERC, Inc./AMRDEC) for sharing their observations and insights regarding the ignition delays of 2-azidoethanamine-red fuming nitric acid systems. The Department of Defense (DOD) High Performance Computing Modernization Office supported this project by supplying supercomputer time. The computer time was made available at the DOD Shared Resource Centers at the U. S. Army Research Laboratory, Aberdeen Proving Ground, MD, and the U.S. Air Force Research Laboratory, Wright-Patterson Air Force Base, OH.

INTENTIONALLY LEFT BLANK.

1. Introduction

In a search for alternatives to hydrazine-based hypergols, the combination of 2-azido-N,N-dimethylethanamine (DMAZ) and (inhibited) red fuming nitric acid (RFNA) was found to yield density-specific impulses (ρ^*I_{sp}) that were competitive with monomethylhydrazine (MMH)-RFNA (Thompson et al., 1998). However, DMAZ-RFNA did not meet “ignition delay” standards set by MMH-RFNA. Therefore, other 2-azidoethanamines were synthesized and tested in an attempt to address this issue (Stevenson, 2002). Some proved to have ignition delays comparable to DMAZ-RFNA, but none had ignition delays that were shorter. Comparing various properties of the compounds that were tested to the ignition delays that were observed for them, Stevenson (2002) identified correlations that provided some design guidance. But they did not lead to the development of 2-azidoethanamines with shorter ignition delays than DMAZ. Moreover, a correlation that was expected between compound basicities (as indicated by their aqueous-phase acid dissociation constants [pK_a]) and ignition delays was not observed. The correlation was expected because proton transfer from nitric acid to a 2-azidoethanamine’s amine N-atom (N_{am}) was thought to be a rate-controlling step in the ignition process for such systems, and pK_a is a measure of the strength of the attraction between a base and a proton. However, the secondary 2-azido-N-methylethanamine (MMAZ), which has a higher pK_a than DMAZ (9.3 versus 8.5), did not ignite in drop-into-drop tests (Stevenson, 2002).

Seeking to explain the difference in the hypergolicities of MMAZ-RFNA and DMAZ-RFNA systems, McQuaid (2004) employed quantum chemistry (QC) models to obtain predictions for the molecular structures and relative energies of a comprehensive set of equilibrium MMAZ conformers, and he compared them to analogous predictions for DMAZ (McQuaid et al., 2002) and 2-azido-N-cyclopropylethanamine. (The latter is a secondary 2-azidoethanamine that is hypergolic with RFNA.) No correlation between parameter predictions and ignition delays was observed. In another study, differences in substituent-mediated basicities for a variety of 2-azidoethanamines were predicted, again based on results from QC models (McQuaid, 2003). Perhaps not surprisingly, given the basicities and ignition delays observed for DMAZ-RFNA and MMAZ-RFNA, a correlation between computed basicities and ignition delays was not observed. The study did suggest the possibility that reactions involving the ethylene chain connecting the amine and azide groups were responsible for the unexpectedly short ignition delays observed for some 2-azidoethanamines. However, we are unaware of any other evidence that supports that hypothesis.

Because DMAZ's complexation and decomposition reactions had been extensively studied in the course of developing a chemical kinetics mechanism for DMAZ-RFNA systems (Chen and McQuaid, 2011), an investigation of analogous reactions involving MMAZ appeared to offer an opportunity to gain a more fundamental understanding of the differences in the two systems' ignition delays, and it comprises this work. Estimates for the thermochemical properties of species considered likely to be important during the pre-ignition and ignition phases of a reacting MMAZ-RFNA system are reported here. Ab initio and density functional theory-based QC methods were employed to obtain estimates for thermochemical parameters. Those parameters were then used in conjunction with the principles of thermochemical kinetics, transition state theory (Steinfeld et al., 1989), canonical variational transition state theory (DaSilva and Bozzelli, 2008), and quantum Rice-Ramsberger-Kassel (QRRK) unimolecular rate theory with master equation analysis (Chang et al., 2000; Dean, 1985; Dean et al., 1991) to calculate rate expressions for elementary reaction steps. An MMAZ-RFNA chemical kinetics mechanism was developed by adding the rate expressions and associated thermochemical data for those steps to a mechanism developed previously for tetramethylethylenediamine (TMEDA)-DMAZ-RFNA systems (Chen, 2013). The new mechanism was then employed as the basis for time-dependent, homogeneous reactor simulations (Kee et al., 1989; Lutz et al., 1988;) for MMAZ-RFNA and DMAZ-RFNA systems. A comparison of the results provides a basis for understanding the difference in ignition delays observed for the two systems. An example of the use of the new mechanism as a formulation screening tool is also provided.

2. Methods

2.1 Reaction Path Characterizations

Potential reaction paths were identified and characterized with QC-based models. All such models were implemented with the Gaussian 09 suite of codes (Frisch et al., 2009). The geometries of molecular structures associated with reaction path stationary points were determined via geometry optimizations performed with MPWB1K/6-31+G(d,p) (Zhao and Truhlar, 2004) and B3LYP/6-31+G(d,p) (Becke, 1993; Lee et al., 1988; Stephens et al., 1994; Vosko et al., 1980) models. Vibrational frequencies and zero-point vibrational energies were computed with the same models. The existence of one (and only one) imaginary frequency in the normal mode analysis of a geometry identified it as a transition state (TS), and the reaction coordinate's vibrational motion was evaluated to establish/confirm the nature of the connected equilibrium structures. Intrinsic reaction coordinate (IRC) walks were also performed for that purpose. Composite methods, including CBS-APNO (Ochterski et al., 1996), CBS-QB3 (Montgomery et al., 1999; Montgomery et al., 2000), G3 (Curtiss et al., 1998), G4 (Curtiss et al., 2007), G3MP2B (Baboul et al., 1999), G3(MP2)//MPWB1K/6-31+G(d,p), and

G3(MP2)//B3LYP/6-31+G(d,p) models were used to predict relative energies. The G3(MP2)//MPWB1K/6-31+G(d,p) and G3(MP2)//B3LYP/6-31+G(d,p) models are referred to in the discussion that follows as G3MP2//B1K and G3MP2//B3GTBas3, respectively.

2.2 Thermodynamic Properties: $\Delta H_f^\circ(298)$, $S^\circ(298)$, and $C_p(T)$

For species for which enthalpies of formation at 298 K [$\Delta H_f^\circ(298)$] were needed, they were derived from enthalpy-of-reaction estimates [$\Delta H_r(298)$] for isodesmic reactions in which previously established $\Delta H_f^\circ(298)$ values for all species except the moiety of interest were available. The $\Delta H_f^\circ(298)$ estimates are listed in appendix A, which also includes the isodesmic reaction schemes, $\Delta H_r(298)$ estimates, and thermodynamic data employed to produce them.

In addition to $\Delta H_f^\circ(298)$ estimates, species' entropies at 298 K [$S^\circ(298)$] and heat capacities from 300 to 1500 K [$C_p(T)$] were estimated if not already available. The programs SMCPs (Sheng, 2002) and ROTATOR (Lay et al., 1996; McQuarrie, 1976) were employed to estimate species' entropies at 298 K [$S^\circ(298)$] and heat capacities from 300 to 1500 K [$C_p(T)$]. SMCPs calculates the contributions of individual vibrational modes to $S^\circ(298)$ and $C_p(T)$ based on the rigid-rotor-harmonic-oscillator approximation and entropy corrections that are required for unpaired electrons, symmetry, and optical isomers. For this study, the molecular geometries, frequencies, and moments of inertia needed as input for the program were obtained from the optimized B3LYP/6-31+G(d,p) structures. For low-frequency vibrational modes corresponding to hindered internal rotation, the modes' SMCPs-calculated contributions to $S^\circ(T)$ and $C_p(T)$ were superseded by values calculated by ROTATOR. ROTATOR calculates the contributions for such modes based on direct summation over the calculated hindrance potential energy levels. The estimates for these properties are listed in appendix A.

2.3 Reaction Rate Expressions

Reaction rates [$k(T)$] were calculated based on the expression

$$k(T) = \frac{k_B T}{h} \exp\left(\frac{\Delta S^\ddagger(T)}{R}\right) \exp\left(\frac{-\Delta H^\ddagger}{RT}\right) \quad (1)$$

where ΔS^\ddagger is the activation entropy, ΔH^\ddagger is the activation enthalpy, k_B is Boltzmann's constant, and h is Planck's constant. $\Delta S^\ddagger(T)$ was calculated from the integral of $C_p(T)$ with respect to $\log(T)$. Estimates were produced for temperatures ranging from 300 to 2000 K. An asymmetric Eckart barrier for H-atom tunneling (Louis et al., 2000; Knyazev et al., 1996; Schwartz et al., 1998) was used to calculate the tunneling factor [$\Gamma(T)$] for reactions involving the abstraction of H-atoms from MMAZ by NO₂. An empirical three-parameter form of the Arrhenius equation

$$k(T) = A' T^n \exp\left(\frac{-E_a}{RT}\right) \quad (2)$$

was then fit to the $k(T)$ data, with the parameters E_a , A' and n being adjusted to give the best representation of $k(T)$.

2.4 Homogenous Reactor Simulations

Predictions for the time-dependent behavior of a homogeneous gas mixture in a closed system were obtained with an in-house computer program that uses the SENKIN subroutine library (Lutz et al., 1988). Time-to-ignition values for adiabatic, constant-pressure processes were obtained and compared. All the newly included reactions were written so that the program computed both their forward and reverse rates. Reverse rates were computed from (rate constant-derived) forward rates and equilibrium constants computed with the thermodynamic parameter expressions derived for the reactants and products.

3. Results and Discussion

3.1 Unimolecular Decomposition of MMAZ

The kinetics of DMAZ's unimolecular decomposition have been studied (Chen and McQuaid, 2011). The dominant mechanism in the process involves coupling a 1,2 H-atom shift with the scission of the N-N₂ bond. It produces an imine [(CH₃)₂NCH₂CHNH] and N₂. On the basis of results obtained with a QCISD(T)/6-31++G(3df,2p)//MPWB1K/6-31+G(d,p) model, the transition state for the path was estimated to be 37.4 kcal/mol higher in energy than DMAZ's ground state. Based on results obtained with the same model, the transition state-ground state energy difference for the analogous MMAZ path is 38.1 kcal/mol. The similarity of the relative energies of the two transition states is reflected in the similarity of their geometric parameters. (See figure 1.)

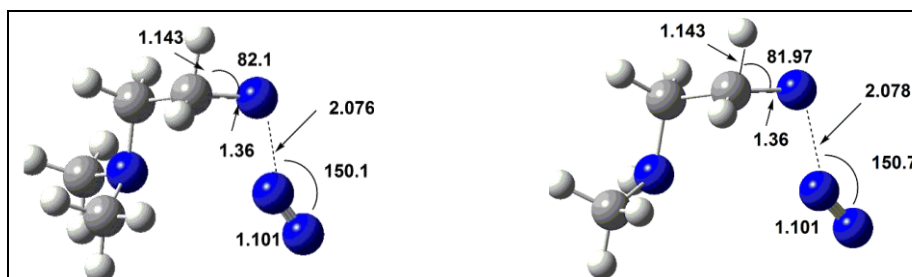


Figure 1. Transition states for N-N₂ bond scission with a 1,2 H-atom shift: MMAZ vs. DMAZ.

The lowest energy conformer MMAZ and the lowest energy conformer of DMAZ are shown in figure 2. In both cases, the azide and amine groups are in relatively close proximity to one another. Because MMAZ is a stronger base than DMAZ, and that difference is associated with differences in the electron clouds of the lone pairs of their amine N-atoms, molecule-dependent differences in the interactions between the amine and azide groups were thought to have the

potential to influence the process. The QC-based results, however, indicate otherwise. Indeed, the similarities in the geometries and relative energies of the transition states for the two molecules indicate that this decomposition mechanism is not responsible for the difference in ignition delays observed for MMAZ-RFNA and DMAZ-RFNA systems.

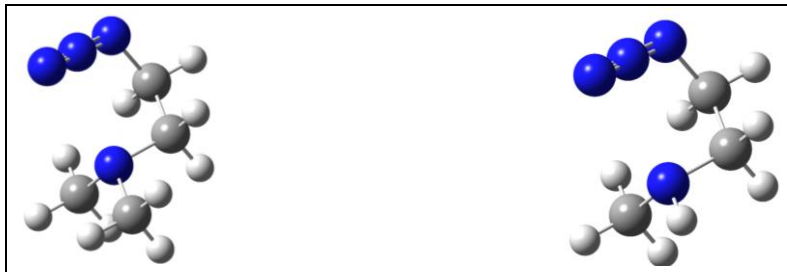


Figure 2. The lowest energy structures of DMAZ and MMAZ.

$\Delta H_f^\circ(298)$ estimates for decomposition products of C–H, N_{am} -H, C–C, and C– N_α (bond) scission reactions were employed to obtain estimates for the corresponding bond dissociation energies (BDEs). The estimates are presented in table 1. BDE estimates for C–H bonds associated with primary and secondary C-atoms adjacent to N_{am} are 91.1 and 89.3 kcal/mol, respectively. These values are similar to BDE estimates found for analogous C–H bonds in DMAZ. For both MMAZ and DMAZ, the BDE estimate for the C–H bond associated with the C-atom adjacent to the azide group is 90 kcal/mol. The BDE estimates for the C– N_3 bonds in DMAZ and MMAZ are 72.8 and 73.8 kcal/mol, respectively. Those energies are slightly lower than the estimates for the energies needed to dissociate C–C bonds: 73.9 kcal/mol for DMAZ and 74.1 kcal/mol for MMAZ. The estimates for the energies needed to dissociate a methyl group from the (secondary) N_{am} of MMAZ and the (tertiary) N_{am} of DMAZ are 81.1 and 77.6 kcal/mol, respectively. The estimate for the energy needed to dissociate MMAZ’s N–H bond is 93.1 kcal/mol. (DMAZ does not have a comparable bond.)

Table 1. MMAZ BDE estimates.^a

MMAZ	BDE (kcal/mol)
C–N Bonds	
H ₃ C–NHCH ₂ CH ₂ N ₃	81.1 (77.6)
CH ₃ NH–CH ₂ CH ₂ N ₃	83.8 (81.2)
CH ₃ NHCH ₂ CH ₂ –N ₃	73.8 (72.8)
C–C Bond	
CH ₃ NHCH ₂ –CH ₂ N ₃	74.1 (73.9)
N–H Bond	
CH ₃ N(–H)CH ₂ CH ₂ N ₃	93.1
C–H Bonds	
H–CH ₂ NHCH ₂ CH ₂ N ₃	91.1 (92.0)
CH ₃ NHC(–H)HCH ₂ N ₃	89.3 (88.4)
CH ₃ NHCH ₂ CH(–H)N ₃	89.8 (90.0)

^aBDE estimates for analogous bonds in DMAZ are in parentheses.

3.2 Complexation of MMAZ With HNO₃

MMAZ-(HNO₃)_x (x = 1,3) complexes are produced via the formation of H-bonds between nitric acid's H-atom and MMAZ's lone-pair sites. The lone-pair sites include: (1) N_{am}, (2) the azido N-atom adjacent to the -CH₂- group (N_α), and (3) the terminal azido N-atom (N_t). Depictions of optimized equilibrium structures for potential complexes are shown in figure 3.

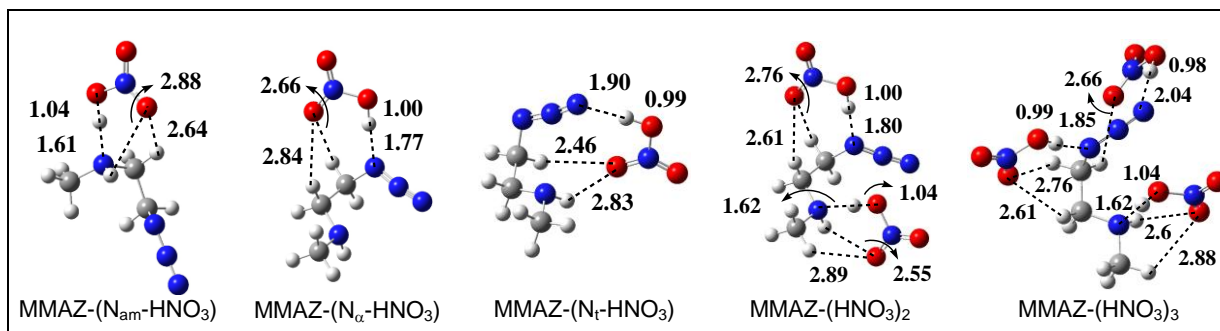


Figure 3. Equilibrium structures for MMAZ-(HNO₃)_x complexes. (Bond distances in Å.)

Table 2 lists the exothermicities that were computed for the reactions leading to these complexes. The exothermicities of analogous DMAZ + HNO₃ complexation reactions are listed for comparison. The exothermicity estimates for the formation of MMAZ-(HNO₃)_x (x = 1–3) complexes are close to those produced for corresponding DMAZ-(HNO₃)_x (x = 1–3) complexes. Since there is little difference, the results lead to the conclusion that differences in complexation energies do not underlie the difference in ignition delays observed for MMAZ-RFNA and DMAZ-RFNA systems.

Table 2. Complexation exothermicities (in kcal/mol): MMAZ-(HNO₃)_x vs. DMAZ-(HNO₃)_x.^a

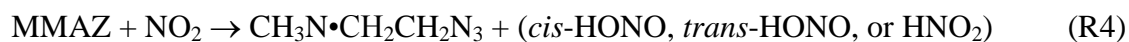
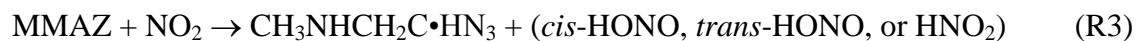
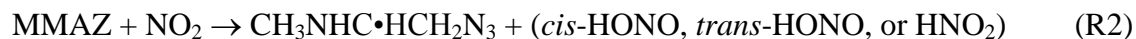
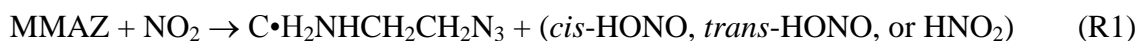
Reaction	CBS-QB3	G4	G3MP2B3	G3MP2// B3GTBas3	G3MP2// B1K
MMAZ + HNO ₃ ↔ MMAZ-(N _{am} -HNO ₃)	14.1 (14.2)	13.2 (13.5)	13.2 (13.6)	13.5 (13.5)	13.2 (13.7)
MMAZ + HNO ₃ ↔ MMAZ-(N _α -HNO ₃)	10.1 (10.1)	9.6 (9.6)	9.5 (9.5)	9.5 (9.5)	9.6 (9.7)
MMAZ + HNO ₃ ↔ MMAZ-(N _t -HNO ₃)	7.7 (6.8)	6.2 (6.3)	6.5 (6.5)	6.6 (6.3)	6.5 (6.6)
MMAZ + 2HNO ₃ ↔ MMAZ-(HNO ₃) ₂	23.0 (24.4)		21.8 (23.1)	22.9 (24.4)	21.8 (23.6)
MMAZ + 3HNO ₃ ↔ MMAZ-(HNO ₃) ₃					27.0 (28.1)

^aValues in parentheses are exothermicities for the corresponding DMAZ + xHNO₃ ↔ DMAZ-(HNO₃)_x reaction.

For comparison, Liu et al. (2011) have modeled TMEDA-(HNO₃)₂ and tetramethylmethylenediamine (TMMA)-(HNO₃)₂ complex formation, finding the former to be 45.0-kcal/mol exothermic and the latter to be 38.7-kcal/mol exothermic. They attribute the difference to stronger electrostatic repulsion in the more sterically constrained TMMA-(HNO₃)₂. Moreover, since TMMA-RFNA has a longer ignition delay than TMEDA-RFNA, they conclude that the complexation exothermicity difference is a contributing factor. They did not, however, present simulations with a comprehensive TMEDA-TMMA-RFNA chemical kinetics mechanism that would support this conclusion and indicate the difference's importance relative to other factors.

3.3 Abstraction of H-Atoms From MMAZ by NO₂

Based on prior studies of other hypergol-RFNA systems (Chen and McQuaid, 2007; McQuaid and Ishikawa, 2006), the abstraction of H-atoms from MMAZ by NO₂ was another class of reactions that was expected to be important in the ignition of MMAZ-RFNA systems. MMAZ has four different nominal H-atom types: (1) those associated with the -CH₃ group, (2) those associated with the -CH₂- group bonded to N_{am}, (3) those associated with the -CH₂- group bonded to N_α, and (4) the one bonded directly to N_{am}. As such, four different “MMAZ radicals” (MMAZ-H•) can be postulated as products: (1) C•H₂NHCH₂CH₂N₃, (2) CH₃NHC•HCH₂N₃, (3) CH₃NHCH₂C•HN₃, and (4) CH₃N•CH₂CH₂N₃. With *cis*-HONO, *trans*-HONO, or HNO₂ being the other product, we define four (overall) reaction types as



The potential energy diagram in figure 4 summarizes the relative energies of stationary points of the three minimum energy paths these four reactions can take. The relative energies of the stationary points of a given path are different for each of the four MMAZ-H• types, but the ordering of the relative energies of the stationary points is the same for R1, R2, and R3. The difference between R4 and the other three is that TS-H is higher in energy than TS-E. Estimates for the relative energies of specific stationary points are listed in table 3. B3LYP/6-31+G(d,p)-based geometries, vibration frequencies, and moments of inertia for all the stationary points of these paths are provided in appendix B.

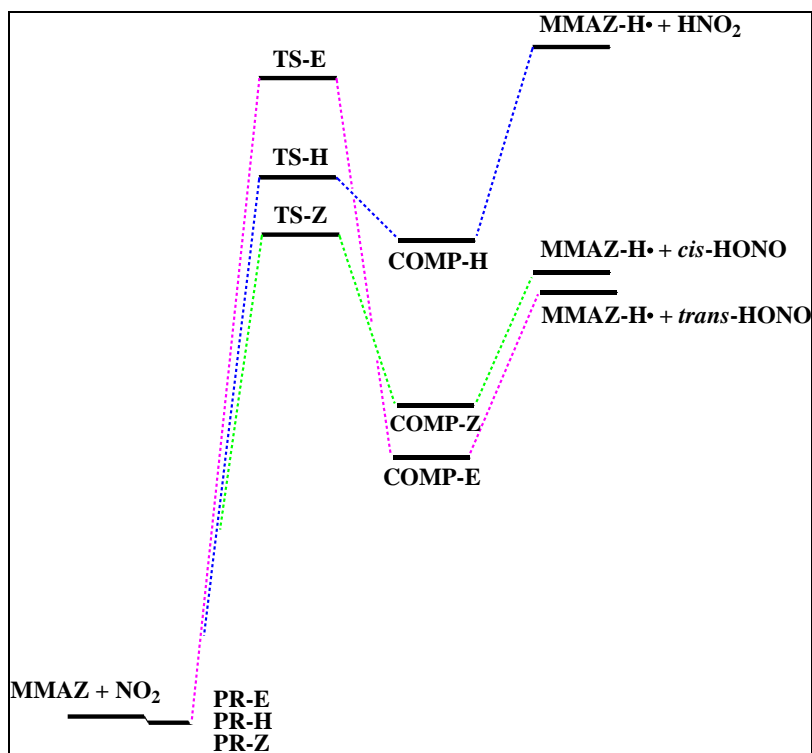


Figure 4. Potential energy diagram for MMAZ + NO₂ H-atom abstraction paths.

Table 3. Relative energies (in kcal/mol) of stationary points for R1–R4 reaction paths.

Reaction Path	CBS-APNO	CBS-QB3	G4	G3MP2B	G3MP2// B3GTBas3	G3MP2// BK1
R1						
PR1-E		-1.8	-2.2	-1.3		
PR1-H		0.3	-2.6	-1.5		
PR1-Z		-0.4	-2.4	-0.6		
TS1-E		20.7	18.6	19.6	18.9	21.3
TS1-H		17.8	16.0	17.8	16.3	18.0
TS1-Z		15.9	14.0	15.3	14.4	15.8
COMP1-E		9.5	7.0	9.0		
COMP1-H		17.0	13.1	15.9		
COMP1-Z		11.4	8.5	10.6		
C•H ₂ NHCH ₂ CH ₂ N ₃ + <i>trans</i> -HONO (R1-E)	15.4	15.6	11.4	12.7	11.7	13.6
C•H ₂ NHCH ₂ CH ₂ N ₃ + HNO ₂ (R1-H)	23.6	23.5	19.3	21.6	20.5	21.8
C•H ₂ NHCH ₂ CH ₂ N ₃ + <i>cis</i> -HONO (R1-Z)	15.9	16.0	12.0	13.4	12.3	14.0
R2						
PR2-E		-1.3	-2.2	-1.4		
PR2-H		0.3	-2.6	-1.6		
PR2-Z		-0.4	-2.4	-0.7		
TS2-E		18.6	17.2	18.4	17.5	20.3
TS2-H			14.0	16.8	15.4	14.9
TS2-Z		13.6	12.6	14.0	13.0	13.5
COMP2-E		6.4	4.9	6.9		
COMP2-H		14.4	11.3	14.1		
COMP2-Z		8.0	6.2	8.3		
CH ₃ NHC•HCH ₂ N ₃ + <i>trans</i> -HONO (R2-E)	13.7	13.1	10.2	11.4		

Table 3. Relative energies (in kcal/mol) of stationary points for R1–R4 reaction paths (continued).

Reaction Path	CBS-APNO	CBS-QB3	G4	G3MP2B	G3MP2// B3GTBas3	G3MP2// BK1
CH ₃ NHC•HCH ₂ N ₃ + HNO ₂ (R2-H)	21.9	21.0	18.1	20.2		
CH ₃ NHC•HCH ₂ N ₃ + <i>cis</i> -HONO (R2-Z)	14.2	13.5	10.8	12.0		
R3						
PR3-E		0.2	-3.1	-1.6		
PR3-H		0.0	-4.0	-1.7		
PR3-Z		-0.1	-3.7	-2.1		
TS3-E		29.8	28.8	30.6	29.4	29.9
TS3-H				24.6	23.0	22.5
TS3-Z		21.0	19.8	21.9	20.4	20.6
COMP3-E		9.7	11.2	10.9		
COMP3-H			13.0	19.1		
COMP3-Z		11.6	10.1	12.4		
CH ₃ NHCH ₂ C•HN ₃ + <i>trans</i> -HONO (R3-E)	13.4	13.8	11.4	13.0	12.0	12.2
CH ₃ NHCH ₂ C•HN ₃ + HNO ₂ (R3-H)	21.6	21.6	19.3	21.8	20.8	20.4
CH ₃ NHCH ₂ C•HN ₃ + <i>cis</i> -HONO (R3-Z)	13.9	14.1	11.9	13.7	12.6	12.7
R4						
PR4-E		0.0	-2.6	-1.6		
PR4-H		-0.9	-3.5	-0.6		
PR4-Z		0.2	-3.1	-1.6		
TS4-E		18.0	14.8	17.3	15.9	22.3
TS4-H		18.3	16.5	18.8	16.6	16.9
TS4-Z		13.9	9.9	11.7	10.7	11.9
COMP4-E		8.5	5.0	9.6		
COMP4-H		15.1	11.3	13.3		
COMP4-Z		9.8	6.9	8.6		
CH ₃ N•CH ₂ CH ₂ N ₃ + <i>trans</i> -HONO (R4-E)	17.6	17.4	13.3	14.4	13.6	15.2
CH ₃ N•CH ₂ CH ₂ N ₃ + HNO ₂ (R4-H)	25.8	25.3	21.2	23.2	22.4	23.5
CH ₃ N•CH ₂ CH ₂ N ₃ + <i>cis</i> -HONO (R4-Z)	18.1	17.8	13.9	15.1	14.2	15.7

Based on IRC walks, prereactive (PR) MMAZ-NO₂ complexes are located between the reactants and transition states. Estimates derived from G4-based results indicate these complexes are 2–4 kcal/mol lower in energy than the MMAZ+NO₂ reactant asymptote. H-bonded complexes (COMP) are located between the products and transition states. The complexes dissociate to MMAZ radicals (MMAZ-H•) and HONO or HNO₂ without a reverse barrier.

For all four reaction/MMAZ-H• types (R1–R4), the reaction channel for *cis*-HONO formation (via TS-Z) has the lowest barrier of the three paths that were characterized. Based on results obtained with the G4 model, the TS-Z transition states for R1–R4 are 14.0, 12.6, 19.8, and 9.9 kcal/mol higher in energy, respectively, than the MMAZ+NO₂ reactant asymptote. For R1–R4, the TS-E transition states (for *trans*-HONO formation) are higher in energy than the TS-Z transition states by 4.6, 4.6, 9.0, and 4.9 kcal/mol, respectively. For R1–R3, the relative energies of transition states for HNO₂ formation (TS-H) are between those of TS-E and TS-Z. For R4, results from the G4 model predict that TS-H is 1.7 kcal/mol higher in energy than TS-E. Based on results from the CBS-QB3 model, the difference is 0.3 kcal/mol.

Overall rate expressions for R1–R4 were produced by combining the results for the three paths that were characterized. Table 4 lists their rates as a function of temperature. Rate constants for expressions that fit the data in table 4 are listed in table 5, and rates computed with the expressions are compared in figure 5. The figure shows that at low temperatures the rate at which the N_{am} -bonded H-atom is abstracted (R4) will be faster than any other. However, as the temperature increases, the abstraction of H-atoms from the primary methyl group (R1) becomes the dominant path. The abstraction of H-atoms from the secondary methyl group bonded to N_α (R3) has a relatively high barrier, and proves to be of little importance. At 300 K, the overall rate for the abstraction of H-atoms from MMAZ by NO_2 is a factor of 18 slower than the overall rate for the abstraction of H-atoms from DMAZ. The possibility that this difference is responsible for the difference in the two systems' ignition delays is considered in more detail in the section presenting results for time-to-ignition values produced by homogeneous reactor simulations.

Table 4. Reaction rates (in $\text{cm}^3\text{-mol}^{-1}\text{-s}^{-1}$) for the abstraction of H-atoms from MMAZ by NO_2 .

Temperature (K)	R1: MMAZ + $\text{NO}_2 \rightarrow \text{C}\cdot\text{H}_2\text{NHCH}_2\text{CH}_2\text{N}_3 + (\text{trans-HONO}, \text{HNO}_2, \text{or cis-HONO})$		
	(<i>trans</i> -HONO via TS1-E)	(HNO_2 via TS1-H)	(<i>cis</i> -HONO via TS1-Z)
300	3.757E-03	6.065E-01	3.057E+00
400	1.240E+01	7.255E+02	1.822E+03
500	2.156E+03	6.254E+04	1.054E+05
600	8.009E+04	1.406E+06	1.850E+06
800	9.842E+06	8.953E+07	8.964E+07
1000	2.231E+08	1.349E+09	1.183E+09
1200	2.069E+09	9.500E+09	7.749E+09
1500	2.255E+10	7.909E+10	6.066E+10
2000	3.124E+11	8.480E+11	6.137E+11
	R2: MMAZ + $\text{NO}_2 \rightarrow \text{CH}_3\text{NHC}\cdot\text{HCH}_2\text{N}_3 + (\text{trans-HONO}, \text{HNO}_2, \text{or cis-HONO})$		
	(<i>trans</i> -HONO via TS2-E)	(HNO_2 via TS2-H)	(<i>cis</i> -HONO via TS2-Z)
300	2.024E-03	1.259E+00	5.121E+00
400	3.634E+00	6.342E+02	1.446E+03
500	4.472E+02	3.253E+04	5.454E+04
600	1.341E+04	5.132E+05	7.292E+05
800	1.298E+06	2.035E+07	2.562E+07
1000	2.582E+07	2.234E+08	2.815E+08
1200	2.190E+08	1.241E+09	1.634E+09
1500	2.168E+09	7.901E+09	1.135E+10
2000	2.690E+10	6.202E+10	1.022E+11
	R3: MMAZ + $\text{NO}_2 \rightarrow \text{CH}_3\text{NHCH}_2\text{C}\cdot\text{HN}_3 + (\text{trans-HONO}, \text{HNO}_2, \text{or cis-HONO})$		
	(<i>trans</i> -HONO via TS3-E)	(HNO_2 via TS3-H)	(<i>cis</i> -HONO via TS3-Z)
300	1.883E-11	7.333E-07	1.226E-04
400	2.934E-06	8.121E-03	2.773E-01
500	5.528E-03	2.926E+00	4.443E+01
600	1.024E+00	1.803E+02	1.636E+03
800	9.584E+02	4.330E+04	2.071E+05
1000	7.460E+04	1.498E+06	4.864E+06
1200	1.589E+06	1.840E+07	4.642E+07
1500	4.023E+07	2.646E+08	5.256E+08
2000	1.306E+09	4.807E+09	7.639E+09
	R4: MMAZ + $\text{NO}_2 \rightarrow \text{CH}_3\text{N}\cdot\text{CH}_2\text{CH}_2\text{N}_3 + (\text{trans-HONO}, \text{HNO}_2, \text{or cis-HONO})$		
	(<i>trans</i> -HONO via TS4-E)	(HNO_2 via TS4-H)	(<i>cis</i> -HONO via TS4-Z)
300	1.606E-01	5.493E-02	9.890E+01
400	1.938E+02	5.451E+01	1.392E+04
500	1.638E+04	4.203E+03	3.247E+05
600	3.577E+05	8.624E+04	3.054E+06
800	2.131E+07	4.678E+06	6.717E+07
1000	3.022E+08	6.170E+07	5.619E+08
1200	2.019E+09	3.888E+08	2.795E+09
1500	1.574E+10	2.833E+09	1.738E+10
2000	1.552E+11	2.585E+10	1.497E+11

Table 5. Kinetic parameters.^a

Reaction		A (s^{-1} or $cm^3 mol^{-1} s^{-1}$)	n	E_a ($kcal/mol$)	Ref.
Abstraction of H-atoms from MMAZ by NO₂					
R1	MMAZ + NO ₂ = C•H ₂ NHCH ₂ CH ₂ N ₃ + HONO	1.69 × 10 ⁻³	4.96424	12.3	b
R2	MMAZ + NO ₂ = CH ₃ NHC•HCH ₂ N ₃ + HONO	8.02 × 10 ⁻⁴	4.71530	10.7	b
R3	MMAZ + NO ₂ = CH ₃ N•CH ₂ CH ₂ N ₃ + HONO	3.24 × 10 ⁻⁷	5.71875	7.8	b
R4	MMAZ + NO ₂ = CH ₃ NHCH ₂ C•HN ₃ + HONO	1.72 × 10 ⁻⁸	5.93404	14.9	b
C•H₂NHCH₂CH₂N₃ + NO₂					
R5	C•H ₂ NHCH ₂ CH ₂ N ₃ + NO ₂ = H ₂ C(ONO)NHCH ₂ CH ₂ N ₃	3.39 × 10 ¹²	0.00000	0.0	c
R6	H ₂ C(ONO)NHCH ₂ CH ₂ N ₃ = ONNHCH ₂ CH ₂ N ₃ + CH ₂ O	2.06 × 10 ¹²	0.41566	42.3	d
R7	H ₂ C(ONO)NHCH ₂ CH ₂ N ₃ = H ₂ C(ONO)NHCH ₂ CHNH + N ₂	8.95 × 10 ¹¹	0.99420	39.3	d
R8	H ₂ C(ONO)NHCH ₂ CH ₂ N ₃ = H ₂ CNCH ₂ CH ₂ N ₃ + HNO ₂	4.26 × 10 ¹²	0.34595	31.8	d
R9	H ₂ C(ONO)NHCH ₂ CH ₂ N ₃ = H ₂ C(O•)NHCH ₂ CH ₂ N ₃ + NO	2.68 × 10 ¹⁶	0.00000	38.4	e
R10	C•H ₂ NHCH ₂ CH ₂ N ₃ + NO ₂ = H ₂ C(NO ₂)NHCH ₂ CH ₂ N ₃	1.13 × 10 ¹²	0.00000	0.0	c
R11	H ₂ C(NO ₂)NHCH ₂ CH ₂ N ₃ = H ₂ C(NO ₂)NHCH ₂ CHNH + N ₂	1.06 × 10 ¹²	1.00973	39.1	d
R12	H ₂ C(NO ₂)NHCH ₂ CH ₂ N ₃ = H ₂ CNCH ₂ CH ₂ N ₃ + <i>trans</i> -HONO	4.92 × 10 ¹¹	0.70316	27.9	d
CH₃NHC•HCH₂N₃ + NO₂					
R13	CH ₃ NHC•HCH ₂ N ₃ + NO ₂ = CH ₃ NHC(ONO)HCH ₂ N ₃	3.39 × 10 ¹²	0.00000	0.0	c
R14	CH ₃ NHC(ONO)HCH ₂ N ₃ = OCHCH ₂ N ₃ + CH ₃ NHNO	6.46 × 10 ¹¹	0.40639	30.9	d
R15	CH ₃ NHC(ONO)HCH ₂ N ₃ = CH ₃ NHC(ONO)HCHNH + N ₂	9.05 × 10 ¹¹	0.97907	38.5	d
R16	CH ₃ NHC(ONO)HCH ₂ N ₃ = CH ₃ NHCHCHN ₃ + HNO ₂	3.53 × 10 ¹¹	0.66938	37.0	d
R17	CH ₃ NHC(ONO)HCH ₂ N ₃ = CH ₃ NCHCH ₂ N ₃ + HNO ₂	8.95 × 10 ¹¹	0.99420	39.3	d
R18	CH ₃ NHC(ONO)HCH ₂ N ₃ = CH ₃ NHC(O•)HCH ₂ N ₃ + NO	2.68 × 10 ¹⁶	0.00000	40.0	e
R19	CH ₃ NHC•HCH ₂ N ₃ + NO ₂ = CH ₃ NHC(NO ₂)HCH ₂ N ₃	1.13 × 10 ¹²	0.00000	0.0	c
R20	CH ₃ NHC(NO ₂)HCH ₂ N ₃ = CH ₃ NHC(NO ₂)HCHNH + N ₂	6.51 × 10 ¹¹	0.99235	37.7	d
R21	CH ₃ NHC(NO ₂)HCH ₂ N ₃ = CH ₃ NHCHCHN ₃ + <i>trans</i> -HONO	1.44 × 10 ¹¹	0.99093	34.5	d
R22	CH ₃ NHC(NO ₂)HCH ₂ N ₃ = CH ₃ NCHCH ₂ N ₃ + <i>trans</i> -HONO	3.65 × 10 ¹²	0.58104	26.5	d
CH₃N•CH₂CH₂N₃ + NO₂					
R23	CH ₃ N•CH ₂ CH ₂ N ₃ + NO ₂ = CH ₃ N(ONO)CH ₂ CH ₂ N ₃	3.83 × 10 ¹¹	0.00000	0.0	f
R24	CH ₃ N(ONO)CH ₂ CH ₂ N ₃ = CH ₃ N(ONO)CH ₂ CHNH + N ₂	5.78 × 10 ¹¹	0.96337	38.5	d
R25	CH ₃ N(ONO)CH ₂ CH ₂ N ₃ = CH ₂ NCH ₂ CH ₂ N ₃ + HNO ₂	2.11 × 10 ¹²	0.28120	35.2	d
R26	CH ₃ N(ONO)CH ₂ CH ₂ N ₃ = CH ₃ NCHCH ₂ N ₃ + HNO ₂	8.64 × 10 ¹¹	0.33682	33.4	d
R27	CH ₃ N(ONO)CH ₂ CH ₂ N ₃ = CH ₃ N(O•)CH ₂ CH ₂ N ₃ + NO	1.40 × 10 ¹⁷	0.00000	8.6	e
R28	CH ₃ N•CH ₂ CH ₂ N ₃ + NO ₂ = CH ₃ N(NO ₂)CH ₂ CH ₂ N ₃	1.91 × 10 ¹¹	0.00000	0.0	f
R29	CH ₃ N(NO ₂)CH ₂ CH ₂ N ₃ = CH ₃ N(NO ₂)CH ₂ CHNH + N ₂	2.94 × 10 ¹¹	0.96958	38.6	d
R30	CH ₃ N(NO ₂)CH ₂ CH ₂ N ₃ = CH ₂ NCH ₂ CH ₂ N ₃ + <i>trans</i> -HONO	1.36 × 10 ¹⁰	0.97416	47.1	d
R31	CH ₃ N(NO ₂)CH ₂ CH ₂ N ₃ = CH ₃ NCHCH ₂ N ₃ + <i>trans</i> -HONO	7.16 × 10 ⁰⁹	1.01858	46.3	d

^a High-pressure-limit rate parameters for $k = A''T^{\frac{1}{2}}\exp(-E_a/RT)$. Calculated for $T = 300$ to 2000 K; ^b <TST>; fit with three parameter modified Arrhenius equation. H tunneling effect has been included; ^c (Park and Gutman, 1998); ^d <TST>; fit with three parameter modified Arrhenius equation; ^e (Caralp et al., 1998); ^f (Lazarou et al., 1994).

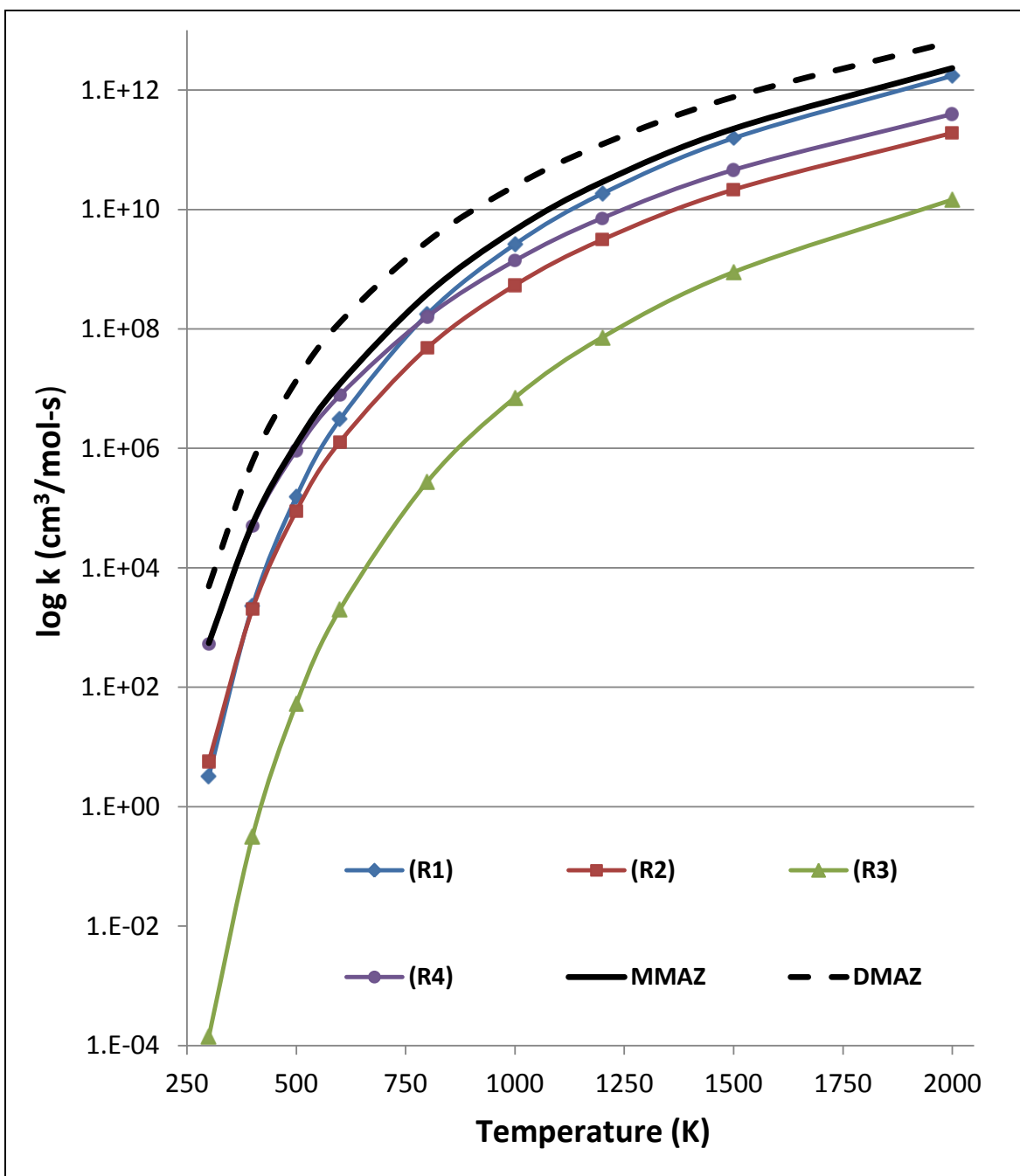


Figure 5. Comparison of the overall rates for R1–R4 as a function of temperature. Overall rates for H-atom abstraction from MMAZ and DMAZ by NO₂ are also shown.

3.4 Radical + NO₂ Reactions

Based on the studies performed to develop the DMAZ-RFNA mechanism, reactions between NO₂ and the first products of H-atom abstraction from the parent, i.e., C•H₂NHCH₂CH₂N₃, CH₃NHC•HCH₂N₃, CH₃NHCH₂C•HN₃, and CH₃N•CH₂CH₂N₃, comprise another class of reactions that was expected to be important for MMAZ-RFNA systems. Potential energy

diagrams for the $\text{C}\cdot\text{H}_2\text{NHCH}_2\text{CH}_2\text{N}_3 + \text{NO}_2$, $\text{CH}_3\text{NHC}\cdot\text{HCH}_2\text{N}_3 + \text{NO}_2$, and $\text{CH}_3\text{N}\cdot\text{CH}_2\text{CH}_2\text{N}_3 + \text{NO}_2$ systems are shown in figures 6–8, respectively. The reaction of $\text{CH}_3\text{NHCH}_2\text{C}\cdot\text{HN}_3$ with NO_2 will not be discussed because, as shown in figure 5, the rate of formation of $\text{CH}_3\text{NHCH}_2\text{C}\cdot\text{HN}_3$ is negligible compared with the rate of formation of the other three radicals. G4-based calculations of total energies at 298 K and B3LYP/6-31+G(d,p)-based geometries, normal mode frequencies, and moments of inertia for all species involved in the $\text{C}\cdot\text{H}_2\text{NHCH}_2\text{CH}_2\text{N}_3 + \text{NO}_2$, $\text{CH}_3\text{NHC}\cdot\text{HCH}_2\text{N}_3 + \text{NO}_2$, and $\text{CH}_3\text{N}\cdot\text{CH}_2\text{CH}_2\text{N}_3 + \text{NO}_2$ systems are provided in appendix C.

In the three cases considered, the first step involves NO_2 addition to the radical site and the formation of a radical-ONO or radical- NO_2 adduct. As shown in figure 6, the formation of $\text{CH}_2(\text{ONO})\text{NHCH}_2\text{CH}_2\text{N}_3$ (R5) is 54.9 kcal/mol exothermic while the formation of $\text{CH}_2(\text{NO}_2)\text{NHCH}_2\text{CH}_2\text{N}_3$ (R10) is 55.2 kcal/mol exothermic. Similarly, figure 7 shows that the formation of $\text{CH}_3\text{NHCH}(\text{ONO})\text{CH}_2\text{N}_3$ (R13) is 55.8 kcal/mol exothermic while the formation of $\text{CH}_3\text{NHC}(\text{NO}_2)\text{CH}_2\text{N}_3$ (R19) is 55.9 kcal/mol exothermic. As shown in figure 8, NO_2 addition to the nitrogen radical site is less exothermic than NO_2 addition to carbon radical sites. The exothermicities for $\text{CH}_3\text{N}(\text{ONO})\text{CH}_2\text{CH}_2\text{N}_3$ and $\text{CH}_3\text{N}(\text{NO}_2)\text{CH}_2\text{CH}_2\text{N}_3$ formation (R23 and R28) are 26.8 and 44.7 kcal/mol, respectively.

As shown in figure 6, the $\text{H}_2\text{C}(\text{ONO})\text{NHCH}_2\text{CH}_2\text{N}_3$ adduct can (1) dissociate back to reactants (R5), (2) proceed via a four-member ring transition state (TS6) to $\text{ONNHCH}_2\text{CH}_2\text{N}_3 + \text{CH}_2\text{O}$,



(3) undergo a concerted 1,2-H shift concomitant with N_2 extrusion and form $\text{H}_2\text{CONONHCH}_2\text{CHNH}$ (via TS7),



(4) eliminate HNO_2 via a five-member ring transition state (via TS8),



or (5) dissociate to the radicals $\text{H}_2\text{C}(\text{O}\cdot)\text{NHCH}_2\text{CH}_2\text{N}_3 + \text{NO}$,

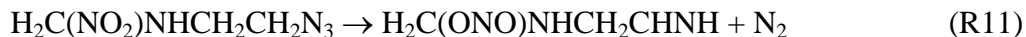


(Reactions that produce closed-shell products, such as R6–R8, are referred to in the discussion that follows as “molecular elimination” paths.)

R6 is 10.5-kcal/mol endothermic and has a transition state that is 42.5 kcal/mol above the ground state of $\text{H}_2\text{C}(\text{ONO})\text{NHCH}_2\text{CH}_2\text{N}_3$. The reaction involves the cleavage of N-O and C-N bonds and the formation of carbonyl ($\text{C}=\text{O}$) and N-N bonds. R7 is 52.7 kcal/mol exothermic and has a transition state that is 39.7 kcal/mol higher in energy than the adduct. This value is slightly higher than that for the transition state for N_2 elimination from the parent (38.1 kcal/mol). R8 is

22.3 kcal/mol endothermic and has a transition state that is 32.0 kcal/mol higher in energy than the adduct. R9 is 39.7-kcal/mol endothermic and does not have a reverse barrier.

$\text{H}_2\text{C}(\text{NO}_2)\text{NHCH}_2\text{CH}_2\text{N}_3$ can (1) dissociate back to reactants (R10), (2) eliminate N_2 and produce $\text{H}_2\text{C}(\text{NO}_2)\text{NHCH}_2\text{CHNH}$ (via TS11),



or (3) eliminate *trans*-HONO via a five-member ring transition state (via TS12),

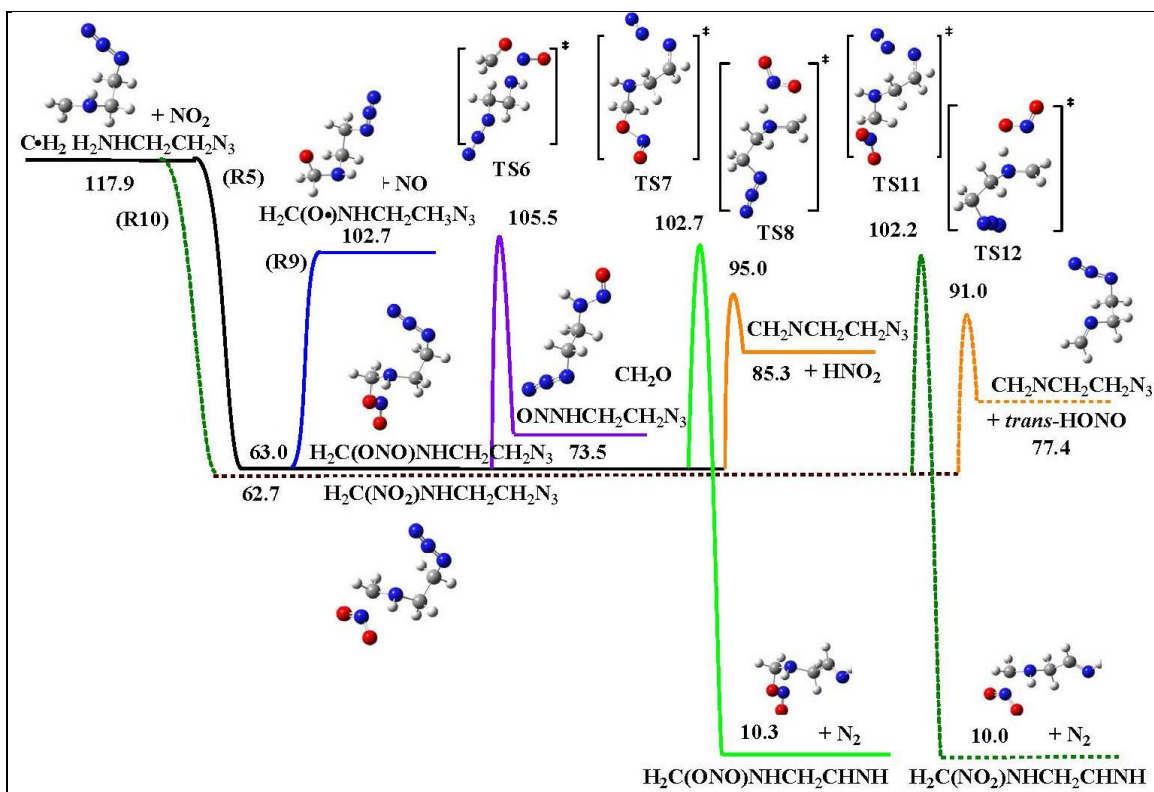


Figure 6. Potential energy diagram for the $\text{C}\cdot\text{H}_2\text{NHCH}_2\text{CH}_2\text{N}_3 + \text{NO}_2$ system: G4-based results.

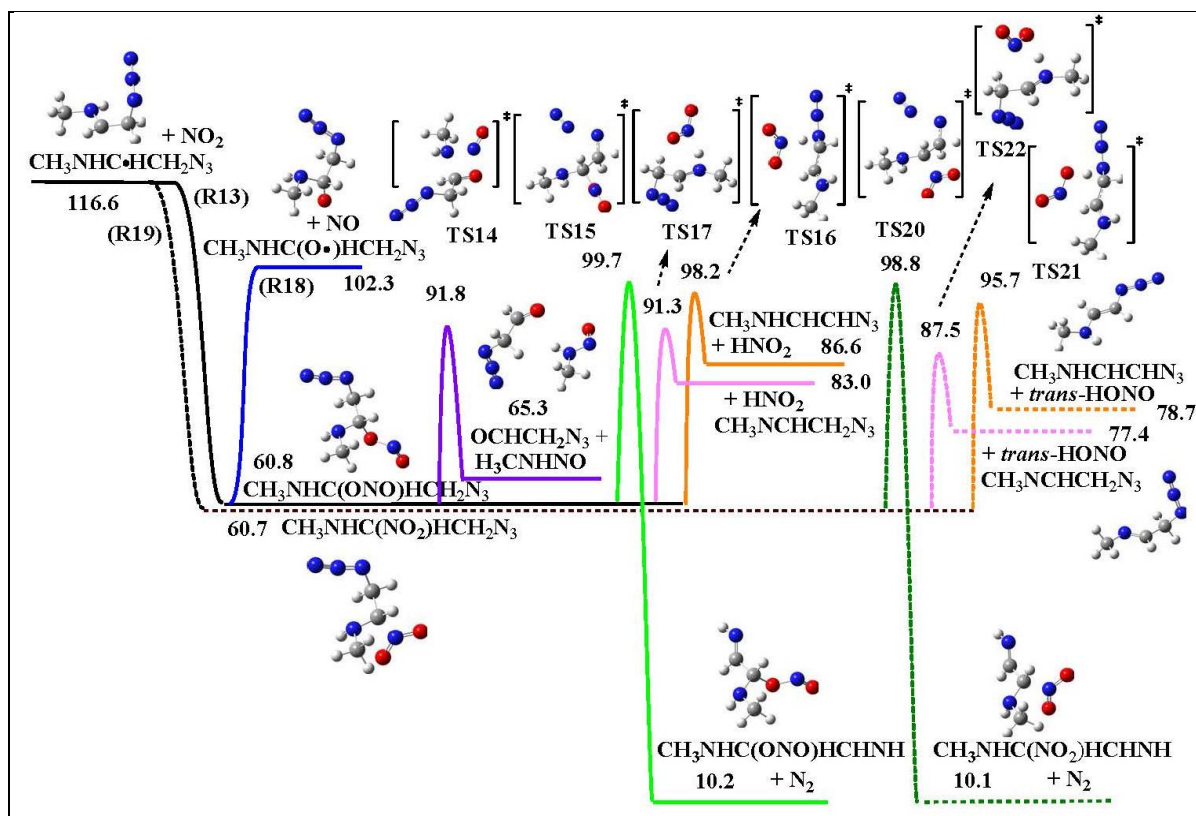


Figure 7. Potential energy diagram for the $\text{CH}_3\text{NHC}\cdot\text{HCH}_2\text{N}_3 + \text{NO}_2$ system: G4-based results.

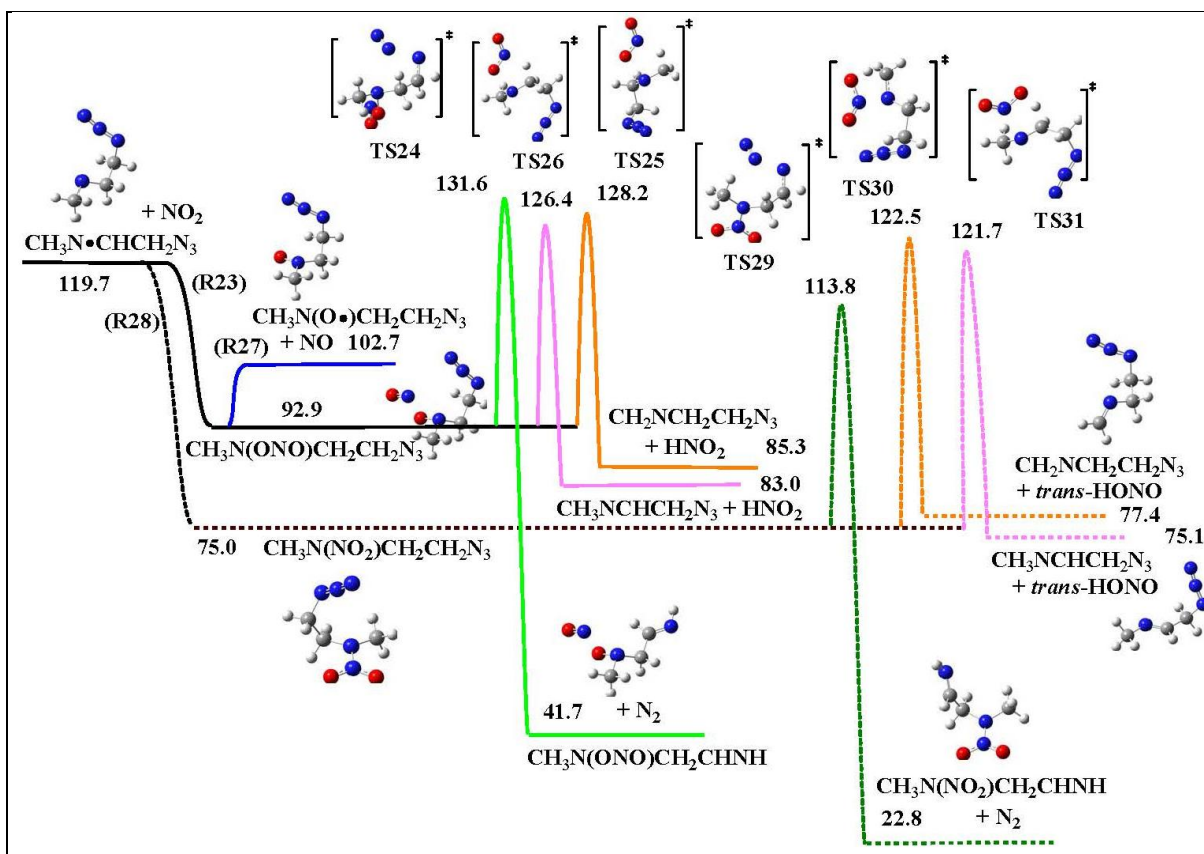


Figure 8. Potential energy diagram for the $\text{CH}_3\text{N}\cdot\text{CH}_2\text{CH}_2\text{N}_3 + \text{NO}_2$ system: G4-based results.

On the basis of results produced by the G4 model, the barrier to N_2 elimination (R11) is 39.5 kcal/mol, and the reaction is 52.7 kcal/mol exothermic. As with N_2 elimination from $\text{H}_2\text{C}(\text{ONO})\text{NHCH}_2\text{CH}_2\text{N}_3$ (R7), the transition state for R11 is slightly higher than that for N_2 elimination from MMAZ. The elimination of *trans*-HONO (R12) is 14.7 kcal/mol endothermic and has a transition state that is 28.3 kcal/mol higher in energy than the adduct.

Figure 7 shows potential energy diagrams for the decompositions of $\text{CH}_3\text{NCH}(\text{ONO})\text{CH}_2\text{N}_3$ and $\text{CH}_3\text{NCH}(\text{NO}_2)\text{CH}_2\text{N}_3$. The N_2 elimination channels for $\text{CH}_3\text{NCH}(\text{ONO})\text{CH}_2\text{N}_3$ (via TS15) and $\text{CH}_3\text{NCH}(\text{NO}_2)\text{CH}_2\text{N}_3$ (via TS20) have 38.9- and 38.1-kcal/mol barriers, respectively. These paths are approximately 50.6 kcal/mol exothermic. R14, which involves a four-member ring transition state (TS14), has a relatively low barrier (31.0 kcal/mol) and is 4.5 kcal/mol endothermic. The HNO_2 elimination channels via five-member ring transition states (TS16 and TS17) have 37.4- and 30.5-kcal/mol barriers, respectively. The barriers to *trans*-HONO elimination via TS21 and TS22 are lower by 2.5 and 3.8 kcal/mol, respectively.

Figure 8 shows paths for the decompositions of $\text{CH}_3\text{N}(\text{ONO})\text{CH}_2\text{CH}_2\text{N}_3$ and $\text{CH}_3\text{N}(\text{NO}_2)\text{CH}_2\text{CH}_2\text{N}_3$. Transition states for R24–R26 are higher in energy than the $\text{CH}_3\text{N}\cdot\text{CH}_2\text{CH}_2\text{N}_3 + \text{NO}_2$ reactant asymptote. The dissociation of $\text{CH}_3\text{N}(\text{ONO})\text{CH}_2\text{CH}_2\text{N}_3$ into $\text{CH}_3\text{N}(\text{O}\cdot)\text{CH}_2\text{CH}_2\text{N}_3$ and NO is 9.8 kcal/mol endothermic. It does not have a reverse barrier.

Figures 9 and 10 compare, respectively, the temperature and pressure dependences of rates for reactions in the $\text{C}\cdot\text{H}_2\text{NHCH}_2\text{CH}_2\text{N}_3 + \text{NO}_2$, $\text{CH}_3\text{NHC}\cdot\text{HCH}_2\text{N}_3 + \text{NO}_2$, and $\text{CH}_3\text{N}\cdot\text{CH}_2\text{CH}_2\text{N}_3 + \text{NO}_2$ systems. In the $\text{C}\cdot\text{H}_2\text{NHCH}_2\text{CH}_2\text{N}_3 + \text{NO}_2$ and $\text{CH}_3\text{NHC}\cdot\text{HCH}_2\text{N}_3 + \text{NO}_2$ systems, although all the transition states for the molecular-elimination channels are comparable to, or lower in energy than, the product asymptotes associated with alkoxy radical formation (R9 and R18), R9 and R18 are dominant at high temperature and low pressure due to their high A factors [$\sim 1 \times 10^{16} \text{ s}^{-1}$]. The elimination of *trans*-HONO (via R12 and R22) is competitive at moderate to high temperatures. Adduct stabilization reactions (R5, R10, R13, and R19) are important at low temperatures and high pressures, with the rates of radical-ONO stabilization (R5 and R13) being faster than those of radical- NO_2 stabilization (R10 and R19). In the $\text{CH}_3\text{N}\cdot\text{CH}_2\text{CH}_2\text{N}_3 + \text{NO}_2$ system, the dissociation of $\text{CH}_3\text{N}(\text{ONO})\text{CH}_2\text{CH}_2\text{N}_3$ into $\text{CH}_3\text{N}(\text{O}\cdot)\text{CH}_2\text{CH}_2\text{N}_3$ and NO (R27) is dominant at all temperatures and pressures. The stabilization of $\text{CH}_3\text{N}(\text{NO}_2)\text{CH}_2\text{CH}_2\text{N}_3$ (R28) is competitive with R29 ($\text{CH}_3\text{NNO}_2\text{CH}_2\text{CHNH} + \text{N}_2$ formation), with the rate of R28 being faster than the rate of R29 at low temperatures and high pressures.

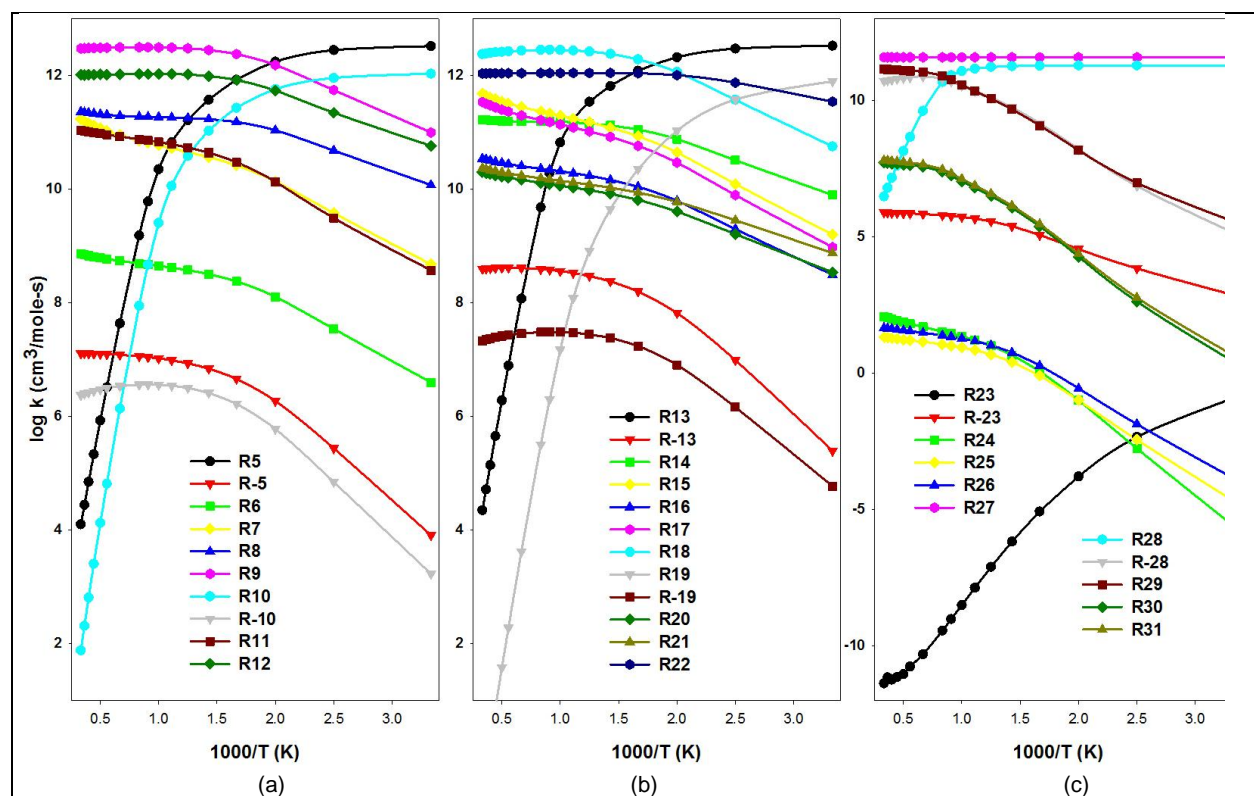


Figure 9. QRRK-derived reaction rates (at 1 atm) as a function of temperature: (a) $\text{C}\cdot\text{H}_2\text{NHCH}_2\text{CH}_2\text{N}_3 + \text{NO}_2$, (b) $\text{CH}_3\text{NHC}\cdot\text{HCH}_2\text{N}_3 + \text{NO}_2$, and (c) $\text{CH}_3\text{N}\cdot\text{CH}_2\text{CH}_2\text{N}_3 + \text{NO}_2$. Note that the scale of the y-axis of (c) differs from that of (a) and (b).

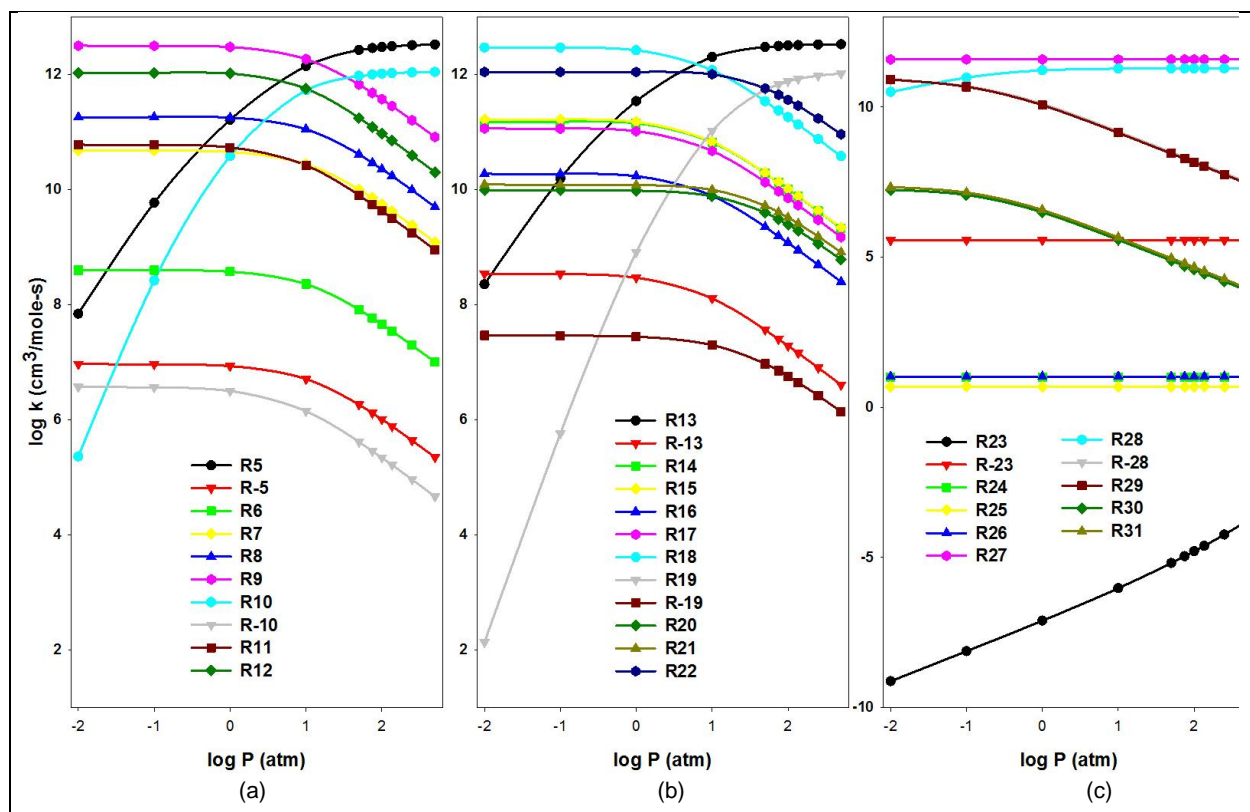


Figure 10. QRRK rate constants at 800 K as a function of pressure: (a) $\text{C}\cdot\text{H}_2\text{NHCH}_2\text{CH}_2\text{N}_3 + \text{NO}_2$, (b) $\text{CH}_3\text{NHC}\cdot\text{HCH}_2\text{N}_3 + \text{NO}_2$, and (c) $\text{CH}_3\text{N}\cdot\text{CH}_2\text{CH}_2\text{N}_3 + \text{NO}_2$. Note that the scale of the y-axis of (c) differs from that of (a) and (b).

3.5 Comparison of Time-to-Ignition Values

Based on results such as those presented in the previous sections, rate expressions for 208 reactions and thermochemical descriptions for 54 species were developed and added to the previously developed TMEDA-DMAZ-RFNA mechanism. Homogeneous reactor simulations were run to estimate time-to-ignition values for DMAZ-RFNA and MMAZ-RFNA systems. Figure 11 shows results obtained for mixtures with oxidizer-to-fuel ratios ranging from 0.25 to 4.0. (This range corresponds to fuel-oxidizer equivalence ratio (ϕ) ranges of 8.89–0.56 for DMAZ and 10.14–0.63 for MMAZ.) All systems were initially at either 75 or 136 atm. The initial temperature in all cases was 300 K. For corresponding initial conditions, the shortest ignition delays observed for the MMAZ-RFNA systems are considerably longer than those for the DMAZ-RFNA systems. These differences are consistent with the differences in the ignition delays observed for the two systems. Moreover, based on sensitivity analyses of the simulations' results, the differences in time-to-ignition are clearly attributable to the difference in the rates at which H-atoms are abstracted from the parent fuel by NO_2 .

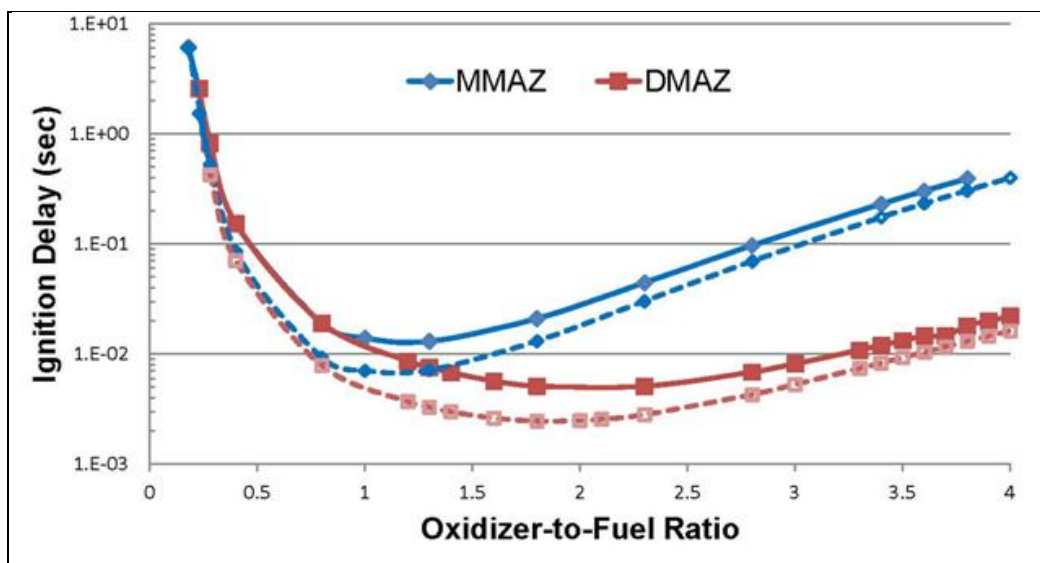


Figure 11. Time-to-ignition values determined in homogenous reactor simulation: MMAZ-RFNA vs. DMAZ-RFNA. Solid line: 75 atm. Dotted line: 136 atm.

Having developed a mechanism that was applicable to any TMEDA-DMAZ-MMAZ-RFNA system, we decided to calculate time-to-ignition values for MMAZ-DMAZ and MMAZ-TMEDA blends. Our interest in the values was motivated by the ignition delays observed for blends of TMEDA and DMAZ (called TEDMAZ). Blends with a DMAZ fraction near 33 wt % have been observed to have shorter ignition delays than either TMEDA-RFNA or DMAZ-RFNA (Stevenson et al., 2008), and the same synergism was observed in time-to-ignition values produced with the TMEDA-DMAZ-RFNA mechanism (Chen, 2013). Because MMAZ is denser than DMAZ and has a lower C-atom/N-atom ratio, a fuel produced by adding MMAZ to DMAZ (or TMEDA) would have a higher $\rho \cdot I_{sp}$ than neat DMAZ (or neat TMEDA), and it might burn more cleanly as well. With respect to producing shorter ignition delays, the possibility envisioned was that the faster H-atom abstraction paths in DMAZ or TMEDA might couple with a relatively fast secondary process in MMAZ to produce an overall ignition process that was faster than achievable by either DMAZ or TMEDA in neat form. But that did not prove to be the case (see figure 12). Time-to-ignition values simply increased with increase in the blend's weight-percent MMAZ. However, in the case of MMAZ-DMAZ blends, MMAZ's negative impact on time-to-ignition values is predicted to be less pronounced than would be expected on the basis of a simple linear interpolation of the separate systems' ignition delays.

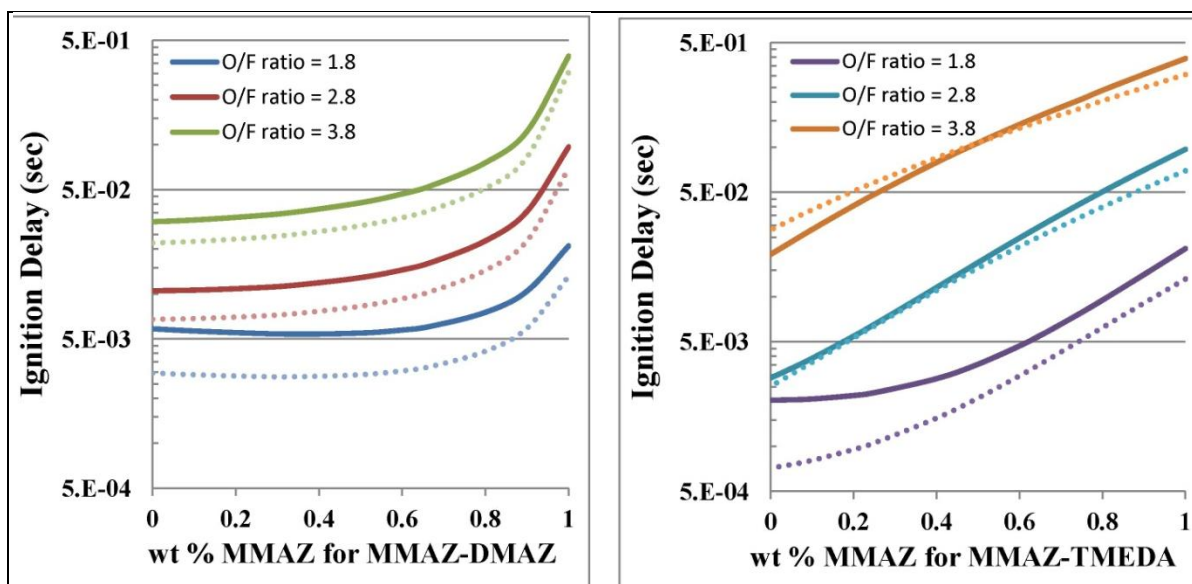


Figure 12. Time-to-ignition values for MMAZ-DMAZ and MMAZ-TMEDA blends. Solid line: 75 atm. Dotted line: 136 atm.

4. Summary

Reaction rate expressions for paths with the potential to be rate-determining steps in the ignition of MMAZ-RFNA systems were estimated on the basis of results obtained from quantum chemistry models and transition state theory. Expressions were obtained for paths involving (1) MMAZ's unimolecular decomposition, (2) MMAZ's complexation with HNO_3 , (3) the abstraction of H-atoms from MMAZ by NO_2 , (4) bimolecular reactions between (radical) intermediates and NO_2 , and (5) the unimolecular dissociation of MMAZ- NO_2 adducts. Together with rate expressions for other potentially important reactions involving products of the parent molecule's decomposition, they were added to an existing finite-rate chemical kinetics mechanism for TMEDA-DMAZ-RFNA systems to produce a mechanism applicable to TMEDA-DMAZ-MMAZ-RFNA systems. Homogeneous reactor simulations produced with the new mechanism predict time-to-ignition values for MMAZ-RFNA systems that are significantly longer than those for comparable DMAZ-RFNA systems. This result is consistent with experimentally measured ignition delays that have been reported for the two systems.

On the basis of an analysis of the computationally obtained results, the difference in the ignition delays is attributable to differences in the rates of NO_2 -mediated abstraction of H-atoms from the parent. As such, the study answered a long-standing question concerning the relative importance of various reactions involved in the ignition of 2-azidoethanamine-RFNA systems. The answer undoubtedly applies to other alkyl amine-based hypergols as well. Given the complexity and rapidity of the reaction chemistry involved in hypergolic ignition, it is doubtful the answer

could have been obtained via experimental means alone. Firmly establishing the correspondence between the rate of this reaction type and ignition delay, the results of this study provide guidance for developing more effective and efficient computationally based means for designing and screening hydrazine alternative hypergols.

5. References

- Anderson W. R. Heats of Formation of HNO and Some Related Species. *Combustion and Flame* **1999**, *117*, 394–403.
- Baboul, A. G.; Curtiss, L. A.; Redfern, P. C.; Raghavachari, K. Gaussian-3 Theory Using Density Functional Geometries and Zero-Point Energies. *Journal of Chemical Physics* **1999**, *110*, 7650–7657.
- Becke, A. D. Density-Functional Thermochemistry III. The Role of Exact Exchange. *Journal of Chemical Physics* **1993**, *98*, 5648–5652.
- Buckley, E.; Herington, E. F. G. Equilibria in Some Secondary Alcohol + Hydrogen + Ketone Systems. *Trans. Faraday Soc.* **1965**, *61*, 1618–1625.
- Caralp, F.; Rayez, M.; Forst, W.; Gomez, N.; Delcroix, B.; Fittschen, C.; Devolder, P. Kinetic and Mechanistic Study of the Pressure and Temperature Dependence of the Reaction $\text{CH}_3\text{O} + \text{NO}$. *Journal of the Chemical Society, Faraday Transactions* **1998**, *94*, 3321–3330.
- Chang, A. Y.; Bozzelli, J. W.; Dean, A. M. Kinetic Analysis of Complex Chemical Activation and Unimolecular Dissociation Reactions Using qRRK Theory and the Modified Strong Collision Approximation. *Zeitschrift fur Physikalische Chemie* **2000**, *214*, 1533–1568.
- Chao, J.; Rossini, F. D., Heats of Combustion, Formation, and Isomerization of Nineteen Alkanols. *J. Chem. Eng. Data* **1965**, *10*, 374–379.
- Chase, M. W., Jr. NIST-JANAF Thermochemical Tables, 4th ed. *Journal of Physical and Chemical Reference Data* **1998**, Monograph 9, 1–951.
- Chen, C.-C.; McQuaid, M. J. Tetramethylethylenediamine/Red Fuming Nitric Acid (TMEDA/RFNA) Reaction Kinetics. Presented at the 34th JANNAF Propellant and Explosives Development and Characterization Subcommittee Meeting, Reno, NV, 13–17 August 2007.
- Chen, C.-C.; McQuaid, M. J. Mechanisms and Kinetics for the Thermal Decomposition of 2-Azido-N,N-Dimethylethanamine (DMAZ). *Journal of Physical Chemistry A* **2011**, *116*, 3561–3576.
- Chen, C.-C. An Updated Finite-Rate, Chemical Kinetics Mechanism for the Gas-Phase Ignition and Combustion of TMEDA-DMAZ and RFNA (TEDMAZ-RFNA). Presented at the 7th Joint Army Navy NASA Air Force (JANNAF) Liquid Propulsion Subcommittee Meeting, Colorado Springs, CO, 29 April–3 May 2013.

- Chen, C.-C.; McQuaid, M. J. A Detail, Gas-Phase, Finite-Rate Chemical Kinetics Mechanism for Modeling the Ignition and Combustion of Methyl and Ethyl Nitrate. Presented at the 7th JANNAF Liquid Propulsion Subcommittee Meeting, Colorado Springs, CO, 29 April–3 May 2013.
- Curtiss, L. A.; Redfern, P. C.; Raghavachari, K. Gaussian-4 Theory. *Journal of Chemical Physics* **2007**, *126*, 84108–84119.
- Curtiss, L. A.; Raghavachari, K.; Redfern, P. C.; Rassolov, V.; Pople, J. A. Gaussian-3 (G3) Theory for Molecules Containing First and Second-Row Atoms. *Journal of Chemical Physics* **1998**, *109*, 7764–7776.
- Cox, J. D.; Wagman, D. D.; Medvedev, V.A. *CODATA Key Values for Thermodynamics*; Hemisphere Publishing Corporation: New York, 1984; p 1.
- DaSilva, G.; Bozzelli, J. W. Variational Analysis of the Phenyl + O₂ and Phenoxy + O Reactions. *Journal of Physical Chemistry A* **2008**, *112*, 3566–3575.
- Dean, A. M. Predictions of Pressure and Temperature Effects Upon Radical Addition and Recombination Reactions. *Journal of Physical Chemistry A* **1985**, *89*, 4600–4608.
- Dean, A. M.; Bozzelli, J. W.; Ritter, E. R. CHEMACT: A Computer Code to Estimate Rate Constants for Chemically-Activated Reactions. *Combustion Science and Technology* **1991**, *80*, 63–85.
- Frisch, M. J.; Trucks, G. W.; Schlegel, H. B.; Scuseria, G. E.; Robb, M. A.; Cheeseman, J. R.; Scalmani, G.; Barone, V.; Mennucci, B.; Petersson, G. A.; Nakatsuji, H.; Caricato, M.; Li, X.; Hratchian, H. P.; Izmaylov, A. F.; Bloino, J.; Zheng, G.; Sonnenberg, J. L.; Hada, M.; Ehara, M.; Toyota, K.; Fukuda, R.; Hasegawa, J.; Ishida, M.; Nakajima, T.; Honda, Y.; Kitao, O.; Nakai, H.; Vreven, T.; Montgomery, J. A.; Peralta, J. E.; Ogliaro, F.; Bearpark, M.; Heyd, J. J.; Brothers, E.; Kudin, K. N.; Staroverov, V. N.; Keith, T.; Kobayashi, R.; Normand, J.; Raghavachari, K.; Rendell, A.; Burant, J. C.; Iyengar, S. S.; Tomasi, J.; Cossi, M.; Rega, N.; Millam, J. M.; Klene, M.; Knox, J. E.; Cross, J. B.; Bakken, V.; Adamo, C.; Jaramillo, J.; Gomperts, R.; Stratmann, R. E.; Yazyev, O.; Austin, A. J.; Cammi, R.; Pomelli, C.; Ochterski, J. W.; Martin, R. L.; Morokuma, K.; Zakrzewski, V. G.; Voth, G. A.; Salvador, P.; Dannenberg, J. J.; Dapprich, S.; Daniels, A. D.; Farkas, O.; Foresman, J. B.; Ortiz, J. V.; Cioslowski, J.; Fox, D. J. Gaussian 09, Revision C.01; Gaussian, Inc., Wallingford, CT, 2013.
- Kee, R. J.; Rupley, F. M.; Miller, J. A. *Chemkin-II: A Fortran Chemical Kinetics Package for the Analysis of Gas-Phase Chemical Kinetics*; SAND 89-8009; Sandia National Laboratories: Albuquerque, NM, September 1989.

- Knyazev, V. D.; Bencsura, A.; Stoliarov, S. I.; Slagle, I. R. Kinetics of the $\text{C}_2\text{H}_3 + \text{H}_2 \rightleftharpoons \text{H} + \text{C}_2\text{H}_4$ and $\text{CH}_3 + \text{H}_2 \rightleftharpoons \text{H} + \text{CH}_4$ Reactions. *Journal of Physical Chemistry* **1996**, *100*, 11346–11354.
- Lay, T. H.; Krasnoperov, L. N.; Venanzi, C. A.; Bozzelli, J. W. Ab Initio Study of α -Chlorinated Ethyl Hydroperoxides $\text{CH}_3\text{CH}_2\text{OOH}$, $\text{CH}_3\text{CHClOOH}$, and $\text{CH}_3\text{CCl}_2\text{OOH}$: Conformational Analysis, Internal Rotation Barriers, Vibrational Frequencies, and Thermodynamic Properties. *Journal of Physical Chemistry* **1996**, *100*, 8240–8249.
- Lazarou, Y. G.; Kambanis, K. G.; Pagagiannakopoulos, P. Gas-Phase Reactions of $(\text{CH}_3)_3\text{N}$ Radicals with NO and NO_2 . *Journal of Physical Chemistry* **1994**, *98*, 2110–2115.
- Lee, C.; Yang, W.; Parr, R. G. Development of the Colle-Salvetti Correlation-Energy Formula Into a Functional of the Electron-Density. *Physical Review B* **1988**, *37*, 785–789.
- Liu, W.-G.; Dasgupta, S.; Zybin, S. V.; Goddard, W. A. First Principles Study of the Ignition Mechanism for Hypergolic Bipropellants: N,N,N',N'-Tetramethylethylenediamine (TMEDA) and N,N,N',N'-Tetramethylnethylenediamine (TMMDA) with Nitric Acid. *Journal of Physical Chemistry A*, **2011**, *115*, 5221–5229.
- Louis, F.; Gonzalez, C. A.; Huie, R. E.; Kurylo, M. J. An Ab Initio Study of the Kinetics of the Reactions of Halomethanes with the Hydroxyl Radical. 1. CH_2Br_2 . *Journal of Physical Chemistry A* **2000**, *104*, 2931–2938.
- Lutz, A.E.; Kee, R. J.; Miller, J. A. *SENKIN: A Fortran Program for Predicting Homogeneous Gas Phase Chemical Kinetics With Sensitivity Analysis*; SAND87-8248; Sandia National Laboratories, Albuquerque, NM, October 1988.
- McQuaid, M. J. *Computational Characterization of 2-Azidocycloalkanamines: Notional Variations on the Hypergol 2-Azido-N,N-Dimethylethanamine*; ARL-TR-2806; U.S. Army Research Laboratory: Aberdeen Proving Ground, MD, 2002.
- McQuaid, M. J. *Computationally Based Measures of Amine Azide Basicity and Their Correlation With Hypergolic Ignition Delays*; ARL-TR-3122; U.S. Army Research Laboratory: Aberdeen Proving Ground, MD, 2003.
- McQuaid, M. J. *The Structure of Secondary 2-Azidoethanamines: A Hypergolic Fuel vs. a Nonhypergolic Fuel*; ARL-TR-3176; U.S. Army Research Laboratory: Aberdeen Proving Ground, MD, 2004.
- McQuaid, M. J.; Ishikawa, Y. H-Atom Abstraction From CH_3NHNH_2 by NO_2 : CCSD(T)/6-311++G(3df,2p)//MPWB1K/6-31+G(d,p) and CCSD(T)/6-311+G(2df,p)//CCSD/6-31+G(d,p) Calculations. *Journal of Physical Chemistry A* **2006**, *110*, 6129–6138.

- McQuaid, M. J.; McNesby, K. L.; Rice, B. M.; Chabalowski, C. F. Density Functional Theory Characterization of the Structure and Gas-Phase, Mid-Infrared Absorption Spectrum of 2-Azido-N,N-dimethylethanamine. *Journal of Molecular Structure (THEOCHEM)* **2002**, 587, 199–218.
- McQuarrie, D.A. *Statistical Mechanics*; Harper & Row: New York, 1976.
- Montgomery, J. A., Jr.; Frisch, M. J.; Ochterski, J. W.; Petersson, G. A. A Complete Basis Set Model Chemistry, VI: Use of Density Functional Geometries and Frequencies. *Journal of Chemical Physics* **1999**, 110, 2822–2827.
- Montgomery, J. A., Jr.; Frisch, M. J.; Ochterski, J. W.; Petersson, G. A. A Complete Basis Set Model Chemistry, VII: Use of the Minimum Population Localization Method. *Journal of Chemical Physics* **2000**, 112, 6532–6542.
- Ochterski, J. W.; Petersson, G. A.; Montgomery, J. A., Jr. A Complete Basis Set Model Chemistry, V: Extensions to Six or More Heavy Atoms. *Journal of Chemical Physics* **1996**, 104, 2598–2619.
- Park, J. Y.; Gutman, D. Reactions of Ethyl, Cyclopentyl, and Cyanomethyl Radicals With Nitrogen Dioxide. *Journal of Physical Chemistry* **1998**, 87, 1844–1848.
- Pittam, D. A.; Pilcher, G. Measurements of Heats of Combustion by Flame Calorimetry, Part 8: Methane, Ethane, Propane, N-Butane and 2-Methylpropane. *J. Chem. Soc. Faraday Trans 1* **1972**, 68, 2224–2229.
- Schwartz, M.; Marshall, P.; Berry, R. J.; Ehlers, C. J.; Petersson, G. A. Computational Study of the Kinetics of Hydrogen Abstraction from Fluoromethanes by the Hydroxyl Radical. *Journal of Physical Chemistry A* **1998**, 102, 10074–10081.
- Sheng, C. Elementary, Pressure Dependent Model for Combustion of C1, C2, and Nitrogen Containing Hydrocarbons: Operation of a Pilot Scale Incinerator and Model Comparison. Ph.D. Dissertation, New Jersey Institute of Technology, Newark, NJ, 2002.
- Steinfeld, J. I.; Francisco, J. S.; Hase, W. L. *Chemical Kinetics and Dynamics*; Prentice Hall: Engelwood Cliffs, NJ, 1989.
- Stephens, P. F.; Devlin, F. J.; Chabalowski, C. F.; Frisch, M. J. Ab-Initio Calculation of Vibrational Absorption and Circular-Dichroism Spectra Using Density-Functional Force-Fields. *Journal of Physical Chemistry* **1994**, 98, 11623–11627.
- Stevenson, W. H. Synthesis and Characterization of Hypergolic Amino Azides. *Proceedings of the 30th JANNAF Propellant Development and Characterization Subcommittee Meeting*, CPIA Publication 708, Colorado Springs, CO, 18–21 March 2002; Vol. II, pp 95–102.

- Stevenson W. H.; McQuaid, M. J. Dissociation Constants of 2-Azidoethanamines in Aqueous Solution. *International Journal of Quantum Chemistry* **2010**, *110*, 1376–1393.
- Stevenson, W. H.; Felton, L. D.; Slocum-Wang, Z. Hypergolic Liquid or Gel Fuel Mixtures. U.S. Patent Application 2008/0127551, 2008.
- Thompson, D. M.; Wilson, B. F.; Stevenson, W. H. Hypergolic Azide Liquid Fuels. *Proceedings of the 1998 JANNAF Propulsion Meeting*, Cleveland, OH, 15–17 July 1998; Chemical Propulsion Information Agency: Columbia, MD; Vol. III, pp 515–523.
- Tsang, W. Heats of Formation of Organic Free Radicals by Kinetic Methods. In *Energetics of Organic Free Radicals*; Martinho Simoes, J.A., Greenberg, A., Liebman, J. F., Eds.; Blackie Academic and Professional: London, 1996; pp 22–58.
- Vosko, S. H.; Wilk, L.; Nusair, M. Accurate Spin-Dependent Electron Liquid Correlation Energies for Local Spin-Density Calculations: A Critical Analysis. *Canadian Journal of Physics* **1980**, *58*, 1200–1211.
- Wiberg, K. B.; Crocker, L. S.; Morgan, K. M. Thermochemical Studies of Carbonyl Compounds 5: Enthalpies of Reduction of Carbonyl Groups. *J. Am. Chem. Soc.* **1991**, *113*, 3447–3450.
- Zhao, Y.; Truhlar, D. G. Hybrid Meta Density Functional Theory Methods for Thermochemistry, Thermochemical Kinetics, and Noncovalent Interactions: The MPW1B95 and MPWB1K Models and Comparative Assessments for Hydrogen Bonding and van der Waals Interactions. *Journal of Physical Chemistry A* **2004**, *108*, 6908–6918.

INTENTIONALLY LEFT BLANK.

**Appendix A. Thermodynamic Property Estimates for Molecular Structures
Involved in 2-azido-N-methylethanamine (MMAZ) Decomposition Paths**

This appendix lists enthalpy of formation estimates [$\Delta H_f^\circ(298)$] for (equilibrium) molecular structures involved in MMAZ decomposition paths presented in this report. The estimates were derived from G4-based results for the enthalpies of reaction [$\Delta H_r(298)$] of isodesmic reactions. The isodesmic reactions, $\Delta H_r(298)$ estimates, and $\Delta H_f^\circ(298)$ estimates are provided in table A-1. G4-based estimates for entropy [$S^\circ(298)$] and heat capacity [$C_p(T)$] are provided for equilibrium and transition state structures in table A-2.

Table A-1. G4-based $\Delta H_f^\circ(298)$ estimates for equilibrium structures involved in paths for the decomposition of MMAZ.

Isodesmic Reaction	$\Delta H_r(298)$ (kcal/mol)	$\Delta H_f^\circ(298)^a$ (kcal/mol)
$\text{MMAZ} + \text{C}_2\text{H}_6 + \text{CH}_3\text{NH}_2 = (\text{CH}_3)_2\text{NH} + \text{CH}_3\text{CH}_2\text{NH}_2 + \text{CH}_3\text{CH}_2\text{N}_3$	0.2	72.4
$\text{C}\cdot\text{H}_2\text{NHCH}_2\text{CH}_2\text{N}_3 + \text{C}_2\text{H}_6 = \text{MMAZ} + \text{C}\cdot\text{H}_2\text{CH}_3$	10.9	109.9
$\text{CH}_3\text{N}\cdot\text{CH}_2\text{CH}_2\text{N}_3 + \text{C}_2\text{H}_6 = \text{MMAZ} + \text{C}\cdot\text{H}_2\text{CH}_3$	9.0	111.8
$\text{CH}_3\text{NHC}\cdot\text{HCH}_2\text{N}_3 + \text{C}_2\text{H}_6 = \text{MMAZ} + \text{C}\cdot\text{H}_2\text{CH}_3$	12.1	108.7
$\text{CH}_3\text{NHCH}_2\text{C}\cdot\text{HN}_3 + \text{C}_2\text{H}_6 = \text{MMAZ} + \text{C}\cdot\text{H}_2\text{CH}_3$	11.0	109.9
$\text{H}_2\text{C}(\text{NO}_2)\text{NHCH}_2\text{CH}_2\text{N}_3 + \text{C}_2\text{H}_6 = \text{MMAZ} + \text{CH}_3\text{CH}_2\text{NO}_2$	4.3	62.7
$\text{H}_2\text{C}(\text{ONO})\text{NHCH}_2\text{CH}_2\text{N}_3 + \text{C}_2\text{H}_6 = \text{MMAZ} + \text{CH}_3\text{CH}_2\text{ONO}$	6.0	63.0
$\cdot\text{OCH}_2\text{NHCH}_2\text{CH}_3\text{N}_3 + \text{C}_2\text{H}_6 = \text{MMAZ} + \text{CH}_3\text{CH}_2\text{O}\cdot$	7.6	81.1
$\text{CH}_3\text{N}(\text{NO}_2)\text{CH}_2\text{CH}_2\text{N}_3 + (\text{CH}_3)_2\text{NH} = \text{MMAZ} + (\text{CH}_3)_2\text{NNO}_2$	-0.3	75.0
$\text{CH}_3\text{N}(\text{ONO})\text{CH}_2\text{CH}_2\text{N}_3 + (\text{CH}_3)_2\text{NH} = \text{MMAZ} + (\text{CH}_3)_2\text{NONO}$	0.1	92.9
$\text{CH}_3\text{N}(\text{O}\cdot)\text{CH}_2\text{CH}_2\text{N}_3 + (\text{CH}_3)_2\text{NH} = \text{MMAZ} + (\text{CH}_3)_2\text{NO}\cdot$	1.3	81.1
$\text{CH}_3\text{NHC}(\text{NO}_2)\text{HCH}_2\text{N}_3 + \text{C}_3\text{H}_8 = \text{MMAZ} + (\text{CH}_3)_2\text{CHNO}_2$	2.3	60.7
$\text{CH}_3\text{NHC}(\text{ONO})\text{HCH}_2\text{N}_3 + \text{C}_3\text{H}_8 = \text{MMAZ} + (\text{CH}_3)_2\text{CHONO}$	4.9	60.8
$\text{CH}_3\text{NHC}(\text{O}\cdot)\text{HCH}_2\text{N}_3 + \text{C}_3\text{H}_8 = \text{MMAZ} + (\text{CH}_3)_2\text{CO}\cdot$	5.0	80.7
$\text{CH}_3\text{NHCHCHN}_3 + \text{CH}_3\text{CH}_2\text{NH}_2 = \text{MMAZ} + \text{CH}_2\text{CHNH}_2$	0.3	97.3
$\text{CH}_2\text{NCH}_2\text{CH}_2\text{N}_3 + (\text{CH}_3)_2\text{NH} = \text{MMAZ} + \text{CH}_2\text{NCH}_3$	-0.8	95.9
$\text{CH}_3\text{NCHCH}_2\text{N}_3 + \text{CH}_3\text{CH}_2\text{NH}_2 = \text{MMAZ} + \text{CH}_3\text{CHNH}$	0.2	93.9
$\text{H}_2\text{C}(\text{NO}_2)\text{NHCH}_2\text{CHNH} + \text{C}_2\text{H}_6 = \text{CH}_3\text{NHCH}_2\text{CHNH} + \text{CH}_3\text{CH}_2\text{NO}_2$	5.6	10.0
$\text{H}_2\text{C}(\text{ONO})\text{NHCH}_2\text{CHNH} + \text{C}_2\text{H}_6 = \text{CH}_3\text{NHCH}_2\text{CHNH} + \text{CH}_3\text{CH}_2\text{ONO}$	7.3	10.3
$\text{CH}_3\text{N}(\text{NO}_2)\text{CH}_2\text{CHNH} + (\text{CH}_3)_2\text{NH} = \text{CH}_3\text{NHCH}_2\text{CHNH} + (\text{CH}_3)_2\text{NNO}_2$	0.5	22.8
$\text{CH}_3\text{N}(\text{ONO})\text{CH}_2\text{CHNH} + (\text{CH}_3)_2\text{NH} = \text{CH}_3\text{NHCH}_2\text{CHNH} + (\text{CH}_3)_2\text{NONO}$	-0.1	41.7
$\text{CH}_3\text{NHC}(\text{NO}_2)\text{HCHNH} + \text{C}_3\text{H}_8 = \text{CH}_3\text{NHCH}_2\text{CHNH} + (\text{CH}_3)_2\text{CHNO}_2$	1.5	10.1
$\text{CH}_3\text{NHC}(\text{ONO})\text{HCHNH} + \text{C}_3\text{H}_8 = \text{CH}_3\text{NHCH}_2\text{CHNH} + (\text{CH}_3)_2\text{CHONO}$	4.0	10.2
$\text{ONNHCH}_2\text{CH}_2\text{N}_3 + \text{CH}_3\text{NH}_2 = \text{H}_2\text{NNO} + \text{MMAZ}$	-0.6	101.2
$\text{OCHCH}_2\text{N}_3 + \text{C}_2\text{H}_6 = \text{CH}_3\text{CHO} + \text{CH}_3\text{CH}_2\text{N}_3$	13.7	29.4
$\text{H}_3\text{CNHNO} + \text{CH}_3\text{NH}_2 = \text{H}_2\text{NNO} + (\text{CH}_3)_2\text{NH}$	1.9	22.0
$(\text{CH}_3)_2\text{CHNO}_2 + \text{C}_2\text{H}_6 = \text{CH}_3\text{CH}_2\text{NO}_2 + \text{C}_3\text{H}_8$	4.0	-34.5
$(\text{CH}_3)_2\text{CHONO} + \text{C}_2\text{H}_6 = \text{CH}_3\text{CH}_2\text{ONO} + \text{C}_3\text{H}_8$	3.4	-31.8
$(\text{CH}_3)_2\text{NNO}_2 + \text{CH}_3\text{CH}_2\text{NH}_2 = \text{CH}_3\text{CH}_2\text{NO}_2 + (\text{CH}_3)_2\text{NNH}_2$	9.9	-2.1
$(\text{CH}_3)_2\text{NONO} + \text{CH}_3\text{CH}_2\text{NH}_2 = \text{CH}_3\text{CH}_2\text{ONO} + (\text{CH}_3)_2\text{NNH}_2$	-6.4	16.3
$(\text{CH}_3)_2\text{NNH}_2 + \text{CH}_3\text{NH}_2 = \text{N}_2\text{H}_4 + (\text{CH}_3)_3\text{N}$	0.7	21.1
$\text{CH}_2\text{CHNH}_2 + \text{C}_2\text{H}_6 = \text{CH}_3\text{CH}_2\text{NH}_2 + \text{C}_2\text{H}_4$	7.4	13.0
$(\text{CH}_3)_2\text{NOH} + (\text{CH}_3)_3\text{CH} = (\text{CH}_3)_2\text{CHOH} + (\text{CH}_3)_3\text{N}$	-23.4	-16.3
$(\text{CH}_3)_2\text{NO}\cdot + (\text{CH}_3)_2\text{CHOH} = (\text{CH}_3)_2\text{CHO}\cdot + (\text{CH}_3)_2\text{NOH}$	31.5	5.7
$\text{CH}_3\text{NHCH}_2\text{CHNH} + \text{C}_2\text{H}_6 + \text{C}_2\text{H}_6 = \text{CH}_3\text{CHNH} + (\text{CH}_3)_2\text{NH} + \text{C}_3\text{H}_8$	-0.8	21.0

^a. $\Delta H_f^\circ(298)$ data (in kcal/mol) used for calculations included $\text{C}_2\text{H}_6 = -20.04 \pm 0.07$ (Pittam and Pilcher, 1972); $\text{C}\cdot\text{H}_2\text{CH}_3 = 28.4 \pm 0.5$ (Tsang, 1996); $\text{C}_3\text{H}_8 = -25.02 \pm 0.12$ (Pittam and Pilcher, 1972); $\text{CH}_3\text{CHO} = -40.80 \pm 0.35$ (Wiberg, et al., 1991); $\text{C}_2\text{H}_4 = 12.54 \pm 0.07$ (Chase, 1998); $(\text{CH}_3)_3\text{CH} = -32.07 \pm 0.15$ (Pittam and Pilcher, 1972); $(\text{CH}_3)_2\text{CHOH} = -65.19$ (Buckley and Herington, 1965); $\text{CH}_3\text{CH}_2\text{OH} = -56.09 \pm 0.07$ (Chao and Rossini, 1965); $\text{NH}_3 = -10.98 \pm 0.084$ (Cox et al., 1984); $\text{CH}_3\text{CH}_2\text{NO}_2 = -25.45$ (Chen and McQuaid, 2013); $\text{CH}_3\text{CH}_2\text{ONO} = -23.40$ (Chen and McQuaid, 2013); $\text{HNO} = 25.6$ (Anderson, 1999); $\text{CH}_3\text{NH}_2 = -5.3$ (Chen and McQuaid, 2011); $\text{CH}_3\text{CH}_2\text{NH}_2 = -12.2$ (Chen and McQuaid, 2011); $(\text{CH}_3)_2\text{NH} = -4.3$ (Chen and McQuaid, 2011); $(\text{CH}_3)_3\text{N} = -6.6$ (Chen and McQuaid, 2011); $\text{CH}_2\text{NCH}_3 = 18.4$ (Chen and McQuaid, 2011); $\text{CH}_3\text{CHNH} = 9.5$ (Chen and McQuaid, 2011); $\text{CH}_3\text{CH}_2\text{N}_3 = 63.8$ (Chen and McQuaid, 2011); $\text{N}_2\text{H}_4 = 23.06$ (Chen and McQuaid, 2011); $\text{H}_2\text{NNO} = 22.88$ (derived from the average of $\Delta H_r(298)$ estimates produced by the G4, CBS-QB3, and G3MP2 models for $\text{H}_2\text{NNO} + \text{NH}_3 = \text{N}_2\text{H}_4 + \text{HNO}$); $\text{CH}_3\text{CH}_2\text{O}\cdot = -3.81$ (derived from the average of $\Delta H_r(298)$ estimates produced by the G4, CBS-QB3, and G3MP2 models for $\text{CH}_3\text{CH}_2\text{O}\cdot + \text{C}_2\text{H}_6 = \text{CH}_3\text{CH}_2\text{OH} + \text{C}\cdot\text{H}_2\text{CH}_3$); $(\text{CH}_3)_2\text{CHO}\cdot = -11.68$ (derived from the average of $\Delta H_r(298)$ estimates of produced by the G4, CBS-QB3, and G3MP2 models for $(\text{CH}_3)_2\text{CHO}\cdot + \text{C}_2\text{H}_6 = (\text{CH}_3)_2\text{CHOH} + \text{C}\cdot\text{H}_2\text{CH}_3$).

Table A-2. $S^\circ(298)$ and $C_p(T)$ estimates for molecular structures involved in MMAZ decomposition paths.^a

Species	$S^\circ(298)$	$C_p(300)$	$C_p(400)$	$C_p(500)$	$C_p(600)$	$C_p(800)$	$C_p(1000)$	$C_p(1500)$
MMAZ	97.36	32.17	37.99	43.42	48.14	55.63	61.16	69.71
C•H ₂ NHCH ₂ CH ₂ N ₃	97.4	34.08	39.32	43.86	47.71	53.83	58.42	65.64
CH ₃ N•CH ₂ CH ₂ N ₃	99.8	29.58	35.28	40.59	45.14	52.19	57.31	65.06
CH ₃ NHC•HCH ₂ N ₃	100.48	31.76	36.25	40.88	45.09	51.9	56.99	64.83
CH ₃ NHCH ₂ C•HN ₃	97.65	31.79	37.89	43.08	47.36	53.93	58.74	66.04
TS1-E	126.39	44.19	51.46	58.1	63.68	72.05	77.83	86.11
TS2-E	119.88	45.06	52.94	59.56	64.81	72.46	77.79	85.73
TS3-E	119.69	45.01	52	58.54	64.15	72.6	78.36	86.42
TS4-E	124.56	42.94	50.22	56.77	62.36	71.05	77.22	86.02
TS1-H	127.52	42.62	50.4	57.34	63.12	71.81	77.87	86.63
TS2-H	122.34	42.79	49.95	56.56	62.06	70.37	76.27	85.13
TS3-H	119.22	43.66	52.52	59.4	64.65	72.29	77.72	85.86
TS4-H	123.03	40.27	47.89	54.81	60.72	69.85	76.31	85.59
TS1-Z	124.88	43.41	51.49	58.65	64.52	73.04	78.75	86.77
TS2-Z	119.89	44.03	52.32	59.48	65.17	73.28	78.83	86.88
TS3-Z	119.06	45.14	51.94	58.21	63.61	71.95	77.82	86.25
TS4-Z	121.26	40.62	48.95	56.82	63.62	73.8	80.42	88.79
H ₂ C(NO ₂)NHCH ₂ CH ₂ N ₃	103.13	36.66	45.16	52.61	58.8	68.16	74.74	84.44
H ₂ C(ONO)NHCH ₂ CH ₂ N ₃	105.03	37.65	46.03	53.33	59.39	68.57	75.04	84.6
•OCH ₂ NHCH ₂ CH ₂ N ₃	96.54	31.27	38.77	45.33	50.78	59.04	64.92	73.68
CH ₃ NHC(NO ₂)HCH ₂ N ₃	100.3	37.56	45.78	53.03	59.1	68.33	74.85	84.49
CH ₃ NHC(ONO)HCH ₂ N ₃	102.33	38.68	46.76	53.85	59.77	68.79	75.18	84.67
CH ₃ NHC(O•)HCH ₂ N ₃	93.61	32.34	39.55	45.88	51.16	59.21	64.97	73.65
CH ₃ N(NO ₂)CH ₂ CH ₂ N ₃	102.4	36.76	45.12	52.53	58.74	68.17	74.81	84.57
CH ₃ N(ONO)CH ₂ CH ₂ N ₃	101.84	38.6	46.79	53.93	59.9	68.98	75.41	84.9
CH ₃ N(O•)CH ₂ CH ₂ N ₃	94.49	31.45	38.5	44.85	50.24	58.56	64.54	73.49
CH ₃ NHCHCHN ₃	93.75	27.32	32.81	37.81	42.08	48.7	53.47	60.7
CH ₂ NCH ₂ CH ₂ N ₃	93.29	27.95	33.28	37.96	42.03	48.6	53.44	60.59
CH ₃ NCHCH ₂ N ₃	92.04	27.53	32.67	37.21	41.19	47.71	52.62	60.07
H ₂ C(NO ₂)NHCH ₂ CHNH	100.89	33.96	41.24	47.3	52.15	59.2	64.08	71.3
H ₂ C(ONO)NHCH ₂ CHNH	101.15	34.75	42.63	48.88	53.72	60.63	65.35	72.27
CH ₃ N(NO ₂)CH ₂ CHNH	95.13	32.96	40.45	46.76	51.88	59.36	64.48	71.88
CH ₃ N(ONO)CH ₂ CHNH	97.4	33.73	41.99	48.59	53.64	60.71	65.44	72.32
CH ₃ NHC(NO ₂)HCHNH	91.83	35.03	43.26	49.68	54.51	61.18	65.67	72.34
CH ₃ NHC(ONO)HCHNH	96.17	36.45	42.86	48.38	53.02	60.02	64.93	72.08
ONNHCH ₂ CH ₂ N ₃	100.53	31.4	37.87	43.23	47.39	53.17	56.99	62.42
OCHCH ₂ N ₃	80.67	21.14	25.10	28.56	31.48	35.95	39.12	43.76
H ₃ CNHNO	70.23	17.47	20.53	23.36	25.77	29.48	32.15	36.2
TS6	105.99	37.72	45.58	52.52	58.36	67.28	73.62	82.99
TS7	111.54	40.17	47.79	54.39	59.9	68.33	74.35	83.34
TS8	106.71	37.01	45.06	52.15	58.11	67.23	73.66	83.1
TS11	110.19	39.17	46.92	53.66	59.31	67.92	74.06	83.19
TS12	105.08	37.21	45.29	52.4	58.38	67.49	73.9	83.26
TS14	100.93	38.41	46.23	53.06	58.78	67.51	73.73	82.99
TS15	108.7	41.1	48.45	54.86	60.24	68.53	74.48	83.41
TS16	103.31	38.73	46.53	53.45	59.28	68.13	74.33	83.4
TS17	104.4	37.83	45.52	52.4	58.25	67.25	73.65	83.07
TS20	106.17	39.97	47.48	54.05	59.58	68.07	74.15	83.23
TS21	103.5	38.93	46.73	53.63	59.43	68.24	74.41	83.44
TS22	104.6	37.99	45.67	52.54	58.38	67.38	73.78	83.16
TS24	107.13	40.93	48.41	54.89	60.33	68.69	74.7	83.63
TS25	101.56	36.82	45.11	52.38	58.45	67.64	74.09	83.43
TS26	100.42	37.28	45.4	52.57	58.59	67.73	74.14	83.45
TS29	106.42	39.06	46.72	53.47	59.15	67.86	74.08	83.28
TS30	101.0	37.01	45.48	52.85	58.97	68.17	74.56	83.72
TS31	100.14	37.72	45.88	53.07	59.09	68.2	74.55	83.7

^a $S^\circ(298)$: cal/K; $C_p(T)$: cal/mol·K

**Appendix B. Geometric Representations, Normal Mode Frequencies, and
Moments of Inertia for Molecular Structures Involved in H-Atom
Abstraction Reactions**

This appendix lists B3LYP/6-31+G(d,p)-based geometries, normal mode frequencies, and moments of inertia for molecular structures involved in reactions R1–R4. Table B-1 presents Cartesian coordinates for MMAZ and MMAZ radical (MMAZ-H•) equilibrium structures. Tables B-2 through B-4 present Cartesian coordinates for TS-E, TS-H, and TS-Z, respectively. Tables B-5 through B-7 present Cartesian coordinates for COMP-E, COMP-H, and COMP-Z, respectively. Table B-8 presents normal mode frequencies and moments of inertia for MMAZ and MMAZ-H•. Table B-9 presents normal mode frequencies and moments of inertia for TS-E, TS-H, and TS-Z. Table B-10 presents the normal mode frequencies and moments of inertia for COMP-E, COMP-H, and COMP-Z.

Table B-1. The Cartesian coordinates of MMAZ and MMAZ radical (MMAZ-H•) equilibrium geometries:
B3LYP/6-31+G(d,p) results.

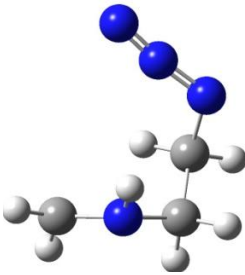
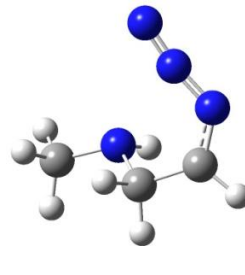
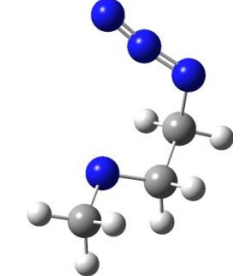
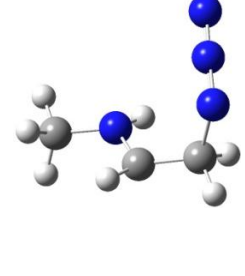
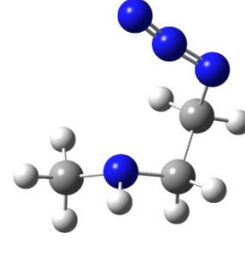
	C•H ₂ NHCH ₂ CH ₂ N ₃	N	0.034294	0.093081	0.051584
		C	0.051049	-0.01583	1.496454
		C	1.237361	0.143134	-0.64335
		C	0.625783	1.211502	2.226085
		N	-0.23274	2.400926	2.045162
		N	0.075366	3.168939	1.135022
		N	0.255328	3.964081	0.342952
		H	-0.96978	-0.19769	1.846573
		H	0.655929	-0.88964	1.771104
		H	2.011992	-0.53502	-0.29855
		H	1.168094	0.342363	-1.70575
		H	0.656276	1.017215	3.301737
		H	1.644076	1.408135	1.873363
		H	-0.68762	0.705263	-0.30177
	CH ₃ NHCH ₂ C•HN ₃	N	0.019576	-0.18051	-0.02157
		C	-0.00705	-0.0883	1.437998
		C	1.345601	0.014661	-0.59257
		C	-1.36581	-0.39189	1.978363
		N	-2.05709	-1.53014	1.705311
		N	-1.62245	-2.40959	0.942145
		N	-1.39187	-3.31792	0.287575
		H	0.728627	-0.82075	1.81339
		H	0.314784	0.893576	1.829508
		H	2.004233	-0.79954	-0.26993
		H	1.281817	-0.02139	-1.68357
		H	1.827043	0.966412	-0.30525
		H	-1.86453	0.253801	2.686112
		H	-0.62986	0.496476	-0.40851
	CH ₃ N•CH ₂ CH ₂ N ₃	N	-0.07603	0.072321	-0.08687
		C	-0.02544	0.199541	1.343984
		C	1.224652	-0.09355	-0.67646
		C	-1.43209	0.307778	1.935313
		N	-2.19328	-0.94869	1.801931
		N	-2.74386	-1.14668	0.717917
		N	-3.32010	-1.45347	-0.21062
		H	0.500613	-0.6592	1.796426
		H	0.556912	1.095648	1.628909
		H	1.147909	-0.13455	-1.76574
		H	1.907985	0.726614	-0.3979
		H	1.700846	-1.02424	-0.32394
		H	-1.37005	0.500911	3.008685
		H	-1.96700	1.140556	1.463715
	CH ₃ NHC•HCH ₂ N ₃	N	0.040421	-0.10355	0.220639
		C	0.110319	0.416719	1.499229
		C	1.22327	-0.15661	-0.61659
		C	-1.11683	0.455395	2.318758
		N	-1.54580	-0.89344	2.899698
		N	-1.9622	-1.70135	2.076839
		N	-2.36995	-2.51698	1.391618
		H	1.072212	0.302303	1.989146
		H	2.029327	-0.65672	-0.07075
		H	1.009849	-0.7417	-1.51448
		H	1.583893	0.837389	-0.92173
		H	-0.97091	1.075988	3.202312
		H	-1.96995	0.858459	1.754909
		H	-0.81748	0.090189	-0.27871
	CH ₃ NHCH ₂ CH ₂ N ₃	N	-0.038	-0.05131	0.051532
		C	0.008846	-0.03904	1.506157
		C	1.257493	0.073253	-0.6029
		C	0.033095	1.390885	2.060196
		N	-1.22373	2.117492	1.805971
		N	-1.38349	2.567154	0.67125
		N	-1.66003	3.062978	-0.31242
		H	-0.89004	-0.53332	1.887824
		H	0.882825	-0.58105	1.915105
		H	1.688917	1.060498	-0.40558
		H	1.996363	-0.68189	-0.2798
		H	1.128041	-0.01138	-1.6853
		H	0.138516	1.358933	3.147075
		H	0.88921	1.949342	1.660337
		H	-0.5081	-0.88602	-0.27368

Table B-2. The Cartesian coordinates of (TS-E) transition states leading to *trans*-HONO formation (R1–R4): B3LYP/6-31+G(d,p) results.

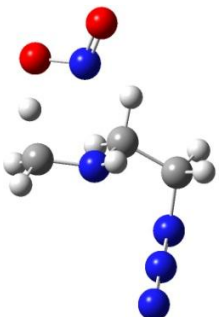
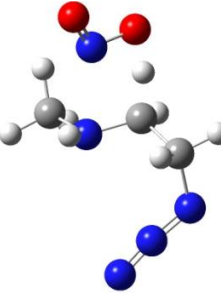
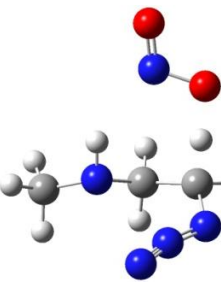
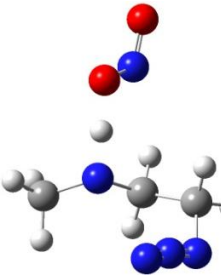
	TS1-E	C	-0.0264	0.00951	-0.00768
		N	-0.00498	0.020326	1.446178
		H	0.932118	0.027921	1.836727
		C	-0.90182	0.822831	2.154054
		H	-1.90803	0.810041	1.730713
		C	0.596131	-1.27211	-0.56735
		N	-0.21672	-2.46984	-0.29152
		N	-0.07898	-2.98074	0.820921
		N	-0.0379	-3.56097	1.795948
		H	0.648762	-1.19166	-1.65477
		H	1.621186	-1.39638	-0.1934
		H	-1.06876	0.079985	-0.33154
		H	0.513086	0.876778	-0.41602
		H	-0.88863	0.622814	3.227942
		H	-0.48104	2.010342	2.079785
		O	0.299729	3.112994	1.983529
		N	1.478152	2.546162	1.854774
		O	2.405767	3.306994	1.747086
	TS2-E	H	-0.00095	0.02248	0.002572
		N	0.000243	0.02142	1.018589
		C	1.331166	0.018138	1.601217
		C	-0.99592	0.834822	1.567923
		C	-2.4119	0.504452	1.109059
		N	-2.93737	-0.73536	1.72177
		N	-2.44882	-1.78957	1.313905
		N	-2.09019	-2.82705	1.022134
		H	-2.45249	0.448022	0.013957
		H	-3.08871	1.296849	1.428586
		H	1.25827	-0.19242	2.671448
		H	1.929894	-0.76456	1.130616
		H	1.842885	0.981168	1.467315
		H	-0.90419	0.903991	2.655506
		H	-0.81349	1.987268	1.107596
		O	-0.56172	3.045615	0.275462
		N	-0.05993	2.400672	-0.75243
		O	0.282068	3.086613	-1.6808
	TS3-E	N	0.000125	-0.00037	-0.00016
		C	0.000144	-0.00053	1.448885
		C	1.329731	0.000592	-0.59706
		H	-0.53684	0.797713	-0.32911
		C	-1.39433	-0.30838	1.992237
		N	-2.01518	-1.52514	1.617017
		N	-1.90841	-1.97993	0.465334
		N	-1.96876	-2.5745	-0.49595
		H	0.691196	-0.78033	1.799042
		H	0.331563	0.947519	1.908816
		H	1.854458	-0.92354	-0.32928
		H	1.236842	0.029057	-1.68583
		H	1.962432	0.848372	-0.28394
		H	-1.45593	-0.23737	3.080803
		H	-2.11429	0.613491	1.64381
		O	-2.83837	1.783606	1.329107
		N	-2.22046	2.289778	0.281743
		O	-2.70558	3.304581	-0.14077
	TS4-E	N	-0.09306	0.045684	-0.00909
		C	-0.0629	0.012851	1.424044
		C	1.172118	-0.00487	-0.69513
		C	-1.29411	-0.70273	2.005204
		N	-1.25015	-2.16177	1.808469
		N	-1.52823	-2.56701	0.678252
		N	-1.76759	-3.07592	-0.30798
		H	0.863146	-0.43175	1.805164
		H	-0.12122	1.069698	1.76216
		H	1.69057	-0.94438	-0.46399
		H	1.015184	0.06819	-1.77267
		H	1.834127	0.816519	-0.37575
		H	-1.31323	-0.55132	3.085402
		H	-2.20664	-0.2696	1.579842
		H	-0.85789	0.896682	-0.39735
		O	-1.43597	1.993797	-0.61349
		N	-1.31909	2.69659	0.494813
		O	-1.86203	3.765529	0.50466

Table B-3. The Cartesian coordinates of (TS-H) transition states leading to HNO₂ formation (R1–R4):
B3LYP/6-31+G(d,p) results.

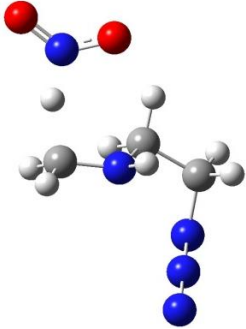
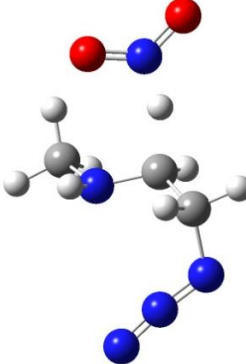

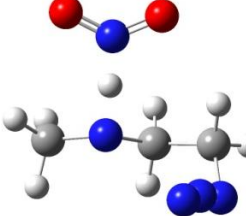
	TS1-H	C	-0.29969	-0.0205	-0.02073
		N	-0.32409	-0.02673	1.434529
		H	0.597854	-0.05648	1.852695
		C	-1.23927	0.758656	2.126739
		H	-2.24185	0.754575	1.69896
		C	0.303885	-1.31233	-0.57477
		N	-0.54169	-2.49393	-0.3262
		N	-0.44701	-3.01097	0.787435
		N	-0.44506	-3.59746	1.759872
		H	0.385355	-1.22781	-1.66023
		H	1.316684	-1.46478	-0.17759
		H	-1.33116	0.075684	-0.37308
		H	0.271781	0.837323	-0.40314
		H	-1.20801	0.626752	3.208005
		H	-0.7625	2.166068	1.963467
		N	-0.07999	3.148508	1.720046
		O	1.006732	2.86607	1.231058
	TS2-H	H	-0.00604	-0.02337	0.00824
		N	0.00345	-0.00114	1.021095
		C	1.34332	0.000661	1.586788
		C	-0.99457	0.787884	1.58616
		C	-2.39365	0.549709	1.067151
		N	-2.99648	-0.71893	1.563061
		N	-2.52359	-1.75599	1.098367
		N	-2.18334	-2.77974	0.740669
		H	-2.40967	0.569516	-0.03132
		H	-3.06011	1.334935	1.424909
		H	1.279021	-0.16207	2.666048
		H	1.920863	-0.81697	1.149302
		H	1.871941	0.944357	1.39872
		H	-0.91956	0.838673	2.67464
		H	-0.68388	2.159982	1.150258
		N	-0.21907	3.135426	0.546309
		O	0.58553	2.813588	-0.31759
		O	-0.58415	4.257889	0.828512
	TS3-H	N	0.029786	-0.06462	0.001951
		C	0.022369	-0.02301	1.457283
		C	1.352276	0.047665	-0.60128
		H	-0.58481	0.654794	-0.35935
		C	0.515263	-1.32847	2.069103
		N	0.038997	-2.54973	1.576198
		N	-1.038	-2.5964	0.962967
		N	-1.99674	-2.8269	0.402096
		H	0.638018	0.788384	1.885895
		H	-1.00843	0.155367	1.786533
		H	1.947981	-0.83888	-0.35986
		H	1.251791	0.088983	-1.6889
		H	1.919761	0.934848	-0.26986
		H	1.578001	-1.42083	2.289816
		H	0.025272	-1.19434	3.422086
		N	-0.51338	-0.95807	4.516426
		O	-1.55455	-0.33212	4.441354
		O	0.051956	-1.35646	5.511073
	TS4-H	N	0.017736	-0.01862	0.008139
		C	0.019969	-0.02902	1.45343
		C	1.329917	0.029205	-0.59433
		C	-1.38641	-0.23283	2.022151
		N	-1.89032	-1.59747	1.774825
		N	-2.44358	-1.78838	0.690472
		N	-2.98412	-2.10146	-0.25727
		H	0.688811	-0.82967	1.803672
		H	0.441452	0.914079	1.845443
		H	1.75608	-0.98576	-0.59512
		H	1.247549	0.364969	-1.63035
		H	2.033806	0.676543	-0.05012
		H	-1.35187	-0.12068	3.10783
		H	-2.06595	0.526168	1.617691
		H	-0.79776	0.924687	-0.52434
		N	-1.36981	1.92097	-0.90617
		O	-2.282	2.322726	-0.19861
		O	-0.97903	2.418328	-1.94716

Table B-4. The Cartesian coordinates of (TS-Z) transition states leading to *cis*-HONO formation (R1–R4):
B3LYP/6-31+G(d,p) results.

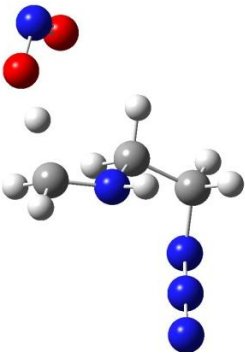
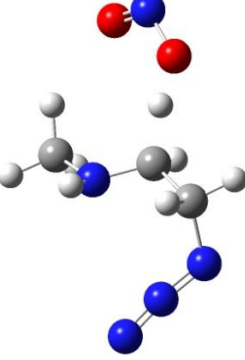
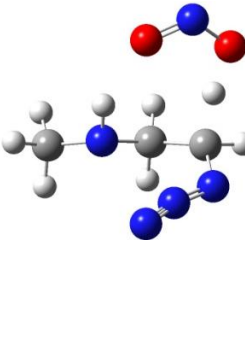
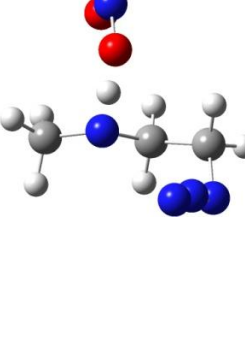
	C	-0.00856	-0.00291	0.002436
	N	-0.0085	-0.00235	1.454447
	H	0.9137	-0.00188	1.872348
	C	-0.97231	0.708063	2.161412
	H	-1.97744	0.59124	1.752393
	C	0.816713	-1.15983	-0.56038
	N	0.210674	-2.4814	-0.31092
	N	0.398357	-2.96777	0.804214
	N	0.509649	-3.53715	1.780781
	H	0.868913	-1.05869	-1.64586
	H	1.84587	-1.12477	-0.17599
	H	-1.04598	-0.09876	-0.3321
	H	0.369619	0.951426	-0.39263
	H	-0.91914	0.548855	3.239913
	H	-0.78424	2.084083	2.092677
	O	-0.67613	3.302889	2.212891
	H	-0.01171	-0.02716	0.000502
	N	-0.0028	0.000293	1.012274
	C	1.322553	0.011091	1.60575
	C	-1.03765	0.727354	1.593794
	C	-2.42096	0.435883	1.042956
	N	-2.96311	-0.87371	1.487374
	N	-2.43254	-1.8706	0.998431
	N	-2.03685	-2.86438	0.614213
	H	-2.42065	0.495484	-0.0541
	H	-3.12635	1.178828	1.414991
	H	1.258652	-0.3386	2.640512
	H	1.973007	-0.66738	1.050051
	H	1.752775	1.021366	1.609571
	H	-0.98764	0.69378	2.68567
	H	-0.90709	2.076286	1.352004
	O	-1.0011	3.294527	1.111595
	N	0.026449	-0.01032	0.01478
	C	0.021003	-0.03905	1.460047
	C	1.356561	0.025032	-0.57619
	H	-0.53355	0.774072	-0.30564
	C	-1.37644	-0.26292	2.011435
	N	-2.15728	-1.33522	1.553287
	N	-2.12299	-1.72599	0.374504
	N	-2.27504	-2.2401	-0.62374
	H	0.658919	-0.87417	1.790828
	H	0.429824	0.869183	1.942237
	H	1.894093	-0.89917	-0.3351
	H	1.267398	0.085037	-1.66397
	H	1.97754	0.871551	-0.23487
	H	-1.42818	-0.2491	3.101759
	H	-2.09114	0.886579	1.806621
	O	-2.77177	1.927423	1.87508
	N	0.027063	-0.01915	0.00297
	C	0.017999	-0.0191	1.446456
	C	1.324146	0.028324	-0.62308
	C	-1.37252	-0.33298	2.002925
	N	-1.75772	-1.74051	1.784014
	N	-2.29117	-2.0025	0.704187
	N	-2.80068	-2.38202	-0.23642
	H	0.741858	-0.76224	1.810827
	H	0.352227	0.960204	1.822077
	H	1.801598	-0.9587	-0.52771
	H	1.214483	0.259752	-1.6841
	H	1.990863	0.764285	-0.15591
	H	-1.36203	-0.19253	3.085531
	H	-2.11419	0.351949	1.576305
	H	-0.94176	0.560518	-0.59104
	O	-1.7861	1.296111	-1.06622
	N	-1.40592	2.515783	-0.85906
	O	-0.35028	2.653196	-0.27412

Table B-5. The Cartesian coordinates of (COMP-E) complexes leading to *trans*-HONO formation (R1–R4):
B3LYP/6-31+G(d,p) results.

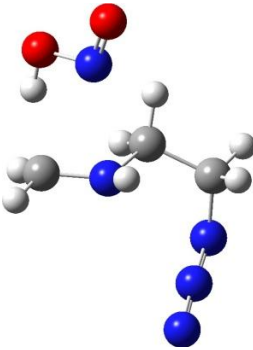
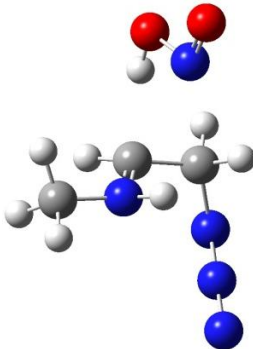
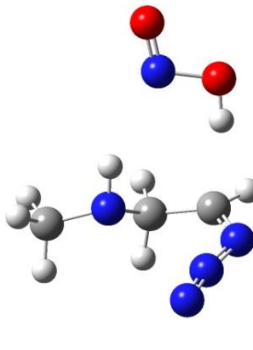
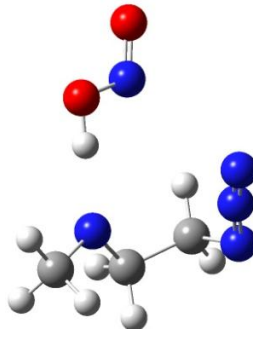
	COMP1-E	C	-0.46062	-0.07879	-1.09999
		N	-0.48683	-0.11895	0.352429
		H	0.434299	-0.10836	0.774004
		C	-1.43928	0.595704	1.056415
		H	-2.428	0.630806	0.608634
		C	0.219807	-1.3189	-1.68251
		N	-0.55877	-2.55215	-1.47075
		N	-0.44591	-3.08991	-0.3684
		N	-0.42077	-3.70112	0.588222
		H	0.304167	-1.20336	-2.76501
		H	1.236678	-1.42341	-1.28004
		H	-1.49497	-0.03478	-1.45398
		H	0.056861	0.819303	-1.47225
		H	-1.38416	0.509667	2.137344
		H	-0.62303	2.381321	0.905045
		O	-0.00489	3.154618	0.785518
	COMP2-E	H	0.89405	-0.64716	-0.53102
		N	0.947286	-0.55948	0.476551
		C	2.299499	-0.45962	0.997102
		C	-0.08334	0.156559	1.053159
		C	-1.46516	-0.08283	0.541861
		N	-2.08303	-1.36779	1.03439
		N	-1.58523	-2.39816	0.586411
		N	-1.2092	-3.41329	0.234964
		H	-1.48956	-0.07306	-0.55611
		H	-2.14359	0.69095	0.900672
		H	2.284925	-0.63195	2.076945
		H	2.924304	-1.22715	0.535301
		H	2.75168	0.524422	0.808296
		H	0.035763	0.33164	2.12029
		H	0.317009	1.911773	0.174129
		O	0.596668	2.629575	-0.45258
		N	0.840109	1.926133	-1.63
		O	1.186358	2.640843	-2.50186
	COMP3-E	N	1.386924	-0.2087	-0.57607
		C	1.463686	-0.37624	0.867582
		C	2.6869	-0.10906	-1.22691
		H	0.8246	0.609707	-0.79003
		C	0.123154	-0.70974	1.451822
		N	-0.68328	-1.70986	0.987413
		N	-0.46921	-2.3094	-0.08196
		N	-0.46227	-2.97526	-1.00644
		H	2.168575	-1.20346	1.063689
		H	1.869681	0.498437	1.407716
		H	3.231474	-1.05247	-1.10738
		H	2.543295	0.059775	-2.29735
		H	3.327457	0.699508	-0.8337
		H	-0.1207	-0.42459	2.468644
		H	-1.18142	0.961001	0.979753
		O	-1.60831	1.821243	0.779273
		N	-0.86952	2.288007	-0.30968
		O	-1.25962	3.333286	-0.68318
	COMP4-E	N	0.026928	-0.06947	-0.00324
		C	0.034666	-0.07085	1.4372
		C	1.323797	0.103259	-0.59905
		C	-1.17807	-0.80462	2.019709
		N	-1.07497	-2.26645	1.839374
		N	-1.47493	-2.71252	0.762098
		N	-1.81282	-3.25677	-0.17504
		H	0.966177	-0.49494	1.842161
		H	-0.00246	0.98233	1.770741
		H	1.953943	-0.7768	-0.39155
		H	1.23648	0.225275	-1.68066
		H	1.852376	0.971367	-0.17456
		H	-1.20847	-0.64253	3.099088
		H	-2.10085	-0.41414	1.577507
		H	-1.43809	0.017736	-1.02347
		O	-2.24122	0.136038	-1.6023
		N	-3.2784	0.177874	-0.69594
		O	-4.32674	0.331465	-1.22296

Table B-6. The Cartesian coordinates of (COMP-H) complexes leading to HNO₂ formation (R1–R4):
B3LYP/6-31+G(d,p) results.

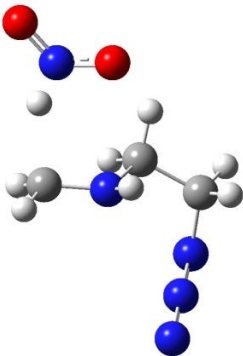
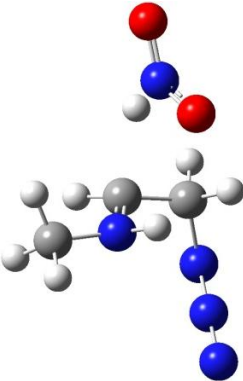
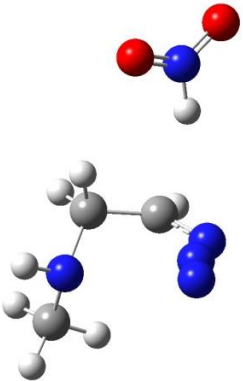
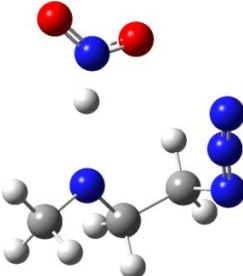
	COMP1-H	C	-0.16818	-0.21874	-1.0521
		N	-0.1656	-0.2158	0.402003
		H	0.760972	-0.13089	0.801289
		C	-1.15835	0.436141	1.112111
		H	-2.15581	0.374941	0.686045
		C	0.555251	-1.44577	-1.61029
		N	-0.1617	-2.70553	-1.34223
		N	0.005046	-3.20497	-0.22898
		N	0.084191	-3.78497	0.744131
		H	0.611357	-1.36103	-2.69747
		H	1.583989	-1.49137	-1.2279
		H	-1.20967	-0.2311	-1.387
		H	0.308765	0.688084	-1.45203
		H	-1.08028	0.363854	2.193353
		H	-0.5389	2.242403	0.906576
	COMP2-H	H	0.856997	-0.69927	-0.91337
		N	0.908475	-0.70583	0.097474
		C	2.263503	-0.68533	0.621091
		C	-0.12198	-0.05345	0.746376
		C	-1.5057	-0.25553	0.219838
		N	-2.10927	-1.58671	0.586743
		N	-1.59476	-2.56696	0.052606
		N	-1.20494	-3.54316	-0.38343
		H	-1.53788	-0.13916	-0.87252
		H	-2.18942	0.473065	0.655329
		H	2.236327	-0.88124	1.696273
		H	2.848701	-1.47456	0.143203
		H	2.762508	0.276404	0.444688
		H	-0.00533	-0.00699	1.827631
		H	0.306772	1.793654	0.20234
	COMP3-H	N	0.358536	1.183527	-2.05885
		C	0.655608	1.079863	-0.63301
		C	1.535928	1.179089	-2.91822
		H	-0.20193	2.009567	-2.23036
		C	1.018412	-0.32881	-0.24715
		N	0.292726	-1.42161	-0.62275
		N	-0.78755	-1.32149	-1.23358
		N	-1.79308	-1.44249	-1.75693
		H	1.476461	1.740568	-0.30145
		H	-0.24278	1.393085	-0.08303
		H	2.04801	0.214667	-2.83573
		H	1.227502	1.303094	-3.95962
		H	2.268544	1.96851	-2.67461
		H	1.99002	-0.5909	0.152313
		H	0.298263	-0.28554	1.854127
	COMP4-H	N	-0.25113	0.088383	2.670698
		O	-0.99231	1.023939	2.414565
		O	-0.07295	-0.44867	3.746025
		N	1.482756	-0.07854	0.016401
		C	1.363727	-0.33493	1.429954
		C	2.710211	-0.54839	-0.56651
		C	-0.09784	-0.35625	1.891721
		N	-0.79096	-1.58309	1.449633
		N	-1.30712	-1.54657	0.331265
		N	-1.8297	-1.6525	-0.67093
		H	1.868489	-1.26873	1.720719
		H	1.886132	0.482274	1.960467
		H	2.738589	-1.64999	-0.54677
		H	2.797365	-0.21371	-1.60224
		H	3.587853	-0.20492	0.003755
		H	-0.12669	-0.37641	2.983137
		H	-0.61931	0.538918	1.536859
		H	0.297721	1.011997	-0.87449
		N	-0.47352	1.665406	-1.20475
		O	-1.41791	1.794952	-0.43288
		O	-0.33872	2.21013	-2.28584

Table B-7. The Cartesian coordinates of (COMP-Z) complexes leading to *cis*-HONO formation (R1–R4): B3LYP/6-31 +G(d,p) results.

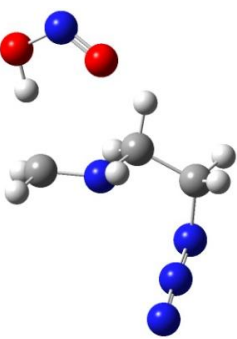
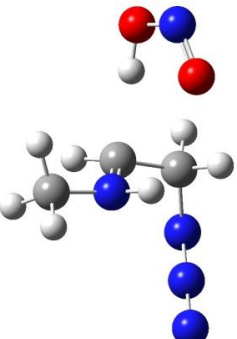
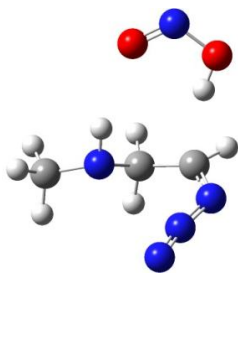
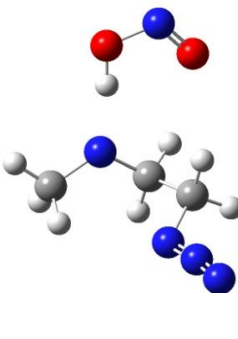
	COMP1-Z	C	-0.16359	-0.30065	-0.93507
		N	-0.00177	-0.18464	0.504248
		H	0.913137	0.154487	0.775189
		C	-1.03261	0.299517	1.287162
		H	-2.03137	-0.01579	0.99864
		C	0.768233	-1.36409	-1.5191
		N	0.406939	-2.73202	-1.10586
		N	0.795418	-3.09	0.006698
		N	1.104825	-3.55918	0.993407
		H	0.685576	-1.35176	-2.60781
		H	1.812964	-1.14088	-1.26319
		H	-1.20185	-0.58027	-1.13738
		H	0.031281	0.658658	-1.43893
		H	-0.82117	0.362126	2.350624
		H	-1.01954	2.225732	0.942128
	COMP2-Z	O	-1.0676	3.227593	0.795417
		N	0.129406	3.660029	0.334214
		O	0.951926	2.80302	0.195013
		H	1.045935	-0.32754	-0.93523
		N	0.959074	-0.64269	0.023392
		C	2.221004	-0.78243	0.727533
		C	-0.16838	-0.18871	0.677707
		C	-1.46219	-0.22432	-0.06855
		N	-2.05668	-1.6048	-0.18453
		N	-1.45162	-2.38027	-0.92108
		N	-0.98026	-3.18073	-1.57878
		H	-1.35041	0.205467	-1.07226
		H	-2.22278	0.347929	0.462548
		H	2.064053	-1.36441	1.639993
		H	2.931686	-1.31993	0.095871
	COMP3-Z	H	2.660905	0.186105	1.006062
		H	-0.19477	-0.42402	1.739728
		H	0.205843	1.760275	0.599491
		O	0.468539	2.733955	0.575305
		N	0.803844	3.058577	-0.70007
		O	0.725893	2.157793	-1.48106
		N	1.399071	-0.24072	-0.70145
		C	1.495071	-0.40895	0.74098
		C	2.688473	-0.22223	-1.37966
		H	0.886783	0.6128	-0.89939
		C	0.145432	-0.6397	1.350817
		N	-0.7399	-1.58122	0.907955
		N	-0.5865	-2.20537	-0.15743
		N	-0.64094	-2.87924	-1.07484
		H	2.142307	-1.28436	0.926697
	COMP4-Z	H	1.974207	0.436639	1.267266
		H	3.175511	-1.19781	-1.27029
		H	2.533189	-0.045	-2.44713
		H	3.386237	0.545011	-1.00123
		H	-0.06418	-0.32398	2.365882
		H	-1.12781	1.128252	0.924395
		O	-1.73737	1.906424	1.008446
		N	-1.3112	2.863821	0.138519
		O	-0.35534	2.55629	-0.5028
		N	1.40375	0.29042	-0.30722
		C	1.15282	0.14750	1.10605
		C	2.33946	-0.64583	-0.86120
		C	-0.21118	-0.51394	1.35032
		N	-0.14500	-1.91734	0.88880
		N	-1.20080	-2.54773	0.93579
		N	-2.10987	-3.22766	0.93431
		H	1.93376	-0.42712	1.62219
		H	1.09164	1.15229	1.54040
		H	1.93009	-1.66578	-0.77866
		H	2.53334	-0.41986	-1.91221
		H	3.28896	-0.64527	-0.30311
		H	-0.43210	-0.47560	2.42444
		H	-0.98645	0.04256	0.81435
		H	0.56380	1.55358	-1.15938
		O	0.14039	2.28521	-1.72518
		N	-0.71171	2.99841	-0.96212
		O	-0.78895	2.63097	0.17769

Table B-8. Normal mode frequencies and moments of inertia for MMAZ and MMAZ radicals (MMAZ-H•): B3LYP/6-31+G(d,p) results.

Species	Frequencies (cm ⁻¹)													MoI (amu-bohr ²)
CH ₃ NHCH ₂ CH ₂ N ₃	60	202	403	660	881	1050	1195	1344	1458	1490	2254	3026	3108	451
	77	266	495	733	985	1144	1264	1379	1478	1496	2923	3061	3110	933
	125	285	582	833	1004	1165	1298	1398	1487	1519	2946	3078	3558	1227
C•H ₂ NHCH ₂ CH ₂ N ₃	25	223	403	616	830	1008	1239	1349	1460	1519	3044	3134		437
	61	274	522	660	864	1065	1279	1371	1473	2251	3088	3250		923
	146	322	576	681	974	1171	1318	1388	1480	3028	3107	3590		1217
CH ₃ N•CH ₂ CH ₂ N ₃	47	129	351	652	935	1042	1210	1378	1423	1484	2955	3041		399
	65	231	518	813	986	1105	1271	1384	1477	2257	2971	3107		1051
	92	286	583	838	1020	1197	1341	1407	1483	2933	2997	3111		1371
CH ₃ NHC•HCH ₂ N ₃	56	181	315	593	774	1095	1245	1373	1473	1554	3007	3136		398
	82	222	511	618	894	1140	1271	1395	1485	2218	3076	3180		1078
	106	287	579	672	1040	1176	1313	1463	1504	2987	3122	3569		1395
CH ₃ NHCH ₂ C•HN ₃	68	201	354	546	893	1085	1169	1374	1478	1516	2947	3109		421
	90	247	380	728	970	1135	1283	1399	1488	2208	2963	3241		959
	151	327	480	777	1033	1156	1321	1457	1497	2936	3059	3519		1300

Table B-9. Normal mode frequencies and moments of inertia (MoI) for H-bonded complexes involved in reactions R1–R4: B3LYP/6-31+G(d,p) results.

Species		Frequencies (cm ⁻¹)															MoI (amu-bohr ²)
COMP1-E	17	50	143	254	428	657	822	896	1039	1266	1344	1439	1488	2254	3090	3173	718
	30	78	170	284	520	686	838	924	1056	1280	1385	1467	1533	2984	3115	3234	3767
	40	112	196	364	580	707	871	988	1181	1305	1389	1484	1750	3019	3124	3560	3927
COMP2-E	24	60	137	198	358	643	774	898	1080	1247	1379	1461	1500	2230	3089	3156	940
	36	79	152	235	522	659	822	909	1139	1282	1395	1477	1553	3003	3132	3246	3123
	41	118	160	292	591	696	856	1044	1175	1316	1427	1486	1756	3022	3134	3563	3423
COMP3-E	24	78	123	214	353	613	746	911	1072	1181	1375	1460	1506	2209	2960	3202	1260
	42	91	141	253	421	687	808	984	1143	1285	1391	1487	1526	2934	3060	3500	2484
	66	113	166	341	537	716	882	1023	1154	1342	1400	1490	1769	2955	3113	3516	3016
COMP4-E	21	64	123	202	369	654	870	956	1062	1214	1382	1432	1487	2252	3008	3122	1398
	33	73	139	255	516	726	905	1000	1123	1272	1392	1472	1513	2946	3018	3122	2044
	39	88	170	304	583	805	948	1020	1199	1339	1404	1483	1754	2972	3057	3199	2655
COMP1-H	16	56	147	266	455	656	828	988	1181	1279	1384	1466	1532	2254	3021	3119	579
	32	93	201	288	523	677	862	1038	1198	1306	1385	1483	1545	2536	3093	3226	3840
	41	115	227	374	580	784	894	1056	1264	1344	1398	1488	1674	3003	3115	3568	4103
COMP2-H	29	64	128	237	367	655	787	1045	1174	1284	1388	1480	1535	2230	3024	3132	913
	35	93	153	258	519	664	829	1077	1176	1316	1404	1486	1556	2721	3087	3156	2931
	50	111	197	292	589	780	898	1139	1248	1378	1464	1498	1677	2996	3131	3557	3313
COMP3-H	22	60	128	203	395	573	790	1036	1136	1301	1389	1481	1519	2207	3008	3115	1042
	23	77	147	269	409	706	872	1065	1150	1333	1411	1486	1534	2945	3025	3212	2803
	53	103	176	325	547	784	932	1111	1183	1376	1456	1492	1685	2953	3067	3547	3296
COMP4-H	27	64	125	247	366	654	874	1017	1196	1274	1393	1432	1489	2253	2971	3058	1406
	36	77	141	300	518	783	941	1061	1211	1341	1396	1471	1600	2862	3010	3122	1885
	45	89	144	310	583	803	987	1122	1222	1381	1407	1483	1685	2945	3018	3122	2556
COMP1-Z	17	54	164	255	435	658	827	943	1040	1268	1345	1418	1489	2254	3020	3121	644
	30	87	173	284	522	688	849	988	1057	1280	1385	1467	1534	2914	3092	3229	3648
	41	130	187	370	581	712	896	999	1183	1309	1391	1484	1666	2990	3115	3564	3868
COMP2-Z	26	63	140	194	361	649	779	924	1080	1247	1379	1463	1500	2230	3032	3133	958
	33	87	150	237	522	661	827	984	1139	1283	1395	1481	1553	2993	3088	3155	2772
	49	121	190	295	589	703	896	1045	1175	1317	1413	1486	1670	3002	3131	3561	3099
COMP3-Z	18	71	118	214	352	611	803	969	1073	1181	1374	1460	1503	2209	2959	3206	1293
	28	86	138	253	420	688	816	984	1144	1284	1382	1486	1522	2934	3060	3336	2271
	65	112	168	338	537	742	882	1024	1153	1341	1400	1490	1687	2955	3112	3528	2921
COMP4-Z	21	77	131	197	441	643	862	1010	1071	1251	1351	1467	1492	2262	3010	3073	1100
	33	82	148	218	481	728	956	1041	1125	1282	1370	1470	1497	2886	3019	3091	2825
	38	112	179	302	584	842	981	1045	1202	1340	1398	1485	1664	2971	3026	3117	3371

Table B-10. Normal mode frequencies and moments of inertia (MoI) for transition states involved in reactions R1–R4: B3LYP/6-31+G(d,p) results.

Species		Frequencies (cm ⁻¹)															MoI (amu-bohr ²)
TS1-E	1120 <i>i</i>	50	152	279	497	581	762	982	1062	1253	1342	1388	1484	1619	3024	3119	690
	24	77	189	307	525	658	827	1036	1171	1278	1352	1464	1518	2254	3070	3157	3566
	44	92	231	379	563	701	897	1055	1186	1285	1385	1479	1531	3004	3097	3539	3736
TS2-E	1045 <i>i</i>	65	142	223	355	600	760	982	1120	1230	1327	1458	1495	1617	3035	3137	878
	34	86	171	263	496	672	862	1043	1140	1282	1380	1479	1513	2244	3093	3139	2874
	56	117	206	309	585	713	912	1053	1173	1308	1385	1483	1541	3013	3096	3527	3198
TS3-E	1104 <i>i</i>	74	163	231	351	551	816	1011	1094	1192	1365	1426	1494	1599	2963	3106	1258
	32	96	174	261	524	666	866	1031	1145	1285	1373	1460	1510	2218	3025	3113	2209
	59	108	203	339	543	714	934	1047	1162	1304	1390	1490	1530	2947	3060	3500	2703
TS4-E	1637 <i>i</i>	49	111	234	362	585	831	999	1088	1249	1373	1419	1482	1713	2977	3070	920
	29	59	145	266	499	662	910	1031	1133	1278	1381	1429	1484	2249	3047	3130	2837
	46	109	191	294	535	800	942	1067	1208	1332	1390	1474	1595	2878	3049	3135	3068
TS1-H	1116 <i>i</i>	46	122	275	457	581	821	985	1080	1279	1344	1411	1490	1660	3020	3117	560
	22	62	209	296	504	659	830	1039	1186	1298	1385	1466	1526	2254	3087	3184	3784
	36	95	241	375	552	691	896	1053	1250	1331	1387	1484	1565	3010	3093	3564	4082
TS2-H	1227 <i>i</i>	62	124	241	317	587	814	977	1139	1290	1376	1461	1501	1658	3019	3131	830
	21	74	167	280	443	664	861	1046	1172	1307	1389	1478	1541	2239	3096	3133	2906
	38	104	212	303	538	683	903	1061	1237	1334	1402	1483	1556	3017	3107	3560	3428
TS3-H	1488 <i>i</i>	57	152	213	396	572	810	993	1141	1298	1380	1459	1494	1672	2955	3116	1076
	19	71	174	295	454	699	869	1046	1160	1300	1393	1482	1518	2227	3054	3137	2481
	43	113	203	340	508	760	914	1057	1192	1349	1406	1489	1530	2943	3069	3547	2993
TS4-H	1354 <i>i</i>	49	109	248	394	582	830	1025	1130	1270	1383	1431	1492	1698	2982	3051	1207
	23	80	147	301	461	657	873	1042	1198	1297	1391	1442	1494	2255	3013	3119	2189
	35	95	182	336	528	806	959	1056	1217	1345	1419	1465	1618	2950	3031	3125	2585
TS1-Z	1319 <i>i</i>	49	149	275	452	582	814	987	1099	1250	1306	1385	1484	1587	3015	3120	584
	21	74	162	289	501	658	832	1045	1170	1279	1341	1445	1492	2252	3073	3165	3599
	36	96	229	379	544	679	892	1056	1188	1288	1382	1470	1523	3009	3091	3565	4066
TS2-Z	1330 <i>i</i>	59	131	226	316	586	799	986	1140	1234	1311	1440	1480	1587	3020	3134	731
	22	107	144	252	463	647	871	1049	1163	1292	1378	1455	1504	2241	3093	3138	2972
	44	120	188	306	539	677	906	1059	1173	1305	1389	1477	1533	3019	3095	3569	3577
TS3-Z	1536 <i>i</i>	75	142	255	353	545	826	1016	1147	1195	1357	1428	1491	1587	2955	3113	1337
	13	114	172	270	469	709	872	1042	1165	1249	1369	1461	1509	2219	2992	3116	1889
	52	120	223	305	534	796	939	1052	1180	1277	1393	1488	1523	2925	3058	3520	2367
TS4-Z	1379 <i>i</i>	55	138	244	333	581	838	1028	1138	1238	1383	1437	1484	1552	2996	3052	1033
	16	81	140	270	486	655	882	1051	1200	1279	1388	1465	1490	2254	3029	3120	2204
	41	108	214	297	539	810	959	1057	1213	1341	1424	1472	1523	2989	3051	3133	2480

**Appendix C. Geometric Representations, Normal Mode Frequencies, and
Moments of Inertia for Molecular Structures Involved in Radical + NO₂
Addition Reaction Paths**

This appendix provides B3LYP/6-31+G(d,p)-based geometries, normal mode frequencies, and moments of inertia for all stationary point structures characterized in the $\text{C}\cdot\text{H}_2\text{NHCH}_2\text{CH}_2\text{N}_3+\text{NO}_2$, $\text{CH}_3\text{NHC}\cdot\text{HCH}_2\text{N}_3+\text{NO}_2$, and $\text{CH}_3\text{N}\cdot\text{CHCH}_2\text{N}_3+\text{NO}_2$ reaction systems. The G4-based sums for the structures' electronic, zero-point vibrational, and thermal energies at 298 K are also listed. Table C-1 presents G4-based energies and moments of inertia. Tables C-2–C-4 present Cartesian coordinate representations and normal mode frequencies for structures in figures 6–8, respectively.

Table C-1. G4-model total energies^a and moments of inertia for molecular structures involved in MMAZ-H• + NO₂ reactions.

Species	G4 Energies at 298 K (Hartrees)	Moments of Inertia (amu-bohr ²)
NO	-129.85624	0; 35; 35
NO ₂	-205.01645	7; 139; 146
CH ₂ O	-114.45032	6; 46; 53
HNO ₂	-205.62781	17; 137; 154
<i>trans</i> -HONO	-205.64039	19; 143; 162
C•H ₂ NHCH ₂ CH ₂ N ₃	-337.21965	437; 923; 1217
H ₂ C(NO ₂)NHCH ₂ CH ₂ N ₃	-542.32286	601; 2897; 3162
H ₂ C(ONO)NHCH ₂ CH ₂ N ₃	-542.32244	579; 3060; 3321
•OCH ₂ NHCH ₂ CH ₃ N ₃	-412.40503	472; 1623; 1884
TS6	-542.25585	586; 3270; 3592
TS7	-542.26025	579; 3555; 3961
TS8	-542.27246	419; 4146; 4319
TS11	-542.26105	668; 3300; 3586
TS12	-542.27887	587; 3314; 3539
ONNHCH ₂ CH ₂ N ₃	-427.86216	388; 969; 1288
CH ₂ NCH ₂ CH ₂ N ₃	-336.66025	165; 2563; 2629
H ₂ C(NO ₂)NHCH ₂ CHNH	-432.902470	307; 2005; 2156
H ₂ C(ONO)NHCH ₂ CHNH	-432.902046	403; 2039; 2326
CH ₃ NHC•HCH ₂ N ₃	-337.22159	398; 1078; 1395
CH ₃ NHC(NO ₂)HCH ₂ N ₃	-542.32603	813; 2108; 2637
CH ₃ NHC(ONO)HCH ₂ N ₃	-542.32601	671; 2586; 3112
CH ₃ NHC(O•)HCH ₂ N ₃	-412.40500	584; 1212; 1676
TS14	-542.27756	652; 2555; 2703
TS15	-542.26509	726; 2871; 3424
TS16	-542.26748	1193; 2173; 3187
TS17	-542.27849	903; 2571; 2912
TS20	-542.26641	850; 2367; 3007
TS21	-542.27134	1023; 2334; 3181
TS22	-542.28447	909; 2440; 2943
CH ₃ NHCHCHN ₃	-336.65818	81; 1992; 2038
OCHCH ₂ N ₃	-317.27214	158; 963; 1054
H ₃ CNHNO	-225.04663	37; 382; 408
CH ₃ NHC(NO ₂)HCHNH	-432.902275	762; 962; 1420
CH ₃ NHC(ONO)HCHNH	-432.902229	794; 1111; 1760
CH ₃ N•CH ₂ CH ₂ N ₃	-337.21668	399; 1051; 1371
CH ₃ N(NO ₂)CH ₂ CH ₂ N ₃	-542.30366	902; 1961; 2109
CH ₃ N(ONO)CH ₂ CH ₂ N ₃	-542.27515	1151; 1724; 2243
CH ₃ N(O•)CH ₂ CH ₂ N ₃	-412.40431	556; 1204; 1469
TS24	-542.21421	1305; 1917; 2346
TS25	-542.21965	665; 2998; 3162
TS26	-542.22253	682; 2754; 3144
TS29	-542.24263	1006; 2036; 2412
TS30	-542.22871	1004; 1955; 2263
TS31	-542.23006	713; 2597; 2970
CH ₂ NCH ₂ CH ₂ N ₃	-336.660253	388; 969; 1288
CH ₃ NCHCH ₂ N ₃	-336.663900	318; 1279; 1506
CH ₃ N(NO ₂)CH ₂ CHNH	-432.882431	482; 1279; 1565
CH ₃ N(ONO)CH ₂ CHNH	-432.852378	629; 1358; 1882

^a Total energy is the sum of electronic, zero-point vibrational, and thermal energies.

Table C-2. The Cartesian coordinates and normal mode frequencies of molecular structures involved in the $C\cdot H_2NHCH_2CH_2N_3+NO_2$ system. (See figure 6 in report.)

Cartesian coordinates				Frequencies (cm ⁻¹)			Cartesian coordinates				Frequencies (cm ⁻¹)		
$H_2C(NO_2)NHCH_2CH_2N_3$							$H_2C(ONO)NHCH_2CH_2N_3$						
N	-0.17546	0.19808	0.131925	33	50	58	N	-0.59779	0.669741	-0.08173	23	52	60
C	0.073759	-0.04475	1.553873	82	134	210	C	-0.23888	-0.07847	1.1201	87	140	206
C	0.931664	0.219174	-0.73139	268	319	385	C	0.37515	0.757802	-1.11537	230	264	342
C	0.426459	1.247903	2.296885	487	492	561	C	0.525011	0.790917	2.125007	392	484	499
N	-0.69968	2.197195	2.344873	581	636	660	N	-0.30477	1.876332	2.678456	582	624	659
N	-0.87261	2.895747	1.346119	697	833	862	N	-0.43024	2.883703	1.982541	704	774	832
N	-1.13452	3.617252	0.509155	886	984	1005	N	-0.61328	3.878082	1.465105	881	977	995
N	1.605684	-1.17446	-0.96722	1047	1146	1215	O	0.664235	-0.51196	-1.76213	1024	1052	1171
O	0.991411	-2.16406	-0.60607	1261	1275	1312	N	1.924593	-1.00664	-1.33985	1189	1261	1292
O	2.689023	-1.15679	-1.52274	1333	1349	1384	O	2.159606	-2.04738	-1.82989	1326	1347	1382
H	-0.84191	-0.454	1.98766	1401	1427	1467	H	-1.16266	-0.42122	1.593858	1395	1410	1476
H	0.868634	-0.78624	1.720837	1486	1495	1521	H	0.365502	-0.97241	0.900304	1486	1495	1514
H	0.664936	0.538305	-1.74133	1673	2255	3006	H	0.009153	1.408883	-1.91169	1760	2255	2989
H	1.751136	0.839501	-0.36629	3024	3089	3102	H	1.322451	1.144104	-0.72754	3028	3065	3094
H	0.660054	1.010137	3.337185	3112	3153	3596	H	0.819403	0.177614	2.979743	3110	3127	3582
H	1.314912	1.722837	1.860152				H	1.442247	1.193614	1.676686			
H	-0.9218	-0.37913	-0.2291				H	-1.50053	0.396693	-0.44536			
TS6							TS7						
C	-0.000216	-0.000234	-0.000375	375i	28	48	N	-0.007468	-0.025589	0.004792	309i	19	37
N	-0.000256	-0.000285	1.816360	57	91	137	C	-0.008526	-0.015433	1.467347	52	80	107
O	1.242039	0.000602	-0.201274	198	209	258	C	1.249746	-0.005374	-0.656087	136	183	209
N	1.252047	1.203398	1.689396	304	337	401	C	-0.173448	1.437814	1.968405	265	304	369
O	2.156160	0.935133	2.355105	455	557	584	N	-1.399696	2.002581	2.117073	436	465	483
H	-0.593756	0.929450	-0.118128	669	699	795	N	-2.157522	2.368780	0.230423	523	600	689
H	-0.603978	-0.895249	-0.244668	921	961	987	N	-2.978955	2.729199	-0.408263	770	827	914
C	-0.967498	0.359961	2.852962	1047	1068	1119	O	2.016795	-1.231934	-0.499359	979	993	1032
H	0.541163	-0.829308	2.061885	1221	1229	1252	N	3.078047	-1.037680	0.420443	1156	1187	1216
C	-1.890535	1.495909	2.390890	1277	1304	1333	O	3.683324	-2.029995	0.588363	1284	1299	1341
N	-2.777516	1.930753	3.486507	1369	1414	1427	H	-0.863228	-0.592557	1.828063	1374	1401	1420
N	-3.806001	1.270822	3.642162	1485	1501	1585	H	0.907905	-0.463084	1.878497	1476	1489	1503
N	-4.787986	0.753446	3.882244	1813	2253	2883	H	1.102084	0.100540	-1.732962	1758	2386	2724
H	-1.566659	-0.524689	3.103536	2923	3002	3042	H	1.871075	0.813900	-0.283050	2862	3000	3066
H	-0.451354	0.668689	3.773747	3050	3125	3472	H	-0.196949	1.455644	3.111234	3104	3125	3593
H	-1.300746	2.372591	2.118063				H	0.692107	2.072343	1.677328			
H	-2.469165	1.191799	1.511149				H	-0.624057	-0.728123	-0.377670			
TS8							TS11						
N	0.029165	-0.004630	-0.003816	269i	15	25	N	-0.010266	-0.023496	0.005490	301i	24	38
C	0.026686	-0.008538	1.456751	73	119	123	C	-0.010203	-0.011078	1.471255	44	72	105
C	1.131215	0.027303	-0.684021	186	239	285	C	1.230440	-0.000313	-0.649343	139	172	242
C	-0.457793	-1.346621	2.005442	321	386	430	C	-0.064502	1.449219	1.972748	309	344	426
N	0.552661	-2.368746	1.668874	525	585	643	N	-1.242904	2.108937	2.115735	465	488	524
N	0.244484	-3.532592	1.926984	715	748	816	N	-1.967576	2.546725	0.225901	556	622	689
N	0.073404	-4.638015	2.117567	853	887	1013	N	-2.764101	2.966238	-0.407951	828	861	916
H	-0.687945	0.672893	-0.483318	1022	1051	1086	N	2.054483	-1.329084	-0.535235	991	1008	1128
O	0.705649	2.265712	-1.328788	1193	1260	1292	O	1.467596	-2.320887	-0.137025	1209	1220	1262
N	-0.530563	2.160677	-1.132266	1317	1342	1376	O	3.219522	-1.267736	-0.884518	1294	1322	1336
O	-1.295272	3.068388	-1.416466	1396	1449	1480	H	-0.910818	-0.519530	1.821011	1373	1420	1425
H	1.031630	0.202506	1.837094	1484	1541	1565	H	0.861687	-0.537591	1.884828	1467	1491	1512
H	-0.642476	0.786346	1.797818	1683	2264	2404	H	1.129838	0.132138	-1.729080	1673	2389	2726
H	2.093479	-0.069528	-0.188861	3018	3050	3068	H	1.910797	0.756051	-0.257257	2852	3005	3088
H	1.089059	0.005092	-1.763110	3112	3156	3282	H	-0.094038	1.464957	3.115262	3115	3155	3600
H	-0.575452	-1.265029	3.093539				H	0.851287	2.016571	1.693974			
H	-1.432434	-1.602333	1.571803				H	-0.622908	-0.732991	-0.370158			

Table C-2. The Cartesian coordinates and normal mode frequencies of molecular structures involved in the $C\cdot H_2NHCH_2CH_2N_3+NO_2$ system. (See figure 6 in report.) (continued).

Cartesian coordinates				Frequencies (cm ⁻¹)			Cartesian coordinates				Frequencies (cm ⁻¹)		
TS12				•OCH ₂ NHCH ₂ CH ₃ N ₃									
N	-0.003732	0.002624	-0.000972	577i	28	37	N	0.03492	-0.214607	0.047945	21	58	103
C	-0.002974	0.001948	1.458114	58	94	155	C	0.124752	-0.028203	1.49065	177	185	266
C	1.108571	-0.001271	-0.670563	218	229	283	C	1.275828	-0.200172	-0.679921	358	465	556
C	-0.966777	-1.050397	2.013153	308	383	417	C	0.428721	1.400561	1.957219	588	642	673
N	-0.494767	-2.422304	1.749398	527	580	646	N	-0.673925	2.267963	1.478547	739	823	878
N	-0.892128	-2.946397	0.707541	670	740	824	N	-0.482024	3.479141	1.558269	982	1006	1045
N	-1.193355	-3.550080	-0.205332	832	904	995	N	-0.417335	4.613023	1.584621	1064	1160	1201
H	-0.654888	0.805277	-0.456815	1025	1042	1084	O	2.039319	0.933911	-0.697053	1246	1313	1326
N	0.564415	2.302858	-1.145317	1186	1201	1269	H	-0.82436	-0.344687	1.937855	1342	1364	1385
O	-0.686194	2.164997	-0.887449	1304	1348	1382	H	0.902654	-0.695461	1.880731	1402	1474	1477
O	0.962891	3.348737	-1.596080	1391	1450	1474	H	1.931604	-1.012968	-0.303806	1502	2259	2900
H	1.007354	-0.188488	1.835005	1484	1545	1612	H	1.077	-0.473961	-1.735187	2925	3009	3034
H	-0.320033	0.994986	1.799627	1697	2098	2256	H	0.478084	1.432613	3.05431	3073	3090	3533
H	1.076467	-0.015395	-1.751141	3034	3043	3092	H	1.383356	1.744906	1.547586			
H	2.064552	-0.164902	-0.177405	3115	3142	3268	H	-0.620485	0.453207	-0.345483			
H	-1.012022	-0.947209	3.099743										
H	-1.974722	-0.892427	1.612538										
H ₂ C(NO ₂)NHCH ₂ CHNH				H ₂ C(ONO)NHCH ₂ CHNH									
N	0.498805	0.479835	-0.106850	48	58	87	N	0.328786	0.457471	-0.102550	44	70	82
C	0.485251	0.525439	1.357328	124	261	293	C	0.492773	0.617744	1.341808	117	197	266
C	1.574810	-0.182100	-0.720024	357	486	524	C	1.391304	-0.180970	-0.797549	314	389	483
C	-0.460343	1.599891	1.829866	564	655	697	C	-0.506333	1.618578	1.862328	516	646	710
N	-1.320244	1.365618	2.731344	759	863	961	N	-1.258211	1.346087	2.846616	767	774	959
N	1.601893	-1.733818	-0.520467	982	1035	1122	O	1.602908	-1.570948	-0.421742	972	1016	1039
O	0.574829	-2.264833	-0.133107	1132	1203	1250	N	2.776342	-1.696846	0.363876	1127	1153	1193
O	2.646910	-2.294069	-0.798949	1263	1307	1343	O	2.945707	-2.808864	0.700232	1237	1280	1327
H	0.217202	-0.427624	1.827974	1361	1416	1426	H	0.397286	-0.313399	1.915420	1363	1403	1418
H	1.500443	0.791523	1.684021	1466	1488	1521	H	1.503848	1.011972	1.515205	1477	1491	1513
H	1.556275	-0.079062	-1.807814	1672	1739	3014	H	1.169218	-0.206079	-1.866776	1737	1762	3010
H	2.543692	0.144301	-0.339426	3018	3070	3081	H	2.333106	0.347950	-0.619914	3018	3055	3058
H	-1.865236	2.205028	2.940862	3149	3446	3558	H	-1.864354	2.138736	3.070391	3120	3444	3543
H	-0.332866	2.567957	1.324225				H	-0.522166	2.569058	1.309932			
H	-0.390475	0.157478	-0.470048				H	-0.562897	0.026700	-0.319868			
N	0.498805	0.479835	-0.106850				N	0.328786	0.457471	-0.102550			
C	0.485251	0.525439	1.357328				C	0.492773	0.617744	1.341808			
ONNHCH ₂ CH ₂ N ₃				CH ₂ NCH ₂ CH ₂ N ₃									
N	-0.071411	-0.106828	0.00596	32	58	64	N	0.040785	-0.425974	0.083692	69	91	110
N	0.05026	-0.394536	1.305612	160	234	301	C	0.011839	-0.265768	1.524298	244	293	400
O	1.119607	-0.073841	1.786264	357	385	583	C	1.062739	-0.032212	-0.545178	524	584	662
C	-1.320608	-0.356282	-0.674969	651	664	704	C	-1.285943	0.430437	1.954779	727	835	880
H	0.717606	0.37194	-0.426181	780	938	1016	N	-2.483028	-0.396469	1.725407	997	1048	1069
C	-2.154777	0.926294	-0.851962	1031	1129	1173	N	-2.932261	-0.411587	0.578622	1105	1209	1244
N	-3.445081	0.642055	-1.5049	1263	1307	1336	N	-3.468785	-0.503263	-0.417081	1285	1344	1369
N	-3.432545	0.602769	-2.735902	1357	1403	1467	H	0.874136	0.304353	1.911813	1385	1473	1486
N	-3.55642	0.550287	-3.863689	1472	1496	1606	H	0.029164	-1.263556	1.978832	1503	1750	2259
H	-1.120676	-0.814991	-1.649665	2252	3029	3050	H	1.941451	0.419372	-0.060914	2954	2996	3029
H	-1.876347	-1.075894	-0.069622	3114	3131	3473	H	1.098927	-0.138874	-1.62997	3061	3112	3139
H	-2.392888	1.339375	0.13008				H	-1.376622	1.400536	1.45018			
H	-1.586947	1.682087	-1.40947				H	-1.255336	0.609726	3.031713			

Table C-2. The Cartesian coordinates and normal mode frequencies of molecular structures involved in the $\text{C}\cdot\text{H}_2\text{NHCH}_2\text{CH}_2\text{N}_3+\text{NO}_2$ system. (See figure 6 in report.) (continued).

Cartesian coordinates				Frequencies (cm ⁻¹)		
CH ₃ NHCHCHN ₃						
C	-0.119645	-0.140774	0.121155	62	117	147
C	-0.037742	-0.153636	1.46004	173	232	317
N	1.12751	-0.13409	2.205777	440	462	518
C	1.117512	0.525269	3.502443	637	687	792
N	-1.378558	-0.296392	-0.503645	962	1004	1050
N	-1.425413	-0.262185	-1.730433	1148	1163	1278
N	-1.598939	-0.250825	-2.857115	1312	1324	1371
H	0.754038	-0.042524	-0.518061	1464	1486	1490
H	-0.949489	-0.242639	2.044521	1522	1732	2252
H	1.961907	0.048506	1.664917	2982	3074	3117
H	0.285881	0.135108	4.09761	3152	3175	3579
H	2.044816	0.294823	4.033431			
H	1.009579	1.619558	3.445762			

Table C-3. The Cartesian coordinates and normal mode frequencies of molecular structures involved in the $\text{CH}_3\text{NHC}\cdot\text{HCH}_2\text{N}_3+\text{NO}_2$ system. (See figure 7 in report.)

Cartesian coordinates				Frequencies (cm ⁻¹)			Cartesian coordinates				Frequencies (cm ⁻¹)		
CH ₃ NHC(NO ₂)HCH ₂ N ₃							CH ₃ NHC(ONO)HCH ₂ N ₃						
N	0.055072	-0.125056	0.034205	48	55	71	N	0.043562	-0.167661	0.065085	44	46	77
C	0.0317	-0.094192	1.438973	122	171	183	C	-0.04732	-0.050086	1.478611	121	170	174
C	1.357111	0.060795	-0.605489	216	267	313	C	1.357048	0.088267	-0.519274	192	255	266
C	-1.311377	-0.558992	2.024466	321	469	507	C	-1.402056	-0.547249	1.995488	320	366	475
N	-1.505827	-2.000357	1.836318	581	634	658	N	-1.550818	-2.002198	1.850278	528	583	633
N	-1.865447	-2.365036	0.713303	710	747	855	N	-1.822082	-2.419264	0.722686	691	759	765
N	-2.214161	-2.844078	-0.253194	913	951	1051	N	-2.090855	-2.941002	-0.248039	901	948	1023
N	0.268911	1.345176	2.036636	1063	1153	1172	O	0.076767	1.328495	1.939681	1048	1076	1155
O	0.618529	1.403499	3.202907	1225	1257	1307	N	1.297579	1.518776	2.64725	1169	1207	1290
O	0.055957	2.293378	1.298415	1324	1371	1378	O	1.413235	2.631481	2.999171	1310	1350	1380
H	-0.635542	0.509995	-0.350623	1422	1462	1485	H	-0.673931	0.388739	-0.38771	1387	1461	1482
H	0.848903	-0.677906	1.8666	1488	1508	1536	H	0.76591	-0.617875	1.943115	1490	1506	1527
H	2.04491	-0.713662	-0.25245	1662	2259	3009	H	2.075207	-0.637391	-0.124768	1764	2260	2998
H	1.241821	-0.062336	-1.684747	3025	3088	3117	H	1.299636	-0.052484	-1.601266	3023	3071	3080
H	1.803743	1.045488	-0.411188	3125	3143	3547	H	1.744534	1.097927	-0.318769	3122	3134	3532
H	-1.308308	-0.389113	3.101041				H	-1.471098	-0.340762	3.063776			
H	-2.129743	0.02277	1.579902				H	-2.214579	-0.005364	1.49306			
TS14							TS15						
N	-0.000176	0.000142	-0.000016	457 <i>i</i>	33	56	N	0.00713	0.003995	-0.003663	288 <i>i</i>	33	40
C	-0.000096	-0.000002	1.762341	100	141	173	C	0.007294	0.004975	1.417273	55	112	122
C	1.325821	-0.000155	-0.585352	181	240	268	C	1.316944	0.001243	-0.64888	159	173	188
C	-1.449733	-0.438692	2.072025	297	314	375	C	-1.435545	-0.17686	1.930738	212	248	304
N	-1.838713	-1.696316	1.398005	442	467	578	N	-1.971283	-1.411264	2.094509	363	430	467
N	-1.591999	-2.743972	1.995379	603	682	721	N	-2.32212	-2.213108	0.20771	500	535	662
N	-1.431798	-3.773166	2.449981	893	920	939	N	-2.583783	-3.073839	-0.426247	748	761	884
O	0.343314	1.177715	2.059083	1041	1061	1138	O	0.512174	1.257178	1.977501	1012	1030	1058
N	-0.6808	1.563305	-0.020302	1146	1196	1235	N	1.766157	1.059102	2.617344	1153	1157	1205
O	-0.018354	2.302649	-0.606147	1303	1334	1344	O	2.17975	2.065058	3.058662	1235	1299	1304
H	-0.673013	-0.604433	-0.472269	1352	1430	1475	H	-0.578649	0.75059	-0.362429	1362	1421	1461
H	0.701529	-0.845497	1.955339	1478	1502	1507	H	0.642097	-0.802688	1.792683	1489	1503	1526
H	1.353368	0.575025	-1.51825	1825	2250	2817	H	1.860115	-0.903513	-0.358564	1758	2395	2743
H	2.009353	0.465142	0.129878	3034	3051	3104	H	1.180852	-0.022672	-1.733014	2865	2997	3079
H	1.638968	-1.026905	-0.791118	3136	3140	3470	H	1.940947	0.870913	-0.395531	3088	3120	3532
H	-1.533615	-0.525417	3.161262				H	-1.434724	-0.180756	3.071613			
H	-2.142564	0.333346	1.736342				H	-2.07404	0.686314	1.640463			
TS16							TS17						
C	0.001996	-0.007535	-0.008615	478 <i>i</i>	36	63	N	0.000369	0.000519	0.000312	248 <i>i</i>	44	49
C	0.025043	-0.008012	1.411841	92	103	131	C	0.000792	-0.000541	1.297516	90	115	132
O	2.570917	-0.001618	1.422068	152	194	244	C	1.243891	0.000096	-0.76564	168	225	228
N	2.653014	-0.24558	0.203889	296	327	392	C	-1.26012	-0.145092	2.094794	302	329	392
H	1.248518	-0.190648	-0.211856	431	489	569	N	-1.370454	-1.563132	2.537569	410	513	587
O	3.707893	-0.474366	-0.360385	574	685	700	N	-1.751654	-2.356792	1.671693	670	745	810
H	-0.501374	-0.864383	-0.471698	813	930	972	N	-2.096475	-3.180233	0.971924	867	913	964
N	-0.14721	-1.089395	2.157019	981	1037	1143	O	-0.628164	2.353574	1.235965	1067	1089	1154
H	0.197816	0.923843	1.936176	1157	1258	1282	N	-1.078963	2.26931	0.065135	1186	1242	1288
H	-0.290244	-1.967022	1.675731	1338	1353	1395	O	-1.609127	3.223767	-0.478523	1298	1355	1395
C	0.297292	-1.175134	3.541966	1419	1457	1468	H	-0.743485	0.718118	-0.36183	1446	1476	1480
H	0.162994	-0.20272	4.020207	1483	1510	1544	H	0.94399	-0.131642	1.826622	1502	1533	1564
H	-0.303765	-1.915651	4.07341	1588	1677	2256	H	2.097368	-0.207531	-0.11592	1698	2247	2424
H	1.356114	-1.446397	3.592828	3046	3050	3125	H	1.190858	-0.763803	-1.545676	3049	3087	3125
N	-0.389364	1.283906	-0.56432	3146	3228	3591	H	1.380935	0.976545	-1.238131	3136	3152	3171
N	-0.090937	1.47987	-1.745427				H	-1.20043	0.452114	3.002378			
N	0.09042	1.784145	-2.82361				H	-2.135	0.166998	1.520228			

Table C-3. The Cartesian coordinates and normal mode frequencies of molecular structures involved in the $\text{CH}_3\text{NHC}\cdot\text{HCH}_2\text{N}_3+\text{NO}_2$ system. (See figure 7 in report.) (continued).

Cartesian coordinates			Frequencies (cm ⁻¹)			Cartesian coordinates			Frequencies (cm ⁻¹)				
TS20						TS21							
N	0.005952	0.010747	-0.004971	264i	38	46	C	-0.000552	-0.000366	-0.000074	964i	32	71
C	0.001936	0.000349	1.39891	53	125	131	C	-0.000961	-0.00032	1.422335	89	99	143
C	1.310791	0.007992	-0.666275	158	174	199	N	2.530652	0.000255	1.287438	160	183	238
C	-1.408002	-0.312375	1.969272	224	302	353	O	2.608059	-0.17691	0.015416	279	313	386
N	-1.799464	-1.59029	2.158982	400	469	490	H	1.270303	-0.118603	-0.177054	427	488	557
N	-2.144617	-2.426955	0.284358	547	622	687	O	3.558501	-0.033373	1.931182	576	677	694
N	-2.373786	-3.309638	-0.331485	723	848	909	H	-0.456713	-0.88252	-0.465035	816	926	953
N	0.424704	1.369155	2.043274	1017	1043	1150	N	-0.182009	-1.076584	2.174718	982	1034	1149
O	0.577289	1.365667	3.255565	1160	1212	1241	H	0.110682	0.941411	1.947323	1156	1239	1275
O	0.51649	2.340319	1.311094	1266	1308	1333	H	-0.271598	-1.962409	1.695128	1282	1340	1373
H	-0.591862	0.744333	-0.367784	1384	1434	1462	C	0.277212	-1.133967	3.557759	1398	1450	1471
H	0.720407	-0.713189	1.803934	1489	1507	1533	H	-0.024974	-0.221128	4.076509	1485	1508	1548
H	1.872245	-0.875351	-0.346758	1655	2397	2753	H	-0.181558	-1.988877	4.056491	1663	1673	2256
H	1.159833	-0.06588	-1.745966	2872	3017	3089	H	1.36982	-1.214598	3.596888	3038	3044	3116
H	1.909829	0.903629	-0.455755	3122	3127	3553	N	-0.457913	1.268128	-0.562412	3150	3220	3589
H	-1.341297	-0.275745	3.10572				N	-0.083741	1.521299	-1.710614			
H	-2.138557	0.47111	1.672703				N	0.1561	1.87075	-2.76322			
TS22						CH ₃ NHC(O·)HCH ₂ N ₃							
N	0.000359	-0.000332	0.000196	416i	45	54	N	0.049506	-0.166927	0.025793	47	63	106
C	0.000423	0.000024	1.298688	87	112	129	C	0.034769	0.000883	1.463699	177	222	251
C	1.245392	0.000376	-0.758965	162	213	246	C	1.370061	-0.003563	-0.579807	268	329	469
C	-1.267758	-0.136118	2.090832	295	297	369	C	-1.265228	-0.685643	2.060529	528	577	673
N	-1.401234	-1.554715	2.525762	420	517	587	N	-1.29142	-2.122126	1.821209	680	783	913
N	-1.774766	-2.340147	1.648862	670	721	823	N	-1.608249	-2.49591	0.689001	942	1008	1064
N	-2.115133	-3.156628	0.938935	865	908	969	N	-1.899216	-2.988728	-0.289279	1107	1140	1146
N	-0.687781	2.362037	0.980692	1070	1089	1152	O	0.059985	1.260563	1.941569	1193	1263	1306
O	-0.827678	3.445775	1.49968	1185	1198	1244	H	-0.593565	0.511883	-0.373071	1330	1360	1452
O	-1.114545	2.179755	-0.214601	1297	1356	1394	H	0.877118	-0.570909	1.897324	1477	1487	1492
H	-0.730044	0.751539	-0.356834	1443	1478	1481	H	2.034061	-0.797574	-0.221003	1516	2253	2927
H	0.936743	-0.167194	1.831304	1503	1544	1603	H	1.288451	-0.103457	-1.665048	2981	3043	3069
H	1.159447	-0.688562	-1.602954	1711	2247	2281	H	1.840924	0.965294	-0.350362	3115	3160	3505
H	1.427746	1.007845	-1.146369	3042	3083	3118	H	-1.251775	-0.54185	3.13912			
H	2.085775	-0.30496	-0.130504	3132	3144	3166	H	-2.142742	-0.18163	1.639408			
H	-1.20869	0.450813	3.005598										
H	-2.132594	0.190341	1.508236										
CH ₃ NHC(NO ₂)HCHNH						CH ₃ NHC(ONO)HCHNH							
N	0.014464	-0.042842	-0.084768	48	69	117	N	0.01112	0.010311	-0.101805	49	79	118
C	-0.064193	-0.137069	1.318428	174	203	228	C	-0.05251	-0.068983	1.315767	172	180	199
C	1.357733	0.085707	-0.646805	297	419	440	C	1.349884	0.055555	-0.681851	265	321	419
C	-1.477778	-0.396329	1.781991	454	634	665	C	-1.478931	-0.264018	1.771035	468	501	655
N	-1.715344	-1.299195	2.634771	717	840	882	N	-1.779138	-1.207024	2.560045	699	757	846
N	0.375338	1.209333	2.038824	1012	1045	1117	O	0.420877	1.155794	1.96756	1001	1026	1053
O	0.907729	1.116914	3.127286	1141	1155	1228	N	1.625176	0.91338	2.684512	1118	1144	1150
O	0.117888	2.243987	1.440682	1256	1292	1328	O	2.013097	1.893234	3.200179	1218	1283	1319
H	-0.596458	0.690468	-0.426941	1402	1425	1462	H	-0.566691	0.768157	-0.448402	1361	1424	1459
H	0.61613	-0.879009	1.735068	1489	1505	1534	H	0.568818	-0.89006	1.682747	1488	1504	1526
H	1.956166	-0.781451	-0.351315	1667	1740	3003	H	1.889717	-0.857926	-0.412969	1746	1762	2998
H	1.287145	0.089191	-1.736918	3025	3085	3125	H	1.266407	0.087097	-1.771016	3012	3078	3097
H	1.881126	0.998496	-0.327959	3144	3452	3548	H	1.949935	0.916515	-0.35268	3120	3448	3538
H	-2.71563	-1.356906	2.838594				H	-2.779376	-1.20245	2.771898			
H	-2.234662	0.249815	1.316057				H	-2.19386	0.46805	1.36798			
N	0.014464	-0.042842	-0.084768				N	0.01112	0.010311	-0.101805			
C	-0.064193	-0.137069	1.318428				C	-0.05251	-0.068983	1.315767			

Table C-3. The Cartesian coordinates and normal mode frequencies of molecular structures involved in the $\text{CH}_3\text{NHC}\cdot\text{HCH}_2\text{N}_3+\text{NO}_2$ system. (See figure 7 in report.) (continued).

Cartesian coordinates				Frequencies (cm^{-1})			Cartesian coordinates				Frequencies (cm^{-1})		
OCHCH₂N₃							H₃CNHNO						
C	-0.094683	0.150122	0.048377	37	70	239	N	0.061776	-0.234856	0.06433	120	221	358
C	0.017028	-0.024593	1.563568	322	485	582	C	-0.01177	-0.019692	1.490082	652	663	991
N	1.402012	0.08425	2.044226	683	720	952	N	1.140949	0.144341	-0.616692	1143	1149	1245
N	1.803017	1.224833	2.288612	1021	1096	1231	O	1.084163	-0.089885	-1.810532	1443	1465	1480
N	2.290697	2.212069	2.562354	1306	1357	1403	H	-0.682248	-0.671579	-0.476776	1523	1600	3031
O	-1.128115	0.406856	-0.50574	1451	1842	2257	H	-0.112614	-0.965799	2.032826	3087	3146	3480
H	0.861554	0.005098	-0.50075	2900	3044	3097	H	0.919668	0.464475	1.789144			
H	-0.667022	0.673186	2.059261				H	-0.852852	0.630737	1.75346			
H	-0.31219	-1.041095	1.804195										

Table C-4. The Cartesian coordinates and normal mode frequencies of molecular structures involved in the $\text{CH}_3\text{N}\cdot\text{CH}_2\text{CH}_2\text{N}_3+\text{NO}_2$ system. (See figure 8 in report.)

Cartesian coordinates				Frequencies (cm^{-1})			Cartesian coordinates				Frequencies (cm^{-1})		
$\text{CH}_3\text{N}(\text{NO}_2)\text{CH}_2\text{CH}_2\text{N}_3$							$\text{CH}_3\text{N}(\text{ONO})\text{CH}_2\text{CH}_2\text{N}_3$						
N	0.082491	0.14461	0.116146	21	44	64	N	0.087487	-0.100235	0.015008	36	55	69
C	-0.045303	0.082934	1.567623	95	135	159	C	0.084354	-0.093537	1.477962	100	179	202
C	1.346158	-0.040248	-0.582061	247	267	359	C	1.40963	0.136603	-0.559334	224	262	279
C	-0.872146	-1.115805	2.045621	418	474	578	C	-1.222319	-0.648125	2.043897	346	421	465
N	-0.201561	-2.392987	1.729963	612	623	657	N	-1.362422	-2.099224	1.82676	541	570	582
N	-0.573288	-2.964812	0.704479	786	817	858	N	-1.796968	-2.457719	0.730725	659	734	844
N	-0.829732	-3.598254	-0.202412	947	985	1033	N	-2.202406	-2.934002	-0.21616	878	990	994
N	-0.912648	0.798309	-0.569852	1069	1143	1187	O	-0.736259	0.994071	-0.393057	1036	1039	1145
O	-0.696673	1.057538	-1.74647	1256	1302	1325	N	-1.765042	0.469136	-1.279789	1171	1236	1259
O	-1.94207	1.049725	0.052526	1344	1361	1379	O	-2.440166	1.343608	-1.657927	1296	1346	1382
H	0.966143	0.014518	1.974237	1402	1442	1476	H	0.910507	-0.734102	1.799933	1399	1447	1469
H	-0.508949	1.004477	1.92992	1486	1492	1508	H	0.260849	0.91968	1.873919	1481	1488	1503
H	1.865057	0.91043	-0.752735	1640	2254	3036	H	1.862535	1.079109	-0.216729	1786	2257	2981
H	1.964496	-0.692978	0.03459	3061	3067	3115	H	2.05569	-0.698123	-0.275357	2996	3047	3093
H	1.170174	-0.516911	-1.546373	3123	3129	3163	H	1.324226	0.155201	-1.64731	3100	3114	3139
H	-0.957502	-1.070563	3.134659				H	-1.225762	-0.511016	3.127516			
H	-1.876369	-1.068867	1.615807				H	-2.077629	-0.099604	1.633561			
TS24							TS25						
N	-0.002588	0.01877	-0.001107	288i	32	46	N	0.001122	0.000538	0.000319	386i	36	58
C	-0.003878	0.008631	1.462777	65	90	136	C	0.001168	0.000502	1.438126	78	96	200
C	1.341871	-0.004789	-0.57102	171	188	219	C	1.233785	-0.00045	-0.62944	245	265	287
C	-1.436794	-0.219119	1.985056	225	279	326	C	-0.162115	1.458296	1.938282	343	451	473
N	-1.95825	-1.469143	2.095408	378	428	480	N	-1.490518	2.01853	1.670769	483	554	582
N	-2.370005	-2.171953	0.175379	520	540	575	N	-1.685246	2.452327	0.532993	665	792	827
N	-2.677967	-2.985975	-0.498204	736	850	905	N	-1.996233	2.90351	-0.459949	870	947	971
O	-0.592131	1.259866	-0.397658	983	1016	1027	H	1.287796	-1.065051	-1.091536	1027	1080	1156
N	-1.715666	0.95548	-1.265855	1124	1164	1223	O	-0.565713	-1.904152	-0.168953	1182	1218	1276
O	-2.215811	1.948545	-1.625242	1236	1279	1299	O	0.262882	-2.426016	-0.929968	1291	1339	1344
H	0.611928	-0.838821	1.774931	1374	1419	1442	N	0.215385	-3.587495	-1.269458	1379	1388	1409
H	0.427309	0.939487	1.867169	1468	1481	1499	H	-0.860617	-0.573611	1.787718	1483	1487	1502
H	1.971927	0.825463	-0.217491	1783	2395	2734	H	0.922202	-0.41545	1.877388	1602	2258	2286
H	1.808486	-0.95356	-0.293954	2898	2969	2993	H	1.257347	0.664671	-1.498288	2976	3007	3034
H	1.265664	0.04182	-1.659162	3096	3104	3138	H	2.115892	0.092637	0.018736	3100	3102	3115
H	-1.419522	-0.291316	3.124832				H	0.632021	2.095969	1.531239			
H	-2.098254	0.642241	1.760515				H	-0.058336	1.442647	3.025332			
TS26							TS29						
N	0.001717	0.001432	-0.000597	351i	31	56	N	0.002047	-0.006364	-0.003335	297i	24	48
C	0.000445	0.00106	1.385143	89	99	216	C	-0.002299	0.0024	1.455043	64	89	122
C	1.288818	0.001825	-0.645895	228	235	276	C	1.226584	0.005583	-0.78894	135	156	201
C	-1.102973	-0.869334	2.003411	317	335	411	C	-0.509345	-1.348218	2.02048	289	324	387
N	-0.785433	-2.310436	1.974178	482	544	589	N	0.313749	-2.430213	2.090458	415	481	519
N	-0.837857	-2.853915	0.869823	668	785	826	N	0.460262	-3.269496	0.221381	622	629	783
N	-0.84886	-3.47622	-0.079934	898	923	1010	N	0.808004	-4.116239	-0.390913	816	885	947
H	-0.299869	1.097111	1.629002	1052	1082	1122	N	-1.14737	0.397179	-0.636225	1011	1044	1139
O	-0.392616	1.905217	-0.441435	1168	1233	1266	O	-1.069978	0.618162	-1.838852	1176	1222	1273
N	-0.625401	2.455295	0.64737	1274	1343	1361	O	-2.15969	0.485226	0.05443	1302	1332	1349
O	-0.912518	3.62772	0.747602	1388	1410	1423	H	1.028794	0.154541	1.779911	1380	1410	1441
H	0.984228	-0.140812	1.856208	1453	1481	1494	H	-0.626431	0.828868	1.804925	1478	1486	1507
H	2.077438	0.52241	-0.084694	1600	2248	2264	H	1.554379	1.025761	-1.022934	1637	2385	2742
H	1.577135	-1.054909	-0.748257	2992	3011	3051	H	1.991863	-0.502436	-0.201961	2943	3033	3065
H	1.196076	0.419006	-1.650474	3052	3129	3131	H	1.071947	-0.531451	-1.724483	3123	3132	3166
H	-1.212125	-0.623077	3.060439				H	-0.379713	-1.343639	3.153496			
H	-2.050922	-0.664761	1.493709				H	-1.591887	-1.481798	1.839937			

Table C-4. The Cartesian coordinates and normal mode frequencies of molecular structures involved in the $\text{CH}_3\text{N}\cdot\text{CH}_2\text{CH}_2\text{N}_3+\text{NO}_2$ system. (See figure 8 in report.) (continued).

Cartesian coordinates				Frequencies (cm^{-1})			Cartesian coordinates				Frequencies (cm^{-1})		
TS30							TS31						
N	0.00066	-0.000691	-0.001423	-1323	29	54	N	-0.000165	0.000076	0.000027	-1377	35	54
C	-0.000047	0.000172	1.450428	97	133	164	C	-0.000158	0.00004	1.344394	91	142	180
C	1.192802	0.000084	-0.618428	239	256	308	C	1.280877	-0.000222	-0.680013	208	223	259
C	-1.375235	0.335213	2.031234	371	432	500	C	-1.174174	-0.700098	2.023726	332	340	450
N	-2.385081	-0.675504	1.667971	547	579	583	N	-0.972084	-2.163556	2.152691	487	527	591
N	-2.952393	-0.517898	0.585168	651	671	828	N	-0.898681	-2.786009	1.092972	613	686	822
N	-3.564869	-0.49177	-0.369359	837	860	992	N	-0.808809	-3.469186	0.190129	856	918	973
H	1.164087	1.234768	-1.021023	1036	1078	1081	H	-0.323916	1.271502	1.475563	1026	1070	1112
N	-0.378125	2.116196	-0.357966	1184	1233	1279	N	-0.444985	2.077069	-0.212332	1167	1257	1267
O	0.585077	2.420522	-1.10281	1297	1322	1350	O	-0.650808	2.429224	0.98119	1295	1301	1350
O	-1.270249	2.882	-0.106977	1379	1389	1423	O	-0.616707	2.80404	-1.147589	1393	1421	1468
H	0.776814	0.647488	1.886	1445	1493	1525	H	0.964635	-0.069749	1.868265	1477	1494	1498
H	0.250305	-1.033094	1.734684	1573	1733	2259	H	2.102996	0.433304	-0.093287	1575	1767	2246
H	2.112435	-0.068159	-0.023437	2982	3012	3025	H	1.523537	-1.05181	-0.884538	2996	3009	3049
H	1.210588	-0.503323	-1.589056	3069	3116	3123	H	1.19238	0.513735	-1.638845	3059	3130	3132
H	-1.690892	1.336641	1.725236				H	-1.293547	-0.346598	3.048432			
H	-1.308623	0.311201	3.121374				H	-2.093525	-0.48615	1.467074			
CH₂NCH₂CH₂N₃							CH₃NCHCH₂N₃						
N	0.040785	-0.425974	0.083692	69	91	110	N	0.007561	0.158768	-0.012568	40	69	186
C	0.011839	-0.265768	1.524298	244	293	400	C	0.012351	-0.166226	1.208674	209	235	308
C	1.062739	-0.032212	-0.545178	524	584	662	C	1.261379	0.113099	-0.739404	428	528	590
C	-1.285943	0.430437	1.954779	727	835	880	C	-1.255176	-0.144064	2.024657	682	851	925
N	-2.483028	-0.396469	1.725407	997	1048	1069	N	-1.521826	-1.458007	2.661309	997	1057	1089
N	-2.932261	-0.411587	0.578622	1105	1209	1244	N	-1.885893	-2.353293	1.895957	1141	1167	1237
N	-3.468785	-0.503263	-0.417081	1285	1344	1369	N	-2.234106	-3.257652	1.304824	1302	1362	1387
H	0.874136	0.304353	1.911813	1385	1473	1486	H	0.91797	-0.497915	1.741478	1438	1477	1479
H	0.029164	-1.263556	1.978832	1503	1750	2259	H	1.149313	-0.554231	-1.600897	1495	1761	2251
H	1.941451	0.419372	-0.060914	2954	2996	3029	H	1.479655	1.109863	-1.138418	2981	2993	3054
H	1.098927	-0.138874	-1.62997	3061	3112	3139	H	2.116803	-0.224107	-0.13387	3073	3090	3111
H	-1.376622	1.400536	1.45018				H	-1.156287	0.553531	2.860797			
H	-1.255336	0.609726	3.031713				H	-2.088717	0.17703	1.392071			
CH₃N(NO₂)CH₂CHNH							CH₃N(ONO)CH₂CHNH						
N	0.051492	0.316783	0.077465	45	55	86	N	0.082491	0.14461	0.116146	55	76	88
C	-0.023832	-0.036740	1.491733	135	149	310	C	-0.045303	0.082934	1.567623	180	206	223
C	1.173010	-0.076583	-0.763552	357	389	468	C	1.346158	-0.040248	-0.582061	275	361	389
C	-0.429033	-1.476949	1.715397	607	631	760	C	-0.872146	-1.115805	2.045621	482	525	580
N	0.337362	-2.263550	2.349089	785	878	963	N	-0.201561	-2.392987	1.729963	704	766	956
N	-1.120553	0.625262	-0.570041	1003	1036	1128	N	-0.573288	-2.964812	0.704479	995	1001	1021
O	-1.053407	0.758608	-1.786033	1137	1154	1258	N	-0.829732	-3.598254	-0.202412	1101	1129	1167
O	-2.128784	0.759414	0.118808	1297	1329	1357	N	-0.912648	0.798309	-0.569852	1234	1253	1290
H	0.962340	0.126873	1.930372	1365	1414	1444	O	-0.696673	1.057538	-1.74647	1364	1425	1444
H	-0.744137	0.635149	1.961953	1467	1484	1510	O	-1.94207	1.049725	0.052526	1461	1480	1501
H	1.448760	0.740781	-1.431416	1637	1732	3043	H	0.966143	0.014518	1.974237	1738	1780	2958
H	2.007833	-0.307682	-0.101202	3045	3083	3120	H	-0.508949	1.004477	1.92992	2993	3042	3097
H	0.939474	-0.957287	-1.371330	3141	3159	3443	H	1.865057	0.91043	-0.752735	3113	3138	3446
H	-0.075884	-3.196293	2.422203				H	1.964496	-0.692978	0.03459			
H	-1.400806	-1.756918	1.288676				H	1.170174	-0.516911	-1.546373			
N	0.051492	0.316783	0.077465				H	-0.957502	-1.070563	3.134659			
C	-0.023832	-0.036740	1.491733				H	-1.876369	-1.068867	1.615807			

Table C-4. The Cartesian coordinates and normal mode frequencies of molecular structures involved in the $\text{CH}_3\text{N}\cdot\text{CH}_2\text{CH}_2\text{N}_3+\text{NO}_2$ system. (See figure 8 in report.) (continued).

Cartesian coordinates				Frequencies (cm ⁻¹)		
CH ₃ N(O•)CH ₂ CH ₂ N ₃						
N	-0.046108	0.101583	0.123832	33	59	86
C	0.01288	0.190951	1.585711	134	203	289
C	1.157985	-0.244825	-0.619705	295	356	463
C	-1.380764	0.068887	2.198279	568	583	654
N	-1.935723	-1.290053	2.055753	765	852	962
N	-2.578488	-1.517263	1.028654	1000	1039	1112
N	-3.200659	-1.865264	0.146069	1115	1211	1261
O	-0.971808	0.739743	-0.482494	1277	1346	1367
H	0.663859	-0.607233	1.953853	1383	1430	1448
H	0.451662	1.157223	1.880418	1471	1477	1480
H	1.880886	0.58333	-0.613819	1516	2259	2985
H	1.628924	-1.128484	-0.180221	3005	3071	3089
H	0.860646	-0.450601	-1.648128	3095	3128	3157
H	-1.308825	0.255467	3.271771			
H	-2.037878	0.817634	1.748478			

NO. OF
COPIES ORGANIZATION

1 DEFENSE TECHNICAL
(PDF) INFORMATION CTR
DTIC OCA

1 DIRECTOR
(PDF) US ARMY RESEARCH LAB
IMAL HRA

1 DIRECTOR
(PDF) US ARMY RESEARCH LAB
RDRL CIO LL

1 GOVT PRINTG OFC
(PDF) A MALHOTRA

1 ARMY RSRCH OFC
(PDF) D MANN

2 ARMY RSRCH OFC
(PDF) CHEMICAL SCI DIV
R ANTHENIEN
J PARKER

9 US ARMY AVN & MIS CMND
(PDF) AMSRD AMR PS PT
C DOLBEER
J LILLEY
N MATHIS
R MICHAELS
G DRAKE
L PLEDGER
J NEIDERT
A DURRETT
D THOMPSON

1 CALIFORNIA INST TECHNOLOGY
(PDF) DIV CHEMISTRY AND CHEM ENG
W GODDARD

1 NEW JERSEY INST TECHNOLOGY
(PDF) DEPT CHEM & ENVIRON SCI
J BOZZELLI

1 NORTH CAROLINA STATE UNIV
(PDF) DEPT CHEM & BIOMOLEC ENG
P WESTMORELAND

3 PURDUE UNIVERSITY
(PDF) SCHOOL OF AERONTC & ASTRNTC
S HEISTER
T POURPOINT
S SON

NO. OF
COPIES ORGANIZATION

1 PRINCETON UNIV
(PDF) DEPT MECH & AEROSPACE ENG
C LAW

3 THE PENNSYLVANIA STATE UNIV
(PDF) DEPT OF MECHL & NUCLEAR ENGRG
G RISHA
S THYNELL
R YETTER

1 STANFORD UNIVERSITY
(PDF) DEPT MECHANICAL ENGINEERING
D DAVIDSON

1 CHEMICAL PROPULSION INFO
(PDF) ANALYSIS CTR
E LIU

2 US ARMY ARMAMENT RDEC
(PDF) RDAR MEE W
R DAMAVARUPU
A SURAPANENI

20 DIR USARL
(15 PDF, RDRL WM
5 HC) B FORCH
RDRL WML
M ZOLTOSKI
RDRL WML B
J BRENNAN
S BUNTE
E BYRD
J CIEZAK-JENKINS
M HURLEY
B RICE
D TAYLOR
N TRIVEDI
RDRL WML D
R BEYER
C CHEN (5 HC, 1 PDF)
M MCQUAID
M NUSCA
Z WINGARD

INTENTIONALLY LEFT BLANK.